Université Claude Bernard - Lyon 1

Institut Camille Jordan - CNRS UMR 5208

École doctorale InfoMaths

Thèse

de l'université de Lyon

pour obtenir le titre de

Docteur en Sciences
Mention : Mathématiques appliquées

présentée par

Nathalie Eymard

Modélisation hybride de l'hématopoïèse et de maladies sanguines

Thèse dirigée par Vitaly Volpert
préparée à l'Université Lyon 1

Jury :

Rapporteurs: Roeland Merks, Professor, University of Leiden
Rapporteurs: Pierre Magal, Professeur, Université de Bordeaux
Jean Clairambault, Directeur de recherche, Inria Paris-Rocquencourt
Mostafa Adimy, Directeur de Recherche, INRIA Grenoble
Ionel S. Ciuperca, Maître de Conférences, Université Lyon
Jacques Demongeot, Professeur, Faculté de médecine, Grenoble
Vitaly Volpert, Directeur de recherche, CNRS Lyon

Résumé :

Cette thèse est consacrée au développement de modèles mathématiques de l'hématopoïèse et de maladies du sang. Elle traite du développement de modèles hybrides discrets continus et de leurs applications à la production de cellules sanguines (l'hématopoïèse) et de maladies sanguines telles que le lymphome et le myélome.

La première partie de ce travail est consacrée à la formation de cellules sanguines à partir des cellules souches de la mœlle osseuse. Nous allons principalement étudier la production des globules rouges, les érythrocytes. Chez les mammifères, l'érythropoïèse se produit dans des structures particulières, les îlots érythroblastiques. Leur fonctionnement est régi par de complexes régulations intra et extracellulaire mettant en jeux différents types de cellules, d'hormones et de facteurs de croissance. Les résultats ainsi obtenus sont comparés avec des données expérimentales biologiques ou médicales chez l'humain et la souris.

Le propos de la deuxième partie de cette thèse est de modéliser deux maladies du sang, le lymphome lymphoblastique à cellules T (T-LBL) et le myélome multiple (MM), ainsi que leur traitement. Le T-LBL se développe dans le thymus et affecte la production des cellules du système immunitaire. Dans le MM, les cellules malignes envahissent la mœlle osseuse et détruisent les îlots érythroblastiques empêchant l'érythropoïèse. Nous développons des modèles multi-échelles de ces maladies prenant en compte la régulation intracellulaire, le niveau cellulaire et la régulation extracellulaire. La réponse au traitement dépend des caractéristiques propres à chaque patient. Plusieurs scénarios de traitements efficaces, de rechutes et une résistance au traitement sont considérés.

La dernière partie porte sur un modèle d'équation de réaction diffusion qui peut être utilisé pour décrire l'évolution darwinnienne des cellules cancéreuses. L' existence de "pulse solutions", pouvant décrire localement les populations de cellules et leurs évolutions, est prouvée.

Mots cléfs : modèles hybrides discret-continus, hématopoïèse, maladies du sang, traitement, résistance.

Abstract :

The thesis is devoted to mathematical modeling of hematopoiesis and blood diseases. It is based on the development of hybrid discrete continuous models and to their applications to investigate production of blood cell (hematopoiesis) and blood diseases such as lymphoma and myeloma.

The first part of the thesis concerns production of blood cells in the bone marrow. We will mainly study production of red blood cells, erythropoiesis. In mammals erythropoiesis occurs in special structures, erythroblastic islands. Their functioning is determined by complex intracellular and extracellular regulations which include various cell types, hormones and growth factors. The results of modeling are compared with biological and medical data for humans and mice.

The purpose of the second part of the thesis is to model some blood diseases, T cell Lymphoblastic lymphoma (T-LBL) and multiple myeloma (MM) and their treatment. T-LBL develops in the thymus and it affects the immune system. In MM malignant cells invade the bone marrow and destroy erythroblastic islands preventing normal functioning of erythropoiesis. We developed multi-scale models of these diseases in order to take into account intracellular molecular regulation, cellular level and extracellular regulation. The response to treatment depends on the individual characteristics of the patients. Various scenarios are considered including successful treatment, relapse and development of the resistance to treatment.

The last part of the thesis is devoted to a reaction-diffusion model which can be used to describe darwinian evolution of cancer cells. Existence of pulse solutions, which can describe localized cell populations and their evolution, is proved.

Keywords: hybrid discrete-continuous models, hematopoiesis, blood diseases, treatment, resistance

Publications

1. N. Bessonov, N. Eymard, P. Kurbatova, V. Volpert. *Mathematical Modelling of Erythropoiesis in vivo with Multiple Erythroblastic Islands.* Applied Mathematics Letters, Volume 25, Issue 9, pp: 1217–1221, 2012.

2. P. Kurbatova, N. Eymard, V. Volpert. *Hybrid model of erythropoiesis.* Acta Biotheoretica, Volume 61, Issue 3, pp: 305-315, 2013.

3. N. Eymard, N. Bessonov, O. Gandrillon, M.J. Koury, V. Volpert. *The role of spatial organization of cells in erythropoiesis.* Journal of Mathematical Biology, Volume 70, issue 1, pp 71–97, 2015.

4. P. Kurbatova, N. Eymard, A. Tosenberger, V. Volpert, N. Bessonov. *Application of hybrid discrete-continuous models in cell population dynamics,* in: BIOMAT 2011, World Sci. Publ., Hackensack, NJ, pp 1–10, 2012.

5. V. Volpert, N. Bessonov, N. Eymard, A. Tossenberger. *Modèle multi-échelle de la dynamique cellulaire,* in: *Le vivant discret et continu.* Nicolas Glade et Angélique stéphanou, Editeurs: Editions Matériologiques, pp: 91–112, 2013.

6. P. Nony, P. Kurbatova, A. Bajard, S. Malik, C. Castellan, S. Chabaud, V. Volpert, N. Eymard, B. Kassai C. Cornu and The CRESim and Epi-CRESim study groups. *A methodological framework for drug development in rare diseases.* Orphanet Journal of Rare Diseases, 9:164, 2014.

7. N. Eymard, P. Kurbatova. *Hybrid models in hematopoiesis.* (submitted 2014).

8. N.Eymard, N.Bessonov, V.Volpert, CRESim Group. *Mathematical model of T-cell lymphoblastic lymphoma: disease, treatment, cure or relapse of a virtual cohort of patients.* (submitted 2014).

9. Awards. Best Poster Prize 8. 9th International Conference for Rare Diseases and Orphan Drugs (ICORD), October 7-9, 2014, The Netherlands.

Remerciements

Je remercie tous ceux, en particulier mon directeur de thèse V. Volpert, qui m'ont permis de mener jusqu'à son terme et de concrétiser ce qui n'a longtemps été qu'un projet. Je tiens également à remercier les rapporteurs et membres du jury de l'intérêt qu'ils ont porté à mon travail.

Contents

Chapter 1

Introduction

The thesis is devoted to the mathematical modeling of hematopoiesis and blood diseases. We will begin this study with modeling of the lineage choice of megakaryocytic-erythroid progenitors. These two lineages lead to the production of erythrocytes and platelets. We will study in more detail the erythroid lineage of hematopoiesis. We will model erythroblastic islands, main functional units of erythropoiesis, in normal and pathological situations. The latter will be considered in the case of multiple myeloma. It is a hematological disorder where malignant cells invade the bone marrow resulting in destruction of erythroblastic islands and, as a consequence, to severe anemia. The methods developed for this modeling are applicable to study other diseases. We will show their application to study T-cell lymphoma where tumor develops in the thymus. One of the important aspects of these disorders is that, similar to other cancers, malignant cells can adapt to treatment and develop resistant clones. We will study this question in the case of lymphoma and in a more abstract setting. In this introductory chapter, we will present a short biological background followed by the discussion of the methods of modeling and by the presentation of the main results of this work.

1.1 Biological background

1.1.1 Hematopoiesis

Hematopoiesis is a complex process which begins with hematopoietic stem cells (HSCs) and results in production of red blood cells (erythrocytes), white blood cells (leucocytes) and platelets. Erythrocytes participate in the transport of oxygen, white blood cells in the immune response, platelets play an important role in blood coagulation. In adult humans hematopoiesis occurs mainly in the bone marrow. Due to consecutive stages of maturation and differentiation HSCs give rise to all lineages of blood cells. Various dysfunctions can affect hematopoiesis and cause blood diseases.

Hematopoietic stem cells are located in specific area, called stem cell niche. In niche, HSCs can be in a nondividing state or it can differentiate in order to keep a steady number of blood cells. Hematopoiesis process has the ability to adapt to changes or to stress by elevating the production rate of blood cells.

HSCs are pluripotent cells, they self-renew or differentiate into different lineages. This first differentiation leads to the appearance of common myeloid progenitors (CMP) and common lymphoid progenitors (CLP). Further differentiation of CMP and CLP give rise, in case of CMP, among others cells, to megakaryocytes and erythrocytes and in case of CLP, to lymphocytes. Secondary lymphoid organs such as thymus, spleen, liver and lymph nodes also participate in final differentiations.

Lineage choice of pluripotent cells

Burst forming unit erythroid progenitors (BFU-E) and burst forming units-megakaryocytic progenitors (BFU-MK) appear due to differentiation of megakaryocytic-erythroid progenitor (MEP). BFU-MKs divide and differentiates and become thrombocytes. This process is called the megakaryopoiesis. Similarly, BFU-Es becomes erythrocytes in the process of erythropoiesis. The next stage of maturation of BFU-E is colony-forming unit-erythroid (CFU-E).
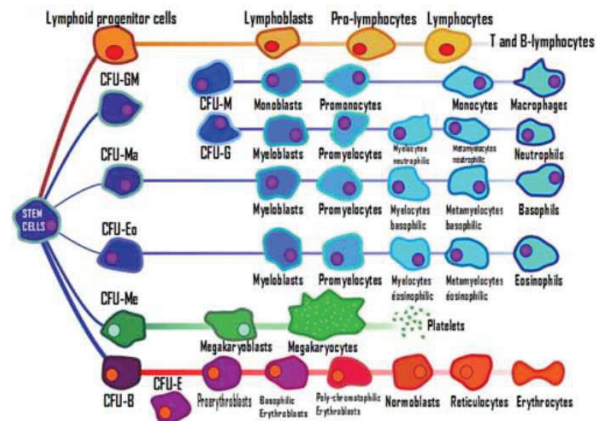
Figure 1.1: All blood cells originate from the stem cell compartment on the left and are released in the blood stream on the right. The lymphoid branch, on top, releases T and B-lymphocytes. The myeloid branch consists of the red lineage (bottom), white lineage in blue and platelets in green.

The complex mechanism that determines commitment of MEP is not completely understood, but it is established that the proteins and transcription factors GATA-1, FLI-1, EKLF play an important role in this process.
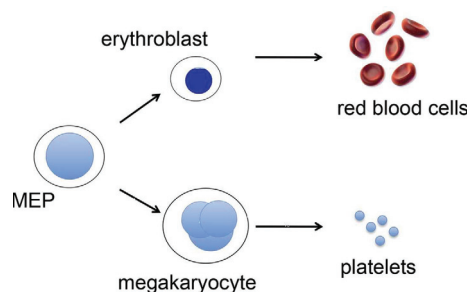
Figure 1.2: Pattern of differentiation of MEP.

Erythropoiesis

Every day, normal adult humans produce $3 \cdot 10^9$ new erythrocytes per Kg of body weight [117], which is approximately $2.1 \cdot 10^{11}$ new erythrocytes for the average 70 Kg person. These new erythrocytes replace the same number of senescent erythrocytes that are removed daily from the circulation. Bleeding or increased rates of erythrocyte destruction (hemolysis) decrease the number of circulating erythrocytes resulting in acute anemia. Acute anemia

14

causes hypoxia that induces stress erythropoiesis in which erythrocyte production is increased until the recovery of normal numbers of circulating erythrocytes. The number of red blood cells should be approximately constant which means that their production should be able to adapt to stress or to diseases.
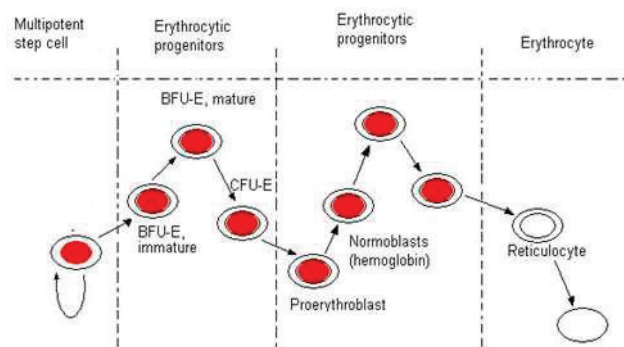
Figure 1.3: Schematic representation of erythropoiesis.

The erythroid lineage of hematopoiesis begins with committed erythroid progenitors that differentiate into more mature cells, the erythroblasts, which subsequently differentiate into reticulocytes. In mammals, the anucleate reticulocytes leave the bone marrow by entering the blood where they become mature erythrocytes. Erythropoiesis is tightly regulated, and its dysregulation results in various blood disorders, such as leukemia, polycythemia and anemia.

The structural unit of mammalian erythropoiesis is the erythroblastic island, which consists of a central macrophage surrounded by as many as several dozen erythroid cells, beginning at the colony-forming unit-erythroid (CFU-E) stage and extending through the reticulocyte stage [40]. The term CFU-E/Pro-EBs describes the erythroid progenitor stage at which the fate decisions are made. CFU-E/Pro-EBs have three possible fates : programmed cell death by apoptosis, proliferation without further differentiation (self-renewal), and terminal differentiation into reticulocytes (Figure 2.10). CFU-E/Pro-EB fate is determined by a complex network of intracellular proteins that has not been completely elucidated and that appears to vary in different biological models. Apoptosis of the CFU-E/Pro-EBs is mainly regulated by Fas, a membrane protein of the TNF receptor family that is activated

15

by Fas-ligand. An important difference between humans and mice is that, among erythroid cells, mature late-stage erythroblasts produce the most Fas-ligand in humans [107], whereas immature early-stage erythroblasts and some CFU-E/Pro-EB themselves, produce the most Fas-ligand in mice [100].

1.1.2 Blood diseases

Two blood diseases, the lymphoma and the multiple myeloma, will be presented in more detail since they will be studied in Chapter 3. These diseases are characterized by invasive processes by tumors of different part of the body that block normal hematopoiesis. For lymphoma, respiratory symptoms shows the early stage of the disease. Symptoms of myeloma are varied and often uncharacteristic.

Multiple Myeloma

Multiple Myeloma (MM) is a blood disease that affects especially elderly people, its frequency increasing with age. This disease is exceptional before the age of forty years. Its incidence is two time more prevalent in men than in women. Causes of the disease are unknown.
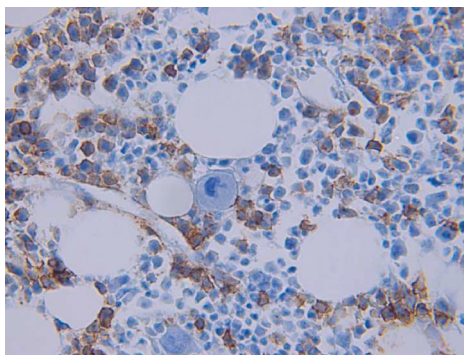
Figure 1.4: Bone marrow. Courtesy of M. Koury.

Medical background. MM is a cancer of the bone marrow that destroys bone tissue, by causing tumors formation inside bones, till the whole bone marrow is replaced by the

tumors.

Clinical presentation. The diagnostic is sometimes suggested by persistent bone pains, fatigue, disturbances related to hypercalcemia, neurological involvement, renal failure, infection and hyperviscosity. The anemia often associated to MM causes by itself symptoms such as weakness, drowsiness, depression, cardiac decompensation and respiratory distress. Some patients are asymptomatic, symptoms like vertebral compression fractures result from bones destruction by the disease and are evidence of generalized disease.

Treatment strategy. MM is presently an incurable hematological malignacy but recent research suggests that therapies designed for long-term cure of the disease should target stem cell. The abnormal erythropoiesis caused by MM is associated with severe normochromic/normocytic anemia. A common complication of MM, anemia indicate in general a poor prognosis. Chemotherapy with melphalan-prednisone is the standard treatment for multiple myeloma. Other treatment modalities include polychemotherapy and bone marrow transplantation. Only 50 to 60 percent of patients respond to therapy. The aggregate median survival for all stages of multiple myeloma is three years. Most patients with multiple myeloma have very significant reductions in the generalized bone marrow infiltration after chemotherapy, permitting comparisons of erythropoiesis in the same individuals at different degrees of bone marrow infiltration. Anemia persists if a remission of patients can not be obtained by chemotherapy and reduces patient's quality of life and sometime blood transfusions are required. It is possible to treat successfully anemia by erythropoietin therapy [101]. Rise of production of erythrocytes after this treatment is simulated in Section 3.1. These malignant cells disrupt erythroblastic island function by either releasing cytokines that are directly cytotoxic to erythroblasts and/or macrophages. Some cytokines can also be indirectly cytotoxic to the marrow erythroid cells by reducing the amount of erythropoietin (EPO), the principal hormonal regulator of erythropoiesis, produced by the kidneys. As the infiltration of the bone marrow space progresses, the malignant cells can physically disrupt the spatial organization of the erythroblastic islands.

17

T Lymphoblastic lymphoma

In industrialized countries, annual cancer incidence in children under than 15 years is estimated to be 140 new cases per million and LBL annual incidence is also estimated between 0.3 to 0.5 case for 100000 children and adolescents, and 85 to 90% are T-cell-lymphoblastic lymphoma [84, 32]. In the current WHO (World Health Organization) classification, T-LBL and T-cell Acute Lymphoblastic Leukemia (T-ALL) are a biologic unit termed "precursor lymphoma/leukemia"[149, 137].The distinction between T-LBL and T-ALL resides in an arbitrary cut-off point of 25% BM infiltration: BM infiltration below 25% is considered T-LBL and above, T-ALL [85]. Non-Hodgkin Lymphoma (NHL) is the third most common form of childhood cancer. LBL represents about 30% of NHL cases in childhood and early adolescence, and 85 to 90% of LBL are T-LBL [84]. Although T-LBL represents around 25% of all NHL in children, it is considered as a rare disease.

Medical background. Lymphoblastic lymphoma (LBL) is a neoplasm developing from immature T- or B-precursor cells [137]. LBL are postulated to arise from precursor B in the bone marrow (BM) or thymic T cells at varying stages of differentiation [52].

Most patients with T-LBL typically present with mediastinal tumor. Other manifestations are lymphadenopathy, frequently with cervical and supraclavicular bulky disease. Pleural or pericardial effusions are also common. The presence of a predominantly anterior mediastinal mass can cause respiratory symptoms from coughing, stridor, dyspnea, edema, elevated jugular venous pressure to acute respiratory distress. About 15–20% of patients exhibit bone marrow infiltration. Less than 5% show CNS (Central Nervous System) involvement [137]. The median age of diagnosis is 8.8 years, and T-LBL are 2.5 times more often diagnosed in male patients [137, 33].

Prognostic factors. The probability of pEFS (probability of event-free survival) in LBL is high, whereas survival in relapsed patients is very poor. As the 5-year EFS (event-free survival) rates are acceptable, the possibility that patients with favorable risk profiles might

be "overtreated" is considered. However, there are currently no validated parameters for use to identify patients with a favorable risk profile. It is of special importance to detect the 10%–30% of patients with a high risk of relapse in order to adapt therapy regimen early. Age older than 14 years [153], CNS involvement trial [1] and unresponse to therapy [155] are identified as possible unfavorable prognostic factors, but this needs confirmation.

Treatment strategy. pEFS in pediatric T-LBLB is currently about 80% [29]. Based on historical studies, the current treatment approach of LBL uses therapy similar to that for childhood acute lymphoblastic leukemia [151], and EFS is actually more than 80% in children and adolescent. Successive studies demonstrated the importance of initial intensive treatment, secondary intensification of chemotherapy, prolonged maintenance therapy and prophylaxis of CNS relapse. Although the development of therapy protocols meant a major step toward curing pediatric patients from LBL, unanswered questions remain. Numerous trials and protocols have been developed on the Berlin-Frankfurt-Muenster (BFM) or LSA2-L2 (American group) backbone to increase event free survival as well as overall survival (OS) and to reduce toxicity within the established therapy regimens [137]. Central nervous system (CNS) prophylaxis is considered as an important element of all LBL protocols, including prophylactic cranial irradiation and Methothrexate (MTX) (high-dose or intrathecal) [137]. Prophylactic irradiation was historically used in all protocols. Several recent trials showed that it was not required any more to achieve an excellent treatment outcome [155, 33, 131]. More trials are needed to evaluate the role of high-dose MTX in pediatric LBL who do not received prophylactic irradiation and an acceptable number of intrathecal MTX. The therapy of LBL is rather long with its total duration of 24 months in most protocols including induction, consolidation and maintenance therapy [137].

1.2 Modeling approaches: multi-scale hybrid model

1.2.1 Modeling literature

Hematopoiesis has been the topic of modeling works for decades. Dynamics of hematopoietic stem cells have been described by Mackey's early works [103, 104]. The author developed hypothesis that aplastic anaemia (lower counts of all three blood cell types) and periodic haematopoiesis in humans are probably due to irreversible cellular loss from the proliferating pluripotential stem cell population. A model for pluripotential stem cell population is described by delay equations. In the later developed model, described by the first order differential equations, a population dynamics of cells capable of both proliferation and maturation was analysed [105]. In Bernard et al. [18] mathematical model was proposed to explain the origin of oscillations of circulating blood neutrophil number. The authors demonstrated that an increase in the rate of stem cell apoptosis can lead to long period oscillations in the neutrophil count. In extension of the previous model Colijn and Mackey in [51] applied mathematical model, described with system of delay differential equations, to explain coupled oscillations of leukocytes, platelets and erythrocytes in cyclical neutropenia. The platelet production process (thrombopoiesis) attracted less attention through years [67, 163]. Cyclical platelet disease was a subject of mathematical modeling in Santillan et al. [132] and was enriched in Apostu et al. [12]. The red blood cell production process (erythropoiesis) has recently been the focus of modeling in hematopoiesis. Pioneering mathematical model which describes the regulation of erythropoiesis in mice and rats has been developed by Wichmann, Loeffler and co-workers [164]. In this work, proposed models were validated by comparing with experimental data. Analysis of the regulating mechanisms in erythropoiesis was enriched in [168]. In 1995, Bélair et al. proposed age-structured model of erythropoiesis where erythropoietin (EPO) causes differentiation, without taking into account erythropoietin control of apoptosis found out in 1990 by Koury and Bondurant in [92]. In 1998 Mahaffy et al. [106] expanded this model by including the apoptosis possibility. Age-stuctured model is detailed in [3] with assumption that decay rate of erythropoietin

depends on the number of precursor cells. In [57] Crauste et al. included in the model the influence of EPO upon progenitors apoptosis and showed the importance of erythroid progenitor self-renewing by confronting their model with experimental data on anaemia in mice. A model of all hematopoietic cell lineages that has been proposed by Colijn and Mackey [50, 51] includes dynamics of hematopoietic stem cells, white cell lineage, red blood cell lineage and platelet lineage. A review of mathematical models and simulation studies, applied to stem cell biology, with particular interest to the hematopoietic system is proposed by Roeder[125].

In recent works a combination of different models is used in order to describe the process of hematopoiesis in its complexity. A hybrid model is suggested in [95] where granulopoiesis is described by ordinary differential equations and stem cell organization by an individual based model.

In this work we consider another type of hybrid models coupling discrete and continuous approaches at the level of each cell. The difference with the preceding works [36] is that ODE are not used to describe cell concentrations of cells but concentrations of proteins inside each individual cell. From this point of view this work can be related to the individual based model in [95]. In our model, cell fate is determined by the combination of discrete and continuous models. Global and local regulation acts at the level of individual cells and not for the whole cell population.

All the previously mentioned approaches did not consider spatial aspects of hematopoiesis. Cellular regulation by cell-cell interaction was neither considered in these models. Multi-scale approaches include both cell population kinetics [24] or erythroid progenitor dynamics [57, 55] and intracellular regulatory networks dynamics in the models [19] in order to give insight in the mechanisms involved in erythropoiesis. Off-lattice discrete-continuous hybrid models, applied to the erythropoiesis modeling, allow to take into account simultaneously interactions at the cell population level, regulation at the intracellular and extracellular levels and to study an importance of the spatial structure [98, 23]. The role of macrophage in stabilizing of erythroblastic island is investigated in [70]. Indeed, macrophages produce

21

growth factors (GF) that influence the fate of cell. According to the distance between cells and macrophage, the quantity of GF received by cells vary.

Multi-scale hybrid model consists in the coupling of two models, with different space and time scales. Such discrete-continuous models are usually called hybrid models [24, 114, 118]. Hybrid discrete-continuous models are widely used in the investigation of dynamics of cell populations in biological tissues and organisms that involve processes at different scales. In this approach biological cells are considered as discrete objects described either by cellular automata ([66], [78], [88], [108], [136], [145]) or by various on-lattice or off-lattice models ([64], [87], [120]) while intracellular and extracellular concentrations are described with continuous models, ordinary or partial differential equations.

1.2.2   Multi-scale hybrid discrete-continuous model

Hybrid models can be based on cellular automata and other lattice models and off-lattice models where cell position in space is not restricted to the nodes of a grid. In cellular automaton model each individual cell can be represented as a single site of lattice, as several connected lattice sites or the lattice site can be larger than an individual cell. A generalized cellular automaton approach is presented by the cellular Potts models (CPM). The CPM is a more sophisticated cellular automaton that describes individual cells, occupying multiple lattice sites, as extended objects of variable shapes. These models take into account surface energy of cell membrane. The CPM effective energy can control cell behaviors including cell adhesion, signalling, volume and surface area or even chemotaxis, elongation and haptotaxis [78], [136]. In each particular CA model, the rules which determine cell motion should be specified. It can be influenced by the interaction of cells with the elements of their immediate surrounding and by processes that involve cellular response to external signals like chemotaxis. The numerous models with gradient fields of chemical concentrations that govern motility of cells have been suggested. Cellular automaton have been used extensively to model a wide range of problems. Different stages of tumor development from initial avascular phase([66], [88]) to invasion ([11]) and angiogenesis ([108], [145]) are studied.

Off-lattice models are important to those biological situations in which the shape of individual cells can influence the dynamics or geometry of the whole population of cells. In off-lattice models, shape of cells can be explicitly modelled and response to local mechanical forces, interaction with neighboring cells and environment can be investigated. Hybrid off-lattice models, not limited in possible directions of cell motion, are widely applied to the modeling of tumor growth and invasion where cell migration should be taken into account ([87], [120]). Another type of off-lattice models, called fluid-based elastic cell model, approach that takes into account cell elasticity, is also applied in tumor growth modeling ([11], [64]).

1.3 Main results of the thesis

The thesis is devoted to mathematical modeling of hematopoiesis and blood diseases. We develop hybrid discrete-continuous models and apply them to study erythropoiesis and lineage choice. We will also use them to model two diseases, lymphoma and myeloma. The last chapter of the thesis is devoted to the analysis of solutions of reaction-diffusion equations which describe Darwinian evolution of cancer cells.

1.3.1 Methods of modeling

A hybrid modeling approach with off-lattice cell dynamics is used in order to study hematopoiesis. Cells will be considered as discrete objects while intracellular and extracellular concentrations will be described with ordinary and partial differential equations. This model will be applied to study the lineage choice of megakaryocytic-erythroid bipotent progenitors, functioning of erythroblastic islands in erythropoiesis and some blood diseases (lymphoma, multiple myeloma).

Intracellular regulation

Cell fate is determined by specific cellular proteins $P_1, ..., P_k$ whose concentrations (or biologic activities) are described by ordinary differential equations :

$$\frac{dP_j}{dt} = \Phi_j(P), \ \ j = 1, ..., k, \tag{1.3.1}$$

where Φ_j are the rates of their production or activation. These proteins will be specified below for intracellular regulation of megakaryocytic-erythroid progenitors and of erythroid progenitors.

Depending on the values of these intracellular proteins, the cell will self-renew, differentiate or die by apoptosis. Precise conditions that determine cell fate will be specified below for each particular application. It should be noted that cell fate depends also on the extracellular regulation, that is on nutrients, hormones, growth factors in the extracellular

$$\frac{\partial c}{\partial t} = d\Delta c - nc + nG(p)$$

cell motion

$$\ddot{x} + \mu \dot{x} + H(\nabla n, c) = 0$$

extra-cellular matrix

cell division, differentiation, death

$$\frac{dp}{dt} = F(p, c)$$

intracellular networks
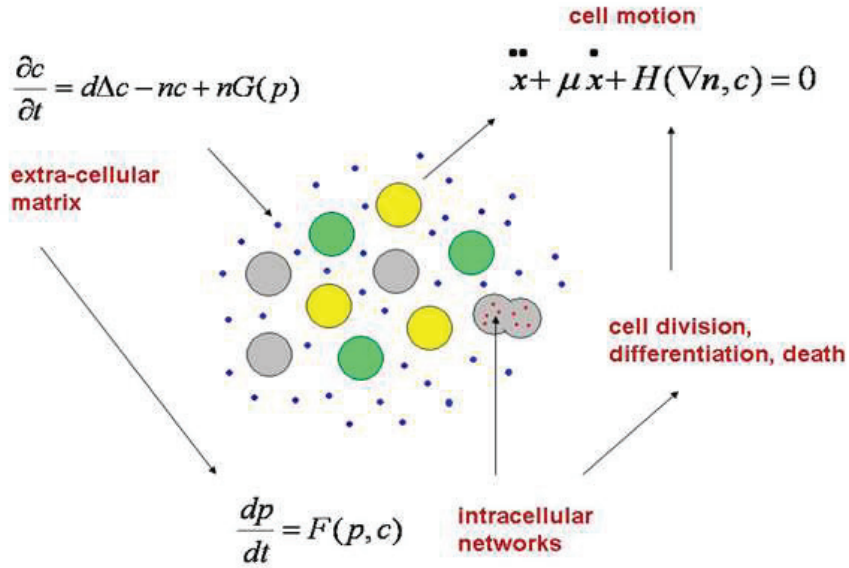
Figure 1.5: Schematic representation of hybrid models. Cells are considered as individual objects. Circles of different colors correspond to different cell types. Intracellular concentrations described by ordinary differential equations determine cell fate. Extracellular substances described by partial differential equations can influence the intracellular regulation. Cells can move due to mechanical forces acting from other cells or because of some other factors.

matrix. These substances can influence the intracellular regulation. Therefore instead of equations (1.3.1) we should consider the equations

$$\frac{dP_i(t)}{dt} = \Phi_i(P(t), \nu(x_i, t)), \quad j = 1, ..., k, \tag{1.3.2}$$

where ν is a vector of extra-cellular concentrations taken at the center $x_i(t)$ of the cell.

Extracellular regulation

The concentrations of the species in the extra-cellular matrix are described by the reaction-diffusion system of equations

$$\frac{\partial \nu}{\partial t} = D \, \Delta \nu + G(\nu, c), \tag{1.3.3}$$

where c is the local cell density, G is the rate of consumption or production of these substances by cells. These species can be either nutrients coming from outside and consumed by cells or some other bio-chemical products consumed or produced by cells. During erythropoiesis, erythroid cells produce Fas-Ligand F_L, which influences the surrounding cells by increasing intracellular Fas activity. The Fas-ligand-producing erythroid cells are mainly immature erythroblasts in murine erythropoiesis [100] and mainly the mature erythroblasts in human erythropoiesis [107]. On the other hand, macrophages produce a growth factor G, which stimulates erythroid cell proliferation. In mice, G is KL/SCF in normal erythropoiesis and BMP4 in stress erythropoiesis. The concentrations of Fas-ligand and of the growth factor in the extracellular matrix are described by the reaction-diffusion equations :

$$\frac{\partial F_L}{\partial t} = D_1 \Delta F_L + W_1 - \sigma_1 F_L, \tag{1.3.4}$$

$$\frac{\partial G}{\partial t} = D_2 \Delta G + W_2 - \sigma_2 G. \tag{1.3.5}$$

Here D_1, D_2 are diffusion coefficients and W_1, W_2 are the rates of production of the corresponding factors. These functions are proportional to the concentrations of the corresponding cells.

In numerical simulations, equations (1.3.4), (1.3.5) are solved by a finite difference method with Thomas algorithm and alternative direction method. Neumann (no-flux) boundary conditions are considered at the boundary of the rectangular domain. Constant space and time steps are used.

The source terms W_1 and W_2 are piece-wise constant functions different from zero at the location of the corresponding cells. Let us explain the definition of these functions with the example of the function W_1 in equation (1.3.4). Consider a cell that produces Fas-ligand. It is shown as a circle in Figure 1.6. For each mesh point ij we consider the grid cells adjacent to this point. Denote by S_{ij} the area of the biological cell inside these numerical cells (grey cells in Figure 1.6). Then the value of the source term in the mesh point ij is written as
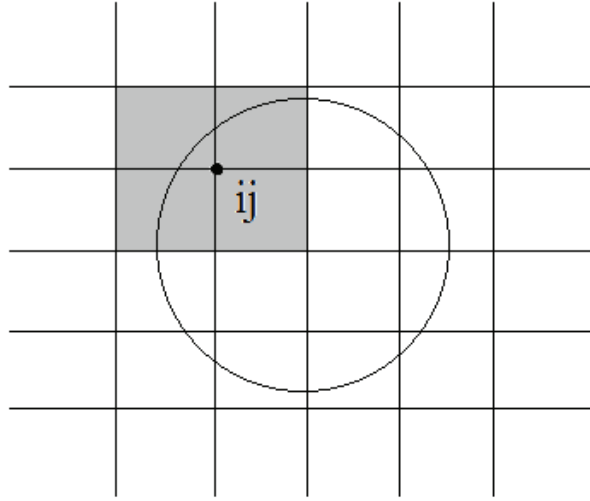
Figure 1.6: Schematic representation of a cell on the numerical grid.

follows: $W_1^{ij} = w_1^0 S_{ij}/(4s)$, where w_1^0 is a constant which measures the normalized intensity of Fas-ligand production, s is the area of the numerical cell. For example, if the grid point ij is inside the biological cell together with all four numerical cells around it, then $W_1^{ij} = w_1^0$.

When the concentrations of various substances in the extracellular matrix are found, we can use them in the equations (1.3.2) for the intracellular concentrations. If cell size is sufficiently small in the length scale determined by the gradients of extracellular concentrations, then the variation of these concentration at the cell size is small. Therefore we use the values of extracellular concentrations at the cell center. These values are found from their values at the grid points by interpolation.

Movement of cells

Since cells divide and increase their number, they can push each other resulting in cell displacement. In order to describe mechanical interaction between cells, we restrict ourselves to the simplest model where cells are presented as elastic spheres. Consider two elastic spheres with centers at the points x_1 and x_2 and with the radii, respectively, r_1 and r_2. If

the distance h_{12} between the center is less than the sum of the radii, $r_1 + r_2$, then there is a repulsive force between them, f_{12}, which depends on the difference between $(r_1 + r_2)$ and h_{12}. If a particle with center at x_i is surrounded by several other particles with centers at the points $x_j, j = 1, ...k$, then we consider the pairwise forces f_{ij} assuming that they are independent of each other. This assumption corresponds to small deformation of the particles. Hence, we find the total force F_i acting on the i-th particle from other particles, $F_i = \sum_i f_{ij}$. The motion of the particles can now be described as the motion of their centers by Newton's second law

$$m\ddot{x}_i + m\mu\dot{x}_i - \sum_{j \neq i} f_{ij} = 0,$$

where m is the mass of the particle, the second term in the left-hand side describes the friction by the surrounding medium, and the third term is the potential force between cells. We consider the force between particles in the following form

$$f_{ij} = \begin{cases} K \frac{h_0 - h_{ij}}{h_{ij} - (h_0 - h_1)} & , & h_0 - h_i < h_{ij} < h_0 \\ 0 & , & h_{ij} \geq h_0 \end{cases},$$

where h_{ij} is the distance between the particles i and j, h_0 is the sum of cell radii, K is a positive parameter, and h_1 accounts for the incompressible part of each cell. This means that the internal part of the cell is incompressible. It allows us to control compressibility of the medium. The force between the particles tends to infinity when h_{ij} decreases to h_0-h_1.

When a cell center crosses the boundary of computational domain, it is removed from the simulations. Under some conditions, cells can also be removed even if they are inside the computational domain. In particular, in the case of cell death or, in the case of blood cells in the bone marrow, if they leave bone marrow into the blood flow. When a new cell appears, we prescribe it initial position and initial velocity.

Cell properties and division

Biological cells considered in hybrid models are characterized by certain parameters such as their type, duration of cell cycle, initial radius and initial values of intracellular proteins. These values are given to each cell at the moment of its birth. Some other cell properties are variable and they can change during it life time. In particular, cell age, radius, position and current values of intracellular proteins. These values are recalculated at every time step.

Some of cell properties can be given as random variables. For example, duration of cell cycle is considered as a random variable with a uniform distribution in the interval $[T - \delta T, T + \delta T]$. Initial protein concentrations can also be considered as random variables in some given range.

Cell fate is determined at the end of cell cycle. At the first stage, they make a choice between apoptosis and survival. If they survive and divide, they make a choice between self-renewal and differentiation. In both cases, the choice is determined by the values of intracellular proteins.

During cell cycle, cell radius grows linearly. It becomes twice the initial radius at the end of cell cycle. Then mother cell is replaced by two daughter cells. Geometrically, two circles with the initial radius are located inside the circle with twice larger radius. The direction of cell division, that is the direction of the line connecting the centers of daughter cells, is random. This is specific for cell division in hematopoiesis. In some other applications, direction of cell division can be prescribed.

Let us also note, that cell volume in the model is not preserved after division. The total volume of the daughter cells is twice less than the volume of the mother cell before its division. Since cells in the bone marrow are sufficiently sparse, preservation of their volume during division is not essential. It can be important in some other applications where cell density is large and the forces acting between cells should be found more accurately.

1.3.2 Hematopoiesis

Hematopoiesis is a complex process that begins with hematopoietic stem cells and results in production of erythrocytes, platelets and leucocytes. This process is controlled by numerous local and global regulatory mechanisms. If some of them do not function properly, various blood diseases can appear. In particular, excessive proliferation of immature cells can lead to leukemia and other malignant diseases.

In this work we will study erythroid lineage of erythropoiesis beginning with lineage choice and then its further progression till mature erythrocytes in the blood flow. We will see that this process is tightly regulated by intracellular proteins, growth factors in the extracellular matrix and hormones.

Lineage choice

We begin to model hematopoiesis with a lineage choice of bipotent megakaryocytic-erythroid progenitor (MEP). In this model, cell-cell interaction can be neglected, and extracellular regulation is not included.

In Section 2.1, we will continue to develop the hybrid model of erythropoiesis. It couples cell dynamics with intracellular and extracellular regulations. It is important to emphasize that we do not impose cell fate as a given parameter (deterministic or stochastic) as it is conventionally done in cell population dynamics. Cell fate is determined by intracellular regulation of protein concentrations and by its environment.

The study of erythropoiesis begins with differentiation of megakaryocytic-erythroid progenitors (MEP) into one of two lineages, BFU-E and BFU-MK. Intracellular regulation of MEP cells is based on the transcription factor GATA-1 and proteins FLI-1 and EKLF. We will show how this regulation determines the lineage choice and the proportion of two types of differentiated cells, BFU-E (burst forming unit erythroid) and BFU-MK (burst forming units-megakaryocytic). The former are engaged in the erythroid lineages, the latter lead to the appearance of platelets.

We will also investigate the role of stochasticity in the intracellular regulation. Random

variations in the initial intracellular concentrations of newly born cells will determine their choice between self-renewal and differentiation. In the case of immature cells MEP, random initial concentrations of intracellular proteins determine their further development and the choice between two lineages. In the case of deterministic initial conditions all cells will have the same fate, and lineage choice cannot be described.

Thus, in this section we have developed hybrid model of MEP cell choice between two lineages, erythroid and megakaryocytic. We have shown how the intracellular regulation based on GATA-1, FLI-1 and EKLF and random initial concentrations of intracellular proteins determine cell fate and proportion of cells of two different lineages.

Erythropoiesis

Production of red blood cells in the bone marrow occurs in small units called erythroblastic islands. They consist of a central macrophage surrounded by erythroid cells with various levels of maturity. Their number can vary from several up to about 30 cells. Some of the erythroid cells produce Fas-ligand that influences the surrounding cells by increasing intracellular Fas activity.

In order to describe erythropoiesis, we use hybrid discrete-continuous models where cells can divide, differentiate, die by apoptosis, move and interact mechanically with each other.

We consider a simplified model of molecular network that integrates multiple microenvironmental influences within the erythroblastic island with those of circulating regulators of erythropoiesis, such as EPO and glucocorticosteroids.

We compare erythropoiesis in mice and in humans. Our modeling results predict a more rapid recovery from acute anemia by mice compared to humans due to the more central location in murine erythroblastic islands of the main producers of Fas-ligand, the early stage-erythroblasts, as compared to the more peripheral location in human erythroblastic islands of the main producers of Fas-ligand, the late-stage erythroblasts. This prediction was confirmed by *in vivo* experimental evidence and clinical observations. Results are also consistent with experiments demonstrating enhanced proliferation *in vitro* of those erythroid

31

(a) in mice   (b) in human
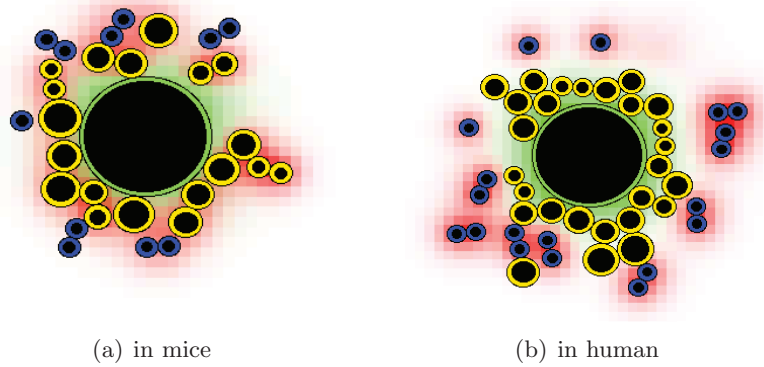
Figure 1.7: Typical structure of an erythroblastic island in the simulations : Fas-ligand produced by early-stage erythroblasts (left) or by late-stage erythroblasts (right). The large cell in the center is a macrophage, yellow cells - CFU-E/Pro-EBs and differentiating erythroblasts, blue - late-stage mature erythroblasts and reticulocytes, level of green - concentration of the growth factor (G) produced by the macrophage, level of red - concentration of Fas-ligand. Black circles inside cells show their incompressible parts.

cells that are most closely associated physically with central macrophages.

Thus, in this section we have developed hybrid model of erythropoiesis. We describe its functioning in normal and stress (anemia) conditions. We obtain a good description of experimental results and of clinical data. We also show that central macrophage is necessary to stabilize erythroblastic islands. Multiple islands without macrophage are unstable and cannot be stabilized by the hormone erythropoietin. On the other hand, erythroblastic islands with macrophages show a stable and robust behavior in a wide range of parameters. Finally, we modeled erythropoiesis in mice and in humans and explained the difference between them. This difference shows that in some cases murine erythropoiesis cannot be used as a biological model of human erythropoiesis.

1.3.3 Blood diseases

Myeloma

Multiple myeloma (MM) is a relatively common disease that is characterized by bone marrow infiltration with malignant plasma cells and, very frequently it leads to a malignancy-

associated chronic anemia. Multiple myeloma cells proliferate and form a tumor that grows and gradually fills the whole space. When it arrives to erythroblastic islands, it destroys them by the direct mechanical contact. Moreover, malignant cells produce Fas-ligand and TRAIL protein which stimulate apoptosis of erythroid progenitors.

(a) (b)
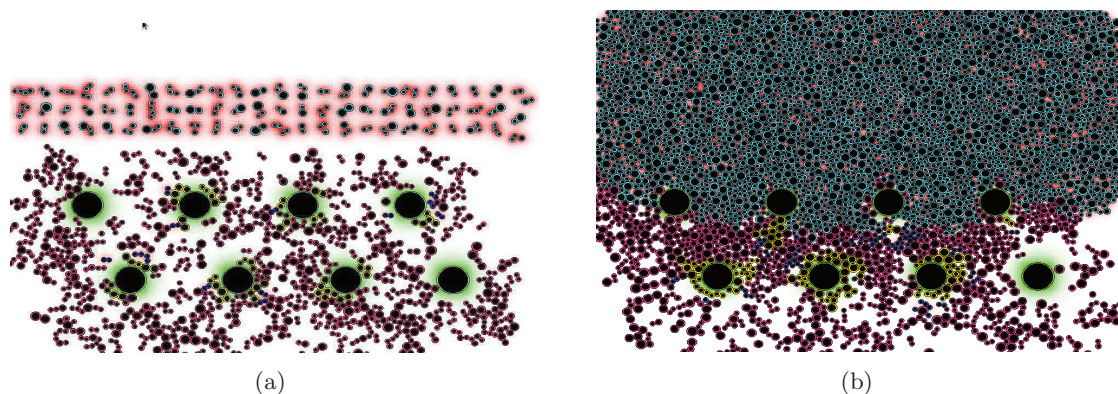
Figure 1.8: Left: erythroblastic islands (at the bottom of the picture), cancer cells (at the top of the picture). Right: disappearance of erythroblastic islands due to the invasion of cancer cells.

In order to model multiple myeloma, we use the model of normal erythropoiesis described above. Moreover, we introduce in the model malignant cells that do not differentiate and do not die by apoptosis. They proliferate and produce Fas-ligand stimulating apoptosis of normal erythroid cells. As a consequence, the normal structure of erythroblastic island is destroyed by mechanical action of tumors and by apoptosis induced by myeloma cells.

One of the consequences of the disease is the destruction of erythroblastic islands and appearance of severe anemia. The organisms tries to resist producing hormone erythropoietin that stimulates production of red blood cells. Treatment with additional erythropoietin can also be considered. In the model, action of erythropoietin is taken into account through the critical level of intracellular protein Fas which determines apoptosis of erythroid progenitors. Erythropoietin increases this critical level and more erythroid progenitors survive resulting in the increased production of erythrocytes.

Thus, we suggest a model of multiple myeloma. We show how it develops and influences

functioning of erythropoiesis. It leads to the development of anemia that can be partially compensated by treatment with hormone erythropoietin.

Lymphoma

Lymphoma is a disease characterized by the appearance of tumor in the thymus, an organ located in the thorax. The volume of the tumor increases and provokes important respiratory difficulties. We study lymphoma development in children and its treatment by chemotherapy. Patients are treated during two years, though according to some estimates, patients can be over-treated. The purpose of this simulation is to study the number of relapses as a function of the duration of treatment and of the doses of drugs, mainly purinethol and methotrexate.

In order to study lymphoma, we begin with modeling of healthy thymus. The model is based on the same approach as we used before to model normal erythropoiesis and multiple myeloma. Cells are considered as individual objects. Their fate is determined by the intracellular regulation and it is influenced by growth factors produced bo other cells.

In Section 3.2, we will model T cells formation in the thymus containing precursors, double negative (DN), double positive (DP) and simple positive (SP) cells. After differentiation, these cells give rise to T lymphocytes. The proportions of each kind of cells remain approximately constant in a healthy individual. Thymus provide a constant T cells production compensating apoptosis. In simulations, apoptosis is modeled by a probability of remaining alive for each cell type. Nurse cells produce growth factor which promotes self-renewal of thymocytes. The thymocytes located sufficiently far from the nurse cells will differentiate else they will self renew.

A single mutated cell begins to proliferate and causes tumor. Malignant cells self-renew at the end of each cell cycle with a given probability. They grow exponentially and invade the thymus and push out normal cells.

The action of chemotherapy on thymus is simulated by intracellular drug concentration given by physiologically based pharmacokinetic model (PBPK) in time, for various values of

parameters. If the intracellular drug concentration reaches some critical level at the end of cell cycle, then the cell dies. Malignant cells are gradually eliminated, the tumor disappears, precursors enter the thymus and recreate its normal structure.

We simulated maintenance treatment and analyzed the number of relapses as a function of duration of treatment. The results of the simulations correspond to the database EuroLB. They show that the duration of treatment can be reduced from 24 month, as it is the case in clinical practice, to 12 month with the same proportion of relapses.

Resistance to treatment. We study the resistance to treatment in the case of lymphoma. Let us recall that malignant cells die if the intracellular concentration of drug reaches some critical level p_c. This value can be different in different cells. Hence different cells have different sensibility to treatment. On the other hand, we assume that when lymphoma cells divide, daughter cells can have different values of p_c in comparison with the mother cell. Since cells with a larger value p_c have a better probability to survive, then more and more resistent cells will emerge in the process of treatment.

In the study of lymphoma, we have developed a hybrid model which describes normal functioning of thymus and the development of the disease. We model treatment of lymphoma and analyze the response of virtual patients to treatment. We show that the duration of treatment can possibly be reduced with the same proportion of relapses. Finally, we model the development of the resistance to treatment.

1.3.4 Existence and dynamics of pulses

Biological cells can be characterized by their genotype. Cells of the same type have a localized density distribution in the space of genotypes. This distribution can evolve under the influence of various external factors. In particular cancer cells can adapt to chemotherapy treatment resulting in appearance of resistant clones. This process is called Darwinian evolution of cancer cells [27]. We studied above the emergence of resistance with hybrid discrete-continuous models in the case of lymphoma treatment. In this chapter we analyze

this process with reaction-diffusion equations. We will consider the scalar reaction-diffusion equation

$$\frac{\partial u}{\partial t} = D \frac{\partial^2 u}{\partial x^2} + F(u, x), \tag{1.3.6}$$

on the whole axis. The typical example of the nonlinearity is given by the function

$$F(u, x) = u^k(1 - u) - \sigma(x)u, \tag{1.3.7}$$

where the first term describe the rate of cell birth and the second term the rate of their death. Let us note that the space variable x here corresponds to cell genotype, $u(x, t)$ is the cell density which depends on x and on time t. The diffusion term describe variation of genotype due to mutations, the mortality term depends on the space variable, that is on cell genotype.

Monostable case

If $k = 1$ and $\sigma(x) = const$, then this equation does not have localized stationary solutions. In order to describe cell populations with localized genotype which correspond to certain cell type, we need to introduce space dependent mortality coefficients. This means that cells can survive only in a certain range of genotypes (survival gap).

Consider now cell population dynamics if there are two survival gaps, that is two intervals of genotype where cells can survive. We will consider the model with global consumption of resources where all cells consume the same nutrients and their quantity is limited. In this case, the function F in (2.2.20) is replaced by the functional

$$F(u, x, J(u)) = u^k(1 - J(u)) - \sigma(x)u, \quad J(u) = \int_{-\infty}^{\infty} u(y, t)dy.$$

Hence we consider a nonlocal reaction-diffusion equation.

Suppose that initially all cells are located in the first survival gap (Figure 1.9). If we increase the mortality coefficient there, then this cell population disappears. Instead of

it, another cell population appears in the second gap. This behavior can be explained as follows. Cells located in the first survival gap consume all nutrients and do not allow cells in the second gap (which are present because of mutations) to proliferate. When cells from the first gap are removed, nutrients become available and cells in the second gap proliferate restoring a similar population with another genotype. This is one of possible mechanisms of emergence of cell clones resistant to chemotherapy in the process of treatment.
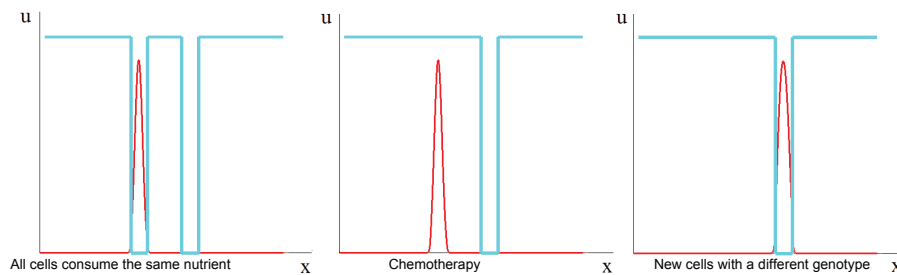
Figure 1.9: Development of the resistance to treatment. In the beginning all cells are located in the first survival gap. They do not appear in the other one because they do not have enough nutrients. If cells in the first survival gap are eliminated by chemotherapy, then more resistent cells in the second survival gap will appear.

Bistable case

Cancer cells can accelerate their proliferation due to cell-cell interaction. In this case the proliferation rate is proportional to u^k with $k > 1$ and not with $k = 1$ considered above. Then we obtain a bistable equation. This equation has stable stationary pulses even in the case where $\sigma(x) \equiv const$. In this case, pulse solutions can easily be constructed analytically. However if the function $\sigma(x)$ is not constant, then this simple analytical construction is not applicable. We study the existence of pulse solutions of this equation in Chapter 4.

We use the the Leray-Schauder method based on topological degree and a priori estimates of solutions. It should be notes that the classical degree construction for elliptic problems in bounded domains is not applicable here since we consider the problem on the whole axis. We apply the degree construction for Fredholm and proper operators with the index zero. Therefore we need to study the properties of the corresponding operators. The

main difficulty of the application of the Leray-Schauder method is related to a priori estimates of solutions. We develop a special approach which allows us to obtain the estimates in weighted Hölder spaces which are introduced in order to define the degree. The following theorem is proved.

Theorem. *If the function $F(w, x)$ satisfies conditions:*

$$F(0, x) = 0, \quad x \geq 0; \quad \frac{\partial F(w, x)}{\partial x} < 0, \quad w > 0, \quad x \geq 0$$

$$F(w, x) < 0, \quad \forall x \geq 0, w > w_+.$$

and the function $F_+(w)$ satisfies conditions:

$$F'_+(0) < 0, \quad F_+(w) < 0 \ \text{for} \ w > w_+$$

$$\int_0^{w_0} F_+(u)du = 0, \quad \int_0^w F_+(u)du \neq 0 \ \forall w \in (0, w_+), w \neq w_0.$$

then the problem

$$w'' + F(w, x) = 0, \quad w'(0) = 0$$

on the half-axis $x > 0$ has a positive monotonically decreasing solution vanishing at infinity. It belongs to the weighted Hölder space E_1.

This theorem affirms the existence of solutions on the half-axis. The existence of pulse solutions on the whole axis can be now obtained by symmetry. We also use this result to prove the existence of pulse solutions for the corresponding nonlocal reaction-diffusion equation.

In the case of time dependent problem, if the mortality rate depends on the genotype, $\sigma = \sigma(x)$, then the pulse will move in the direction where this function is less. In this

case we have a gradual change of cell genotype due to small mutations. This evolution will also lead to the emergence of cell clones better adapted to treatment. Thus, there are two different mechanisms of cell evolution. In one of them, cell genotype can have large changes, jumps to other survival gaps ($k = 1$), in the other one these changes are continuous.

Analyzing the reaction-diffusion equations, we proved the existence of pulse solutions for local and nonlocal reaction-diffusion equations. We suggested two possible mechanisms of the resistance to treatment. These mechanisms are based on the evolution of cancer cells in the space of genotypes and on survival of more adapted cells.

Chapter 2

Hematopoiesis

2.1 Lineage choice

2.1.1 Introduction

In this section, we discuss intracellular regulation of bipotent MEP (megakaryocytic-erythroid progenitor) between thrombocytic and erythroid lineage. MEP can differentiate into BFU-E (burst forming unit erythroid) progenitors or BFU-MK (burst forming units-megakaryocytic) progenitors or self-renew in order to give rise to the two lineages of blood cells.

The 'hybrid' model that couples two relevant scales, intracellular protein regulation with extracellular matrix is used to model lineage choice. An intracellular regulation of progenitors allows to simulate this choice. Cell-cell interaction can be neglected, and the model does not include extracellular regulation. Cell movement and their spatial position play an important role in cell's decision between self-renewal, differentiation and apoptosis based on intracellular protein concentrations. We have performed numerical simulations to model the behavior of MEP and we obtained all the expected behavior (appearance of two lineages) concerning the commitment of progenitors by changing the parameters of equations of an hybrid model.

2.1.2   Intracellular regulation

The complex mechanism that induces commitment of MEP is not completely understood but the role of some growth factors and transcription factors has been established. Indeed, the erythroid transcription factor (zinc finger factor) GATA-1 is required for the differentiation and maturation of erythroid/megakaryocytic cells [38]. Endogenous EKLF (erythroid Kruppel-like factor) promotes the erythroid lineage choice while FLI-1 (Friend Leukemia Integration 1) overexpression inhibits erythroid differentiation [38]. Interactions between FLI-1 and EKLF are also involved [38], EKLF represses FLI-1 [72, 30, 144].

We will take into account intracellular regulation of MEP with GATA-1 and transcription factors FLI-1 and EKLF. We assumed that distribution of hormones Epo and Tpo is uniform in the bone marrow. Moreover according to biological observations there is no communication between these cells. Therefore extracellular regulation is not present in this model.

Let u be the concentration of the transcription factor EKLF, v the concentration of FLI-1 and w of GATA-1. FLI-1 can form complexes with the other two factors. We will denote them by $[uv]$ and $[vw]$. Then the intracellular regulation can be described as follows:

$$u + w \underset{k_1^-}{\overset{k_1^+}{\longleftrightarrow}} [uw], \quad [uw] \overset{k_2}{\longrightarrow} n_1 u, \quad v + w \underset{k_3^-}{\overset{k_3^+}{\longleftrightarrow}} [vw], \quad [vw] \overset{k_4}{\longrightarrow} n_2 v.$$
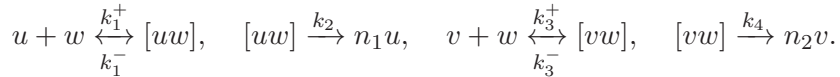
Taking into account the mass balance $w + [uw] + [vw] = w_0$, we obtain the system of equations for these concentrations:

$$\frac{du}{dt} = -k_1^+ u(w_0 - [uw] - [vw]) + (k_1^- + n_1 k_2)[uw], \tag{2.1.1}$$

$$\frac{dv}{dt} = -k_3^+ v(w_0 - [uw] - [vw]) + (k_3^- + n_2 k_4)[vw], \tag{2.1.2}$$

$$\frac{d[uw]}{dt} = k_1^+ u(w_0 - [uw] - [vw]) - k_1^- [uw], \tag{2.1.3}$$

$$\frac{d[vw]}{dt} = k_3^+ v(w_0 - [uw] - [vw]) - k_3^- [vw]. \tag{2.1.4}$$

Intracellular regulation described by this system of equations should be completed by conditions of self-renewal of the progenitors or their commitment to one of the two lineages. We will suppose that if concentrations of FLI-1 and EKLF are less than some critical values at the end of cell cycle, then differentiation does not hold and the cell self-renews. If at least one of these two concentrations is greater than the critical level, then the cell differentiates. In this case, it becomes BFU-MK if the concentration of FLI-1 is greater than the concentration of EKLF, and it becomes BFU-E otherwise (Figure 2.1).

In this model, transcription factors FLI-1 and EKLF influence the commitment of progenitors in a MEP cell lineage with the following rules (cf. Figure: 2.1):

- If $[\text{FLI-1}] < [\text{FLI-1}]_{crit}$ and $[\text{EKLF}] < [\text{EKLF}]_{crit}$ then self-renewal.

- If $[\text{FLI-1}] > [\text{FLI-1}]_{crit}$ and $[\text{EKLF}] < [\text{EKLF}]_{crit}$ then BFU-MK production.

- If $[\text{FLI-1}] < [\text{FLI-1}]_{crit}$ and $[\text{EKLF}] > [\text{EKLF}]_{crit}$ then BFU-E production.

- If $[\text{FLI-1}] > [\text{FLI-1}]_{crit}$, $[\text{EKLF}] > [\text{EKLF}]_{crit}$ and $[\text{FLI-1}] > [\text{EKLF}]$ then BFU-MK production else $[\text{FLI-1}] < [\text{EKLF}]$ BFU-E production.

Lineage choice by MEP depends on the different parameters and on the initial conditions of GATA-1, FLI-1 and EKLF. Two behaviors of bipotent MEP can be observed. The statement of rules, given above, which determine MEP fate according to intracellular concentrations is summarized in the figure 2.1.
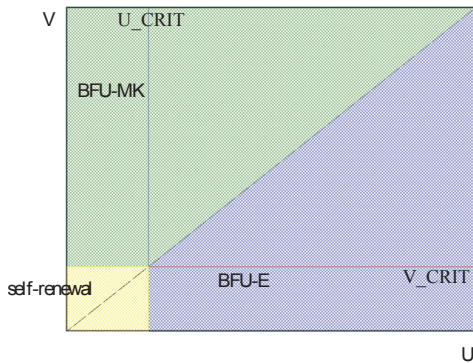
Figure 2.1: Phase space: concentration u on x-axis, v on y-axis. If the concentrations at the end of cell cycle are as the coordinate point belongs to yellow region, the considered cell self-renews. In blue region, the cell differentiates into BFU-E. In green region, the cell differentiates into BFU-MK. Cell fate depends on the concentrations u and v.

2.1.3 Results

We carry out numerical simulations of the model presented in the previous section. Cell cycle duration is taken to be 12 hours with a random perturbation uniformly distributed between 0 and 7 hours. Initial concentrations are equal to a random value between 0 and 0.05 for u and v, and between 0 and 0.09 for w. Initial concentrations of $[uw]$ and $[vw]$ are equal to zero. Daughter cells have the same values of intracellular concentrations as mothers cells at the moment of cell division. The critical values of u and v, for which differentiation occurs, are taken equal 0.2.

Figures 3.11, 3.15 and 2.4 show the results of numerical simulations. In subfigures (a) we present evolution of intracellular concentrations u and v in time in 10 different cells. These concentrations determine the cell fate according to Figure 2.1. The initial concentration of u and v in each cell is randomly distributed in the square $[0, 0.05] \times [0, 0.05]$. Subfigures (b) and (c) show snapshots of cell populations and the evolution of cell number in time.

(a) Concentrations u and v in 10 cells

(b) Snapshot of cell population

(c) Number of MEP (red) and BFU-MK (green) cells as a function of time
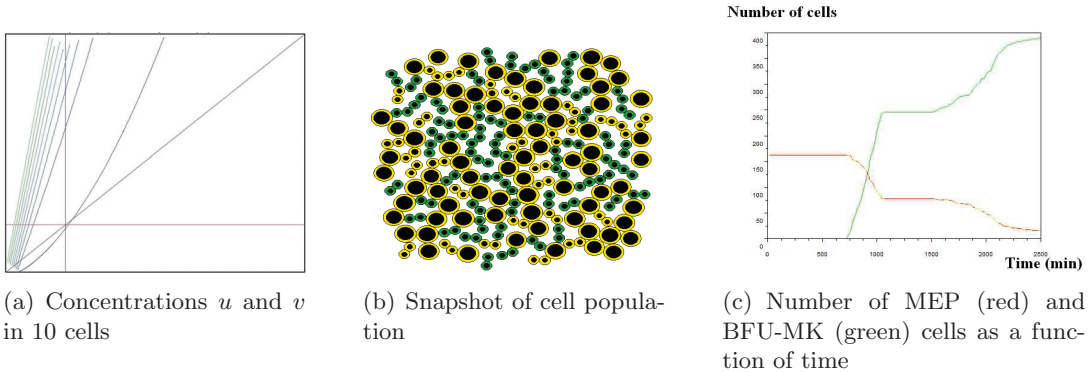
Figure 2.2: Evolution of the population of MEP cells for the values of parameters $k_1^+ = 0.005$, $k_1^- = 0.008$, $k_2 = 0.01$, $k_3^+ = 0.005$, $k_3^- = 0.008$, $k_4 = 0.1$. In Figure 2.2(a), curves of the phase space are majority located above the first bisector. MEP cells self-renew and differentiate into BFU-MK cell lineage as shown in Figure 2.1. The Figures 2.2(b) and 2.2(c) show the evolution towards BFU-MK cells and gradual disappearance of self-renewal.

Depending on the values of parameters, different regimes of cell population dynamics are observed. If production of the intracellular concentration u (EKLF) is slower than of the concentration v (FLI-1), then cells MEP basically differentiate into the BFU-MK

(a) Concentrations u and v in 10 cells

(b) Snapshot of cell population

(c) The same cell population some time later
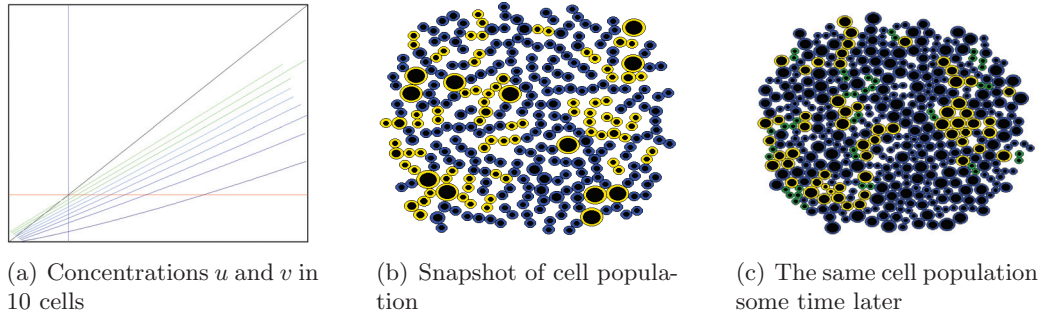
Figure 2.3: Evolution of the population of MEP cells for the values of parameters $k_1^+ = 0.005$, $k_1^- = 0.008$, $k_2 = 0.1$, $k_3^+ = 0.005$, $k_3^- = 0.008$, $k_4 = 0.2$. MEP cells self-renew and differentiate into BFU-E cell lineage. In Figure 2.3(a), curves of the phase space are majority located bellow the first bisector, there is commitment into BFU-E lineage as shown in Figure 2.1. The Figures 2.3(b) and 2.3(c) show the evolution towards BFU-E cells and gradual disappearance of self-renewal.

(a) Concentrations u and v in 10 cells

(b) Snapshot of cell populations

(c) Number of MEP cells (red), BFU-MK (green) and BFU-E (blue) as a function of time
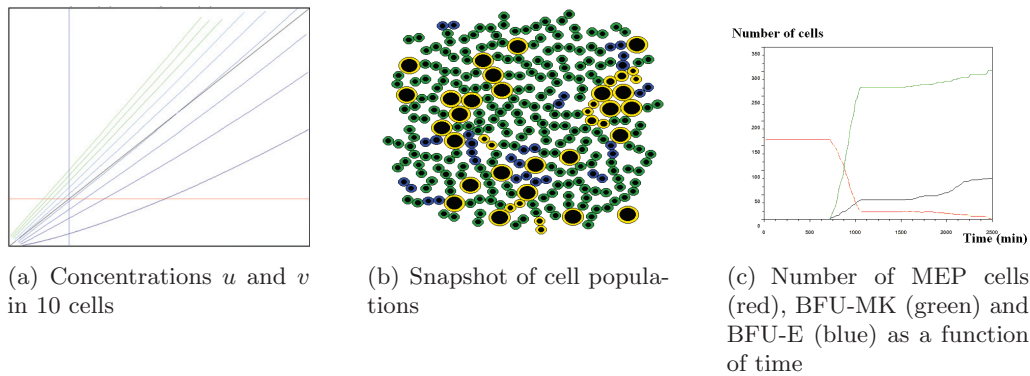
Figure 2.4: Evolution of the population of MEP cells for the values of parameters $k_1^+ = 0.002$, $k_1^- = 0.003$, $k_2 = 0.1$, $k_3^+ = 0.004$, $k_3^- = 0.00329$, $k_4 = 0.1$. Both lineages of differentiated cells BFU-E and BFU-MK are present. In Figure 2.4(a), curves of the phase space are distributed around the first bisector, there is commitment into BFU-E and BFU-MK lineage as shown in Figure 2.1. The Figures 2.4(b) show the coexistence of the three type of cells. Figure 2.4(c) show the evolution towards BFU-E and BFU-MK cells and gradual disappearance of self-renewal.

lineage. There is weak self-renewal observed for the values of parameters in Figure 3.11, and after several cell cycles all cells differentiate. An opposite situation is shown in Figure 3.15 where MEP cells differentiate into BFU-E. As before, the self-renewing activity is weak and after several cell cycles all cells differentiate. For the intermediate values of reaction

rates, both lineages of differentiated cells are present (Figure 3.16). If we decrease the rate of production of the intracellular proteins EKLF and FLI-1, then some of the MEP cells can remain undifferentiated and preserve their self-renewal capacity. Let us also note that the distribution of initial protein concentrations can influence the dynamics of the cell population.

Thus we show how intracellular regulation of MEP cells influence their differentiation in one of the two lineages. The balance between them can be controlled by the hormones EPO stimulating production of erythrocytes and TPO stimulating production of platelets. Their concentrations influence the parameters of the intracellular regulation of the MEP cells and can increase production of one of the two cell types decreasing production of the other one.

2.2 Erythropoiesis

2.2.1 Introduction

The erythroid lineage of hematopoiesis begins with early erythroid progenitors that differentiate into more mature cells, the erythroblasts, which subsequently differentiate into reticulocytes. They leave the bone marrow and enter the bloodstream where they finish their differentiation and become erythrocytes. Erythropoiesis occurs in the bone marrow within small units, called erythroblastic islands. *In vivo*, erythroblastic islands consist of a central macrophages surrounded by erythroid cells of different maturation stage. Progenitor stage of colony-forming units-erythroid (CFU-Es) are situated close to macrophage while reticulocytes are at the periphery of the island [40]. CFU-Es make a choice between three possible fates. They can increase their number without differentiation, differentiate into reticulocytes or die by apoptosis. Complex intracellular protein regulation determines CFU-E fate.

We develop a multi-scale model of erythroblastic islands which takes into account intracellular regulation, cell-cell interaction and extracellular regulation. The intracellular regulation of erythroid progenitors describes the choice between self-renewal, differentiation and apoptosis. Intracellular regulatory mechanisms involved in progenitor cell fate are numerous and not completely known. This is an active area of biological research where new data appear and where there is no clear understanding of the underlying biological mechanisms. Therefore different approaches are possible in describing intracellular regulation.

Three models of intracellular regulation of erythroid progenitors are presented in this chapter. The first model (Section 2.2.2) is suggested in [20]. It is based on the interaction of two proteins: Erk (Extracellular signal-regulated kinases) and Fas. They inhibit each others expression. ERK promotes self-renewal, while Fas controls differentiation and apoptosis.

The second model (Section 2.2.3) takes in count three proteins, Erk, BMP4 (Bone Morphogenetic Protein 4) and Fas. These proteins control differentiation, self-renewal and apoptosis of erythroid progenitors. This model can also be considered as a more general

example applicable in other situations where each of cell fates is controlled by some protein.

According to more recent data, the third model contains four proteins: activated glucocorticosteroid receptor (GR), activated BMPR4 receptor (BMP-R), transcription factor GATA-1 and activated caspases (Section 2.2.4). This model describes intracellular dynamics represented by regulatory networks based on specific protein competition. This intracellular dynamical level, represented by ordinary differential equations, is influenced by extracellular substances represented by partial differential equations. The cell fate depends on its environment, the extracellular regulation and on the intracellular regulation. Stochasticity due to random events (cell cycle duration, orientation of the mitotic spindle at division) and small population effects also plays an important role.

2.2.2 Regulation by proteins Erk and Fas

Intra- and extra- cellular regulation

Recent studies have proposed that there is competition between two key proteins: ERK, which stimulates proliferation without differentiation, and Fas which stimulates differentiation and apoptosis [128]. ERK is involved in a self-renewal loop, while Fas controls differentiation and also triggers cell apoptosis. Fas is activated by extracellular Fas-ligand that is produced by mature erythroblasts and reticulocytes [107]. This regulation demonstrates a bistable behaviour that provides the choice between cell self-renewal and differentiation or apoptosis [62, 55]. One of the most important regulator of erythropoiesis is erythropoietin (EPO), a hormone released by the kidneys in quantities that are inversely proportional to the number of erythrocytes in blood. EPO protects erythroid progenitors from apoptosis through the binding to the erythropoietin receptor (EPO-R) [92].

Based on the current knowledge, in a first model (2.2.2), we decided to focus on a simplified regulatory network based on two proteins, Erk and Fas, responsible respectively for cell self-renewal and proliferation and cell differentiation and apoptosis [107, 128]. These proteins are antagonists: they inhibit each other's expression. They are also subject to external regulation, through feedback loops.

One of these feedback loops is based upon the population of reticulocytes. They produce Fas-ligand which is fixed to their exterior cell membrane. Fas-ligand activates Fas, a transmembrane protein and influences progenitor differentiation and apoptosis. Another feedback control is related to mature erythrocytes in bloodstream. Their quantity determines the release of erythropoietin and other hormones, called growth factors. Erythropoietin is known to inhibit erythroid progenitor apoptosis [92] and to stimulate immature erythroid progenitor self-renewal [61]. Other hormones, like glucocorticoids [62, 55], also increase progenitor self-renewal by activating Erk.

The simplified system of Erk-Fas interactions considered as the main regulatory network for erythroid progenitor fate is then [55]

$$\frac{dE}{dt} = (\alpha(Epo, GF) + \beta E^k)(1 - E) - aE - bEF, \qquad (2.2.5)$$

$$\frac{dF}{dt} = \gamma(F_L)(1 - F) - cEF - dF, \qquad (2.2.6)$$

where E and F denote intracellular normalized levels of Erk and Fas. Equation (2.2.5) describes how Erk level evolves toward maximal value 1 by activation through hormones (function α of erythropoeitin, denoted by Epo, and other growth factors, denoted by G) and self-activation (parameters β and k). In the meantime, Erk is linearly degraded with a rate a and is inhibited by Fas with a rate bF. Equation (2.2.6) is very similar, only there is no proof for Fas self-activation. Fas is however activitated by Fas-ligand, denoted by F_L, through the function $\gamma(F_L)$, it is degraded with a rate d and it is inhibited by Erk with a rate cE. Critical values of Erk and Fas, denoted by E_{cr} and F_{cr}, correspond to self-renewal and apoptosis, respectively, when they are reached. If at the end of the cell cycle intracellular concentrations of Erk and Fas do not reach their critical values, then cell differentiates.

Reticulocytes and erythrocytes (differentiated cells) produce Fas-ligand.

$$\frac{\partial F_L}{\partial t} = D_{F_L}\Delta F_L + W_{F_L} - \sigma_{F_L}F_L, \qquad (2.2.7)$$

48

where $W_{F_L} = k_{F_L} C_{ret}$ is a source term depending on the number of reticulocytes, σ_{F_L} is degradation rate, and D_{F_L} is diffusion rate. If the diffusion coefficient D_{F_L} is sufficiently small, then Fas-ligand is concentrated in a small vicinity of reticulocytes. In this case, Fas-ligand influences erythroid progenitors when they are sufficiently close to reticulocytes.

Results

The goal is to compare results of computations and experimental results. This experimental data gives the increase in the size of the culture erythroid progenitors and the ratio of reticulocytes and erythrocytes (differentiated cells) for six days (cf. experimental data in Table 6.1 and value of parameters in Table 6.7 of Section 6.2).

Biology experience. Biological date were obtained under the following conditions: Normal bone marrow cells were prepared from 19 days old SPAFAS embryos and grown as T2ECs in a medium consisting of α-modification of Eagle's medium (α-MEM) containing 10% FBS (Gibco BRL); 1% normal chicken serum (NCS; Gibco BRL); 10^{-4} M betamercaptoethanol (Sigma); 5 ng/ml TGF-α; 1 ng/ml TGF-β1; 10^{-6} M Dexamethasone and 1 % of a 100 X antibiotics solution(penicillin plus streptomycin; Flow Laboratories) as previously described [75]. T2ECs were induced to differentiate at 10^5 cells/ml by the concomitant removal of TGF-α, TGF-β and Dex from the medium and the addition of 10 ng/ml insulin and of 5% Anemic Chicken Serum (ACS). The differentiation level was assessed by acidic benzidine staining for revealing hemoglobin-containing(mature) cells. The preparation of ACS as well as the estimation of the level of differentiation by acidic benzidine staining have been previously described [74].

Simulation of cells culture. The simulation begins with a culture of 98 progenitors (see Figure 2.5). Behavior of the culture depends on the quantities of Erk and Fas in the cells. At first, these progenitors have low random initial quantities. This small perturbation is made to induce the appearance of the first reticulocytes. If the initial values of Erk and Fas (E_0 and F_0) are equal to 0, only one choice can be observed (differentiation or self-renewal).

49
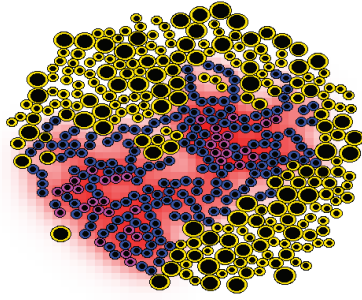
Figure 2.5: Growth of cells culture. After several divisions, progenitors (yellow) become reticulocytes (blue) which produce a growth factor: Fas-ligand (red halo). After one cycle, reticulocytes become erythrocytes (purple): cells do not divide in this model.
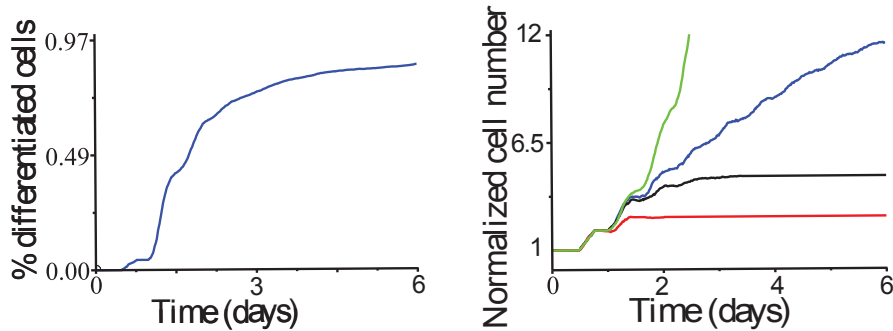
Figure 2.6: Left: proportion of differentiated cells (reticulocytes, erythrocytes) to all cells over time. Right: accumulation of total number of cells. Different curves correspond to different amplitude of stochastic variation of initial activities of ERK and Fas in newly formed cells. Blue curve corresponds to the case where the initial activity of ERK is between 0 and 0.015, Fas between 0 and 0.01, with a uniform probability distribution. Red, black and green curves correspond to σ=0.15, 0.01, 0.007 respectively (see the explanation in the text). Normalized cell number: the ratio of the current cell number to the initial cell number. The initial cell number is 2.10^5 for the experiment and 98 for the numerical simulations. Curves made with the mean of 3 simulations.

Reticulocytes produce a protein Fas-ligand which promotes differentiation and apoptosis.

Comparison between *in vivo* and *in silico* cells culture. The quantities of proteins in the cells are given by the equations (2.2.5)-(2.2.6), so the behavior of the progenitors depends on the parameter values of the system. The most significant are α and γ. For exemple with α=0.000037 all the progenitors choose division, with α=0.000035 all the progenitors choose differentiation after one cycle. To do some comparison between simulation and experimental results, curves of cells number as a function of time are set out.

The evolution of the cells culture is similar *in vitro* experiment and in the calculation.

Almost all the progenitors no longer divide and become reticulocyte. After one cellular cycle, reticulocytes all become erythrocyte.

The role of stochasticity in initial conditions. Curves of Figure 2.6 show the influence of initial conditions. In this simulation, initial quantities of Erk and Fas are randomly distributed between between 0 and c. If c is less than 0.005, each division give only progenitors. If c is between 0.005 and the threshold there is self-renewal and differentiation. If the thresholds are exceeded, it is possible that some or all cells die during the first division. In this case the next generation born of surviving cells was similar behavior to that shown by the curves.

2.2.3 Regulation by proteins, glucocorticoids and transcriptions factors

Extracellular regulation

A population of cells is numerically simulated in a 2D computational domain which is a rectangle. Each cell is a discrete object, an elastic ball, considered to be circular and composed of two parts: a compressible part at the border and a hardly compressible part at the center. All newborn cells have the same radius r_0 and linearly increase in size until the end of their cycle, when they reach twice the initial radius. When a cell divides, it gives birth to two small cells side by side, the direction of division being chosen randomly. From a biological point of view, cell cycle proceeds through G_0/G_1, S, G_2 and M phases. We assume the duration of G_0/G_1 phase is a random variable with a uniform distribution in some given interval [79], other phase durations are supposed to be constant.

Several cell types are computed. Erythroblasts, which are immature erythroid cells, also known as erythroid progenitors. They follow the growth rules explained above and their fate is determined as described in Section 2.2. They either self-renew and give two cells of the same type, or differentiate and give two reticulocytes, or die by apoptosis, depending on their exposition to growth factors and Fas-ligand.

Reticulocytes, are almost mature red blood cells that leave the bone marrow and en-

ter the bloodstream after ejecting their nuclei. In this individual-based model, they are differentiated cells which stay in the bone marrow a little while after being produced, and leave the bone marrow (computational domain) at the end of one cell cycle. Contrarily to erythroblasts, reticulocytes do not have a choice to make, they only express Fas-ligand on their surfaces, thus influencing the development of surrounding erythroblasts.

Organization and modeling of erythropoiesis

Erythropoiesis represents a continuous process maintaining an optimal number of circulating red blood cells and tissue oxygen tension. It occurs mainly in the bone marrow where erythroid progenitors, immature blood cells, which can proliferate and differentiate, undergo a series of transformations to become erythroblasts (mature progenitors) and then reticulocytes which subsequently enter the bloodstream and mature into erythrocytes. At every step of this differentiation process, erythroid cells can die by apoptosis (programmed cell death) or self-renew [73], [75]. Numerous external regulations control cell fate by modifying the activity of intracellular proteins. Erythropoietin (Epo) is a hormone synthesized in the kidney in response of decrease in tissue oxygen level. Epo promotes survival of early erythroblast subsets by negative regulation of their apoptosis through the action on the death receptor Fas [92].

Glucocorticoids [73], [75] and some intracellular autocrine loops [75], [135] induce self-renewal. Previously considered by the authors [55], [70], Erk (from the MAPK family) promoting cell self-renewal inhibits Fas (a TNF family member) [128]. The cell fate depends on the level of these proteins. In addition to global feedbacks, there is a local feedback control through cell-cell interaction, during which Fas-ligand produced by mature cells binds to the membrane protein Fas inducing both differentiation and death by apoptosis [107].

The process of erythroid maturation occurs in erythroblastic islands, the specialized niches of bone marrow, in which erythroblasts surround a central macrophage which influences their proliferation and differentiation [40], [154]. However, erythropoiesis has been mainly studied under the influence of Epo, which can induce differentiation and prolifera-

tion *in vitro* without the presence of the macrophage. Hence, the roles of the macrophage and the erythroblastic island have been more or less neglected.

We will use a hybrid discrete-continuous model developed in [21], [24] in order to bring together intracellular and extracellular levels of erythropoiesis as well as to study the importance of spatial structure of erythroblastic islands in the regulation of erythropoiesis. We focus in particular on the role of the macrophage in erythroid cell proliferation and differentiation and its role in the erythroblastic island robustness. To our knowledge, this is the first attempt to model erythropoiesis by taking these aspects into account. In the previous models [70], [97] it was supposed that Fas-ligand was produced by mature erythroid cells [107]. This assumption corresponds to human erythropoiesis. In this work we study the production of red blood cell in mice taking into account the co-expression of Fas and Fas-ligand by immature erythroid progenitors, particularly in spleen [91].

Erythroblastic islands

Production of red blood cells in the bone marrow occurs in small units called erythroblastic islands. They consist from a central macrophage surrounded by erythroid cells with a various level of maturity. Their number can vary from several cells up to about 30 cells. Some of the erythroid cells produce Fas-ligand which influences the surrounding cells by increasing intracellular Fas activity. These are immature cells in murine erythropoiesis [91] and more mature cells in human erythropoiesis [107]. On the other hand, macrophages produce a growth factor (like SCF, Ephrin-2 or BMP-4 [124]) which stimulates proliferation. In addition, immature cells are subject to a feedback control mediated by mature red blood cells circulating in the bloodstream, representing the action of Epo. Concentration of Epo in the computational domain is supposed to be uniform, so all cells are similarly influenced by Epo (Figure 2.7).

The concentrations of Fas-ligand F_L and of the growth factor G, produced by macrophages,
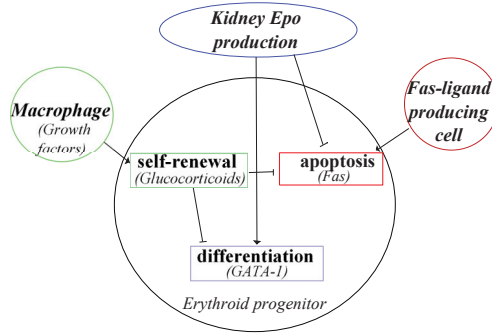
Figure 2.7: Intracellular and extracellular regulation that determine erythroid progenitor fate.

in the extracellular matrix are described by the reaction-diffusion equations:

$$\frac{\partial F_L}{\partial t} = D_1 \Delta F + W_1 - \sigma_1 F_L, \qquad (2.2.8)$$

$$\frac{\partial G}{\partial t} = D_2 \Delta G + W_2 - \sigma_2 G. \qquad (2.2.9)$$

where W_1 and W_2 are the constant source terms, the last terms in the right-hand sides of these equations describe their degradation, D_1 and D_2 are diffusion coefficients.

Complete intracellular regulatory mechanisms involved in erythroid progenitor cell fate are very complex and not yet elucidated. Based on the current knowledge, we consider a simplified regulatory network with three groups of proteins and hormones. The first group, denoted by u, consists of proteins and hormones, such as protein Erk, BMP4 and glucocorticoids, involved into self-renewal. The second group, denoted by v is represented by GATA-1 [5], promoting erythroid progenitor differentiation. The last group, denoted by w, is represented by protein Fas inducing apoptosis. Moreover, self-renewal proteins inhibits apoptotis and differentiation. Intracellular regulation in erythroid progenitors is described by the ordinary differential equations:

$$\frac{du}{dt} = \gamma_1 \tag{2.2.10}$$

$$\frac{dv}{dt} = \gamma_2(1 - \beta_1 uv) \tag{2.2.11}$$

$$\frac{dw}{dt} = \gamma_3(1 - \beta_2 uw), \tag{2.2.12}$$

At the end of cell cycle, if $u < v$, progenitors differentiate, if $u > v$, then progenitors self-renew. If $w > w_{cr}$, then the cell dies by apoptosis at any moment of time during cell cycle. The quantity w being different in different cells, some of them die and some other cells survive. The intracellular regulation is influenced by the extracellular variables through the coefficients γ_1 and γ_3:

$$\gamma_1 = \gamma_1^0 + \gamma_1^1 G, \quad \gamma_2 = \gamma_2^0 + \gamma_2^1 Epo, \quad \gamma_3 = \gamma_3^0 + \gamma_3^1 F_L.$$

The concentration of Epo is constant in these simulations. Therefore the value of the coefficient γ_2 is the same for all cells, while the values of the coefficients γ_1 and γ_3 depend on the cell position with respect to the macrophage and to other erythroid cells. Indeed, γ_1 depends on the quantity of G produced by the macrophage. This quantity is calculated for each cell at each moment of time. Similarly, the quantity of F_L influences γ_3. Let us note, that the threshold w_{cr} also depends on the concentration of Epo. Since Epo downregulates cell apoptosis, w_{cr} increases with the increase of Epo.

After each cell division, initial concentrations u, v, w in the daughter cells are set equal to the half of the concentration in the mother cell. Cell cycle is taken 24 hours plus/minus random value between 0 and 12 hours. The first generation of progenitors has the initial concentrations of u, v, w given as a random variable uniformly distributed in the intervals $[0, u_0]$, $[0, v_0]$ and $[0, w_0]$. Random perturbations in initial conditions are important to describe experiments in cell culture without macrophages (not presented here). In this case, if the initial protein concentrations are the same for all cells, they will have the same

fate. However the experiments show this fate can be different for different cells.

A typical structure of erythroblastic islands is shown in Figure 2.13. It consists of a macrophage and two other types of cells, immature progenitors (yellow) and reticulocytes (blue). Macrophage expresses a growth factor (green) driving nearby erythroblasts toward self-renewal. In mice Fas-ligand (red) is produced by undifferentiated cells (Figure 2.13, left), while in human by differentiated cells (Figure 2.13, right). We will consider below only erythropoiesis in mice. The results of modeling will be compared with experiments in the subsequent work. Model of human erythropoiesis can be found in [70].

With a suitable choice of extracellular and intracellular parameters, functioning of the island is stable (Figure 2.8, left). It contains in average 25 erythroid progenitors and 5 reticulocytes. The influence of the most important parameters on the erythroblastic island is estimated and shown in Figure 2.8 and 2.9. Periodic oscillations in the number of cells are related to the cell cycle.

An important characteristic of erythroblastic islands is the rate of production of progenitors and reticulocytes, which determine the number of erythrocytes in blood. We study how this production depends on the parameters w_{cr}, γ_1 and γ_2^0. First, we will focus on the global feedback control mediated by Epo. When w_{cr} increases, the size of the island also increases due to decreased apoptosis of immature progenitors. Consequently, there are more cells at the perimeter of the island. They have a tendency to differentiate since they are far from the macrophage which promotes self-renewal. Therefore, increasing of the Epo level increases the production of reticulocytes (Figure 2.8, right).

Increase of γ_1 promotes self-renewal and augments the number of immature progenitors. Consequently, the number of reticulocytes also increases (Figure 2.9, left). When we increase the value of γ_2^0, which influences the differentiation rate, the number of reticulocytes decreases. For sufficiently large values of this parameter, the island disappears after several cell cycles (Figure 2.9, right). Let us note that we split here the action of Epo on cell differentiation from its action to downregulate apoptosis. *In vivo*, Epo acting on both of them stimulates production of erythrocytes.

56
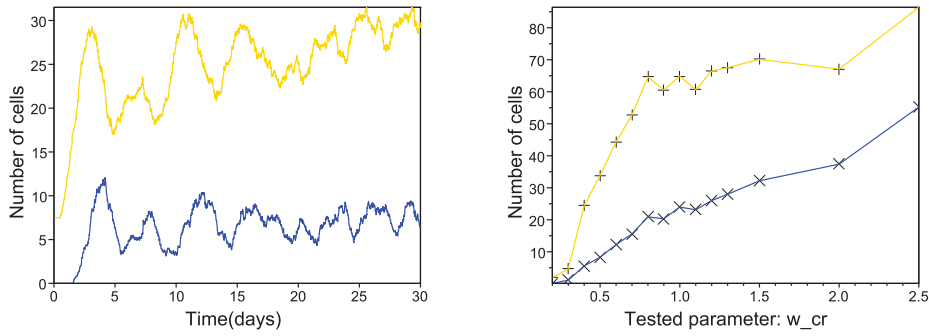
Figure 2.8: The number of progenitors (red curve) and reticulocytes (blue curve) in time (left). Average in time number of progenitors and reticulocytes for different values of the parameter w_{cr} (right). Each curve is obtained as a mean value for 10 simulations.
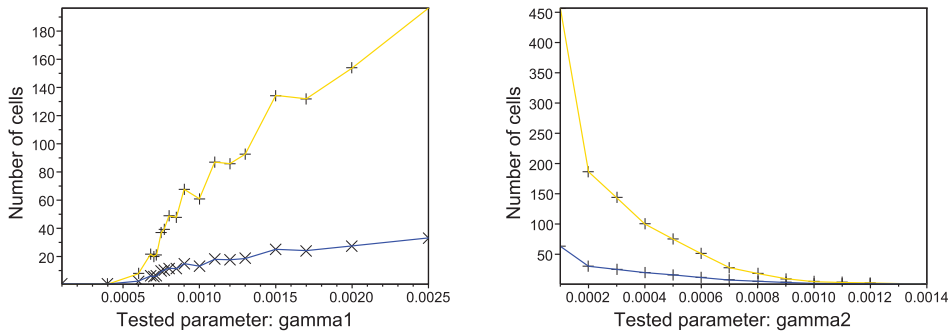
Figure 2.9: Average in time number of progenitors and reticulocytes for different values of γ_1 (left) and γ_2^0 (right) (mean values for 10 simulations).

Tis new model of erythropoiesis taking into account intracellular and extracellular regulations and cell-cell interaction. Competition between three groups of proteins that determine the cell fate has been considered with continuous models (ordinary differential equations) whereas cells have been studied as discrete objects. Extracellular regulatory network are described by partial differential equations. The model suggests an important role of macrophages in functioning of erythroblastic islands and production of mature red blood cells. Without macrophages, erythroblastic islands quickly lose their stability and either die out or abnormally proliferate [70]. Macrophages control the size of erythroblastic islands which show their capacity to rapidly increase production of mature cells in

57

response to stress (anemia, hypoxia). This response is based on the increased production of erythropoietin and glucocorticoids. Analysis of feedback by Epo and of the role of central macrophage in erythroblastic islands give a new insight into the mechanisms of control of erythroid cell proliferation and differentiation. More detailed description of the intracellular regulation and comparison with experimental data will be presented in the subsequent papers.

2.2.4 Regulation by activated glucocorticosteroid receptor, activated BMPR4 receptor, transcription factor GATA-1 and activated caspases

Introduction

The functional unit of mammalian erythropoiesis, the erythroblastic island, consists of a central macrophage surrounded by adherent erythroid progenitor cells (CFU-E/Pro-EBs) and their differentiating progeny, the erythroblasts. Central macrophages display on their surface or secrete various growth or inhibitory factors that influence the fate of the surrounding erythroid cells. CFU-E/Pro-EBs have three possible fates : a) expansion of their numbers without differentiation, b) differentiation into reticulocytes that are released into the blood, c) death by apoptosis. CFU-E/Pro-EB fate is under the control of a complex molecular network, that is highly dependent upon environmental conditions in the erythroblastic island.

Methods and results: A model was developed in which cells are considered as individual physical objects, intracellular regulatory networks are modeled with ordinary differential equations and extracellular concentrations by partial differential equations. We used the model to investigate the impact of an important difference between humans and mice in which mature late-stage erythroblasts produce the most Fas-ligand in humans, whereas early-stage erythroblasts produce the most Fas-ligand in mice. Although the global behaviors of the erythroblastic islands in both species were similar, differences were found, including a relatively slower response time to acute anemia in humans. Also, our modeling approach was very consistent with *in vitro* culture data, where the central macrophage in

reconstituted erythroblastic islands has a strong impact on the dynamics of red blood cell production.

The specific spatial organization of erythroblastic islands is key to the normal, stable functioning of mammalian erythropoiesis, both *in vitro* and *in vivo*. Our model of a simplified molecular network controlling cell decision provides a realistic functional unit of mammalian erythropoiesis that integrates multiple microenvironmental influences within the erythroblastic island with those of circulating regulators of erythropoiesis, such as EPO and glucocorticosteroids, that are produced at remote sites.
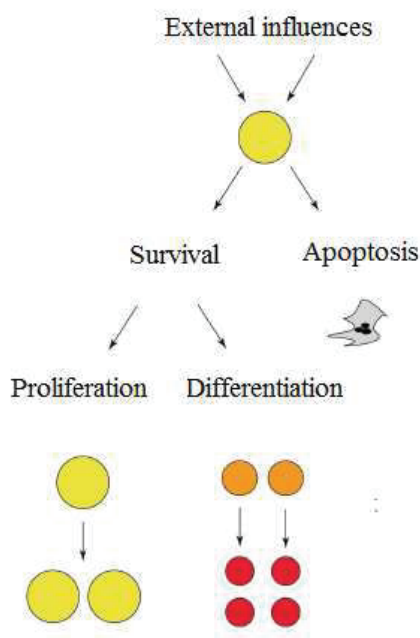
Figure 2.10: Schematic representation of erythroid progenitor cell decision making. Large yellow circles represent erythroid progenitors at the CFU-E/proerythroblast stage of differentiation. Their fate is determined by intracellular regulation which can be influenced by extracellular substances including Fas-ligand and EPO. This intracellular regulatory network is shown in greater detail in Figure 6.2. Erythroid progenitors have one of three possible fates : die by apoptosis, proliferate without differentiation (self-renewal), or terminally differentiate.

Differentiation from hematopoietic stem cell (HSC) through the CFU-E/Pro-EB stage of erythropoiesis requires the hematopoietic growth factor Kit ligand/stem cell factor (KL/SCF) [58]. At the CFU-E/Pro-EB stage of differentiation, the KL/SCF requirement is lost, and a

dependency upon the hormone erythropoietin (EPO) to prevent apoptosis begins [92, 167]. This EPO-dependency persists throughout the period that the CFU-E/Pro-EBs make decisions about their fate. EPO is produced by the kidneys in quantities that are inversely and exponentially proportional to the number of erythrocytes in blood [93]. EPO gene transcription is regulated by hypoxia-inducible factor (HIF), a transcription factor that rapidly accumulates in the kidney EPO-producing cells when oxygen delivery to the kidneys is reduced [93]. Through specific receptors (EPO-R) on erythroid progenitors EPO prevents their apoptosis via down-regulation of Fas and up-regulation of Bcl-xL, an anti-apoptotic protein [107, 100, 81]. Thus, EPO is the major regulator of erythropoiesis that directly links the tissue hypoxia caused by decreased circulating erythrocytes to the rates of new erythrocyte production. Although increased EPO production and the other changes of stress erythropoiesis are similar in humans and mice, one prominent difference is that during hypoxic stress, mice have an extensive expansion of splenic erythropoiesis. This enhanced murine splenic erythropoiesis during hypoxic stress is mediated by bone morphogenetic protein 4 (BMP4), a protein produced by other hematopoietic and non-hematopoietic cells [119]. This BMP4 expression in the spleen increases self-renewal of erythropoietic progenitors including the CFU-E/Pro-EBs.

The differentiation of erythroid progenitors and erythroblasts depends upon multiple transcription factors including, most prominently, GATA-1, the zinc finger-containing component of transcription factor complexes that binds to the DNA sequence (A/T)GATA(A/G). GATA-1 is required for the differentiation of HSCs to the erythroid-committed progenitor stages and for the terminal differentiation of the CFU-E/Pro-EBs to reticulocytes [38]. The complexity of erythroid differentiation related to species, organ, and stress conditions complicates understanding of erythropoiesis and its mathematical modeling. In this report, we develop mathematical models which will allow us to consider various hypotheses about the organization of mammalian erythropoiesis.

Mathematical modeling

Mathematical modeling of erythropoiesis was first based on the dynamics of hematopoietic stem cells, erythroid progenitors and erythroid precursors [164]. Subsequently, stimulated [165] and suppressed erythropoiesis were modeled [168]. An age-structured model describing erythroid cell dynamics, including an explicit control of differentiation by EPO, was proposed [16] and further developed [2, 3, 106]. Age-structured models of erythropoiesis were also used to study stress erythropoiesis [57, 133]. The modeling methods used in these works were based on ordinary differential equations, delay differential equations and transport (age-structured) equations. Spatial cell organization, as found in erythroblastic islands, was not included in any of these studies. Moreover, in all these previous models, as in other models of hematopoiesis, the rates of self-renewal, differentiation and apoptosis were considered as given parameters.

In order to describe spatial cell organization and functioning of erythropoiesis *in vivo* and *in vitro*, we develop in this work a hybrid model of erythropoiesis in which cells are considered as individual objects, intracellular regulatory networks are described by ordinary differential equations and concentrations of biochemical substances in the extracellular matrix are described by partial differential equations. The quantities and activities of intracellular proteins determine cell fate by self-renewal, differentiation or apoptosis. Therefore, most importantly, we do not impose the corresponding rates as parameters, but rather we obtain them as a result of modeling of the molecular network. This model is based on our previous investigations in which we studied intracellular regulation of erythroid progenitors [55, 62], developed individual cell-based models of hematopoiesis [26, 19, 22] and hybrid models of hematopoiesis [19, 70, 80, 97].

Although spatial organization of erythropoietic cells has not been included in most published models, an erythroid progenitor's fate depends on its environment, and the outcome among self-renewal, differentiation and apoptosis depends upon the erythropoietic progenitor cell's spatial situation. Consequently, spatial organization of erythropoietic cells is important for their function. We previously modeled erythroblastic islands consider-

ing their specific structure: a macrophage at the center surrounded by closely associated erythroid progenitors with the more mature erythroblasts and reticulocytes located at progressively peripheral locations from the central macrophage [70]. To study the role of the central macrophage, we modeled erythroblastic islands without it, i.e., as foci of erythroid progenitors surrounded by reticulocytes. Within the range of tested parameters, however, these erythroblastic islands modeled without macrophages were very heterogeneous in development. After several cell cycles, these islands without central macrophages diminished and disappeared or, conversely, they expanded exponentially, with the difference between these two fates depending on their initial size and stochastic perturbations. However, assuming that the central macrophage releases pro-survival cytokines, we demonstrated that it induced a very significant stabilizing effect on the erythroblastic island [70].

In this work we continue the development of the hybrid model of erythropoiesis. Taking into account recent biological data we will present a modified (in comparison with [70]) intracellular regulation. Moreover we will consider two different cases which correspond to human and murine erythropoiesis. In the former, Fas-ligand, the secreted protein which determines erythroid progenitor differentiation and apoptosis is produced by more mature erythroid cells, while for the latter by early erythroblasts and erythroid progenitors themselves. We will demonstrate that although the quantitative behavior of the system in these two cases is similar, there is some difference between them. In particular, hematocrit recovery *in vivo* after anemia is faster in mice than in humans.

Due to obvious limitations of *in vivo* investigation of erythropoiesis, especially in humans, detailed analysis of the structure and functioning of erythroblastic islands have not been performed. *In vitro* experiments on CFU-E/Pro-EBs co-cultured with macrophages were considered as a biological model of *in vivo* erythropoiesis, and such experiments showed that erythroid cell properties strongly depend on their position with respect to adherence to a central macrophage [124]. Mathematical modeling performed herein gives a good description of *in vitro* experimental results and confirms the importance of the spatial organization of cells in erythroblastic islands. Moreover, numerical simulations show that erythropoiesis

in erythroblastic islands with macrophages can be stable, indicating that this stabilization is an important role of macrophages in erythroblastic islands. Thus, erythropoiesis is determined by intracellular and extracellular regulations, cellular environment, local and remote feedbacks, and stochastic perturbations. The hybrid models presented here take each of these aspects into account and obtain good agreement with experimental results.

Before division, cells increase their size. When two daughter cells appear, the direction of the axis connecting their centers is chosen randomly from 0 to 2π. Cell cycle duration is taken to be 18 hours with a random perturbation uniformly distributed between -3 and 3 hours [75]. Intracellular and extracellular regulations and equations of motion represent the main features of the hybrid model of erythropoiesis. More detailed description of the hybrid model is given in [70]. The two-dimensional model considered in this work is appropriate to describe the experiments in cell cultures where the third dimension can be neglected.

We used the conventional Thomas algorithm and alternative direction methods to solve two-dimensional reaction-diffusion equations. Ordinary differential equations were solved by the Euler method. Numerical simulations were carried out with the original software developed by the authors.

One simulation takes about 10 hours of the CPU time on a modern PC. Each point in Figures 2.12, 2.15 and 2.16 represent an average of 10 simulations. This is sufficiently representative and it would be difficult to increase essentially the number of simulations because of the computational complexity.

Intracellular regulation and cell fate

Intracellular regulation of erythroid progenitors. A detailed description of the intracellular regulation of erythroid progenitors is presented in Appendix 1. We will use here a simplified model which retains the most important features of this regulation but allows us to reduce the number of unknown parameters. We will consider here an intracellular regulation of CFU-E/Pro-EBs where each of the possible cell fates (self-renewal, differentiation, or apoptosis) is determined by different proteins. Consider the simplified kinetics of

63
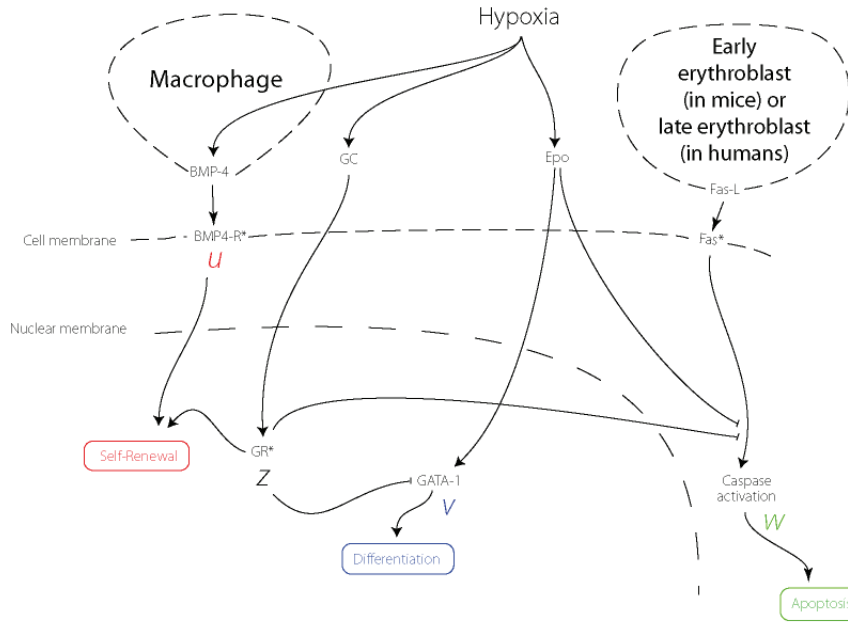
Figure 2.11: Scheme for the modeling of erythropoietic fate based on simplification of the biological scheme in Figure 6.2 (see Appendix 1). Four major variables that play a role in the intracellular regulation of CFU-E/Pro-EBs and affect the fate decisions to undergo apoptosis, terminal differentiation, or self-renewal are retained from Figure 6.2. They include : 1) the concentration of activated glucocorticosteroid receptor (z) that determines the rate of self-renewal in normal, steady-state erythropoiesis and in more limited hypoxia states in which adjustments of EPO concentrations maintain a stable number of circulating erythrocytes; 2) the concentration of activated BMP4 receptor (u) that determines the rate of expansion of the CFU-E/Pro-EB population in periods of hypoxic stress; 3) the concentration of GATA-1 (v) that determines the rate of terminal differentiation; and 4) the concentration of activated caspases (w) that determine the rate of apoptosis when elevated and the rate of terminal differentiation when reduced. The major extracellular mediators that affect the intracellular variables have been retained. These extracellular mediators include : 1) the concentration of glucocorticosteroid hormone (GC) that varies with degree of stress including that associated with hypoxia; 2) the expression of BMP4 by central macrophages that increases with hypoxia-induced stress; 3) the concentration of EPO which varies inversely with the degree of hypoxia; and 4) the expression of Fas by erythroid progenitor cells, which varies inversely with the EPO concentration and 5) Fas-ligand, which is produced by other erythroid cells in the erythroblastic island, specifically by early stage erythroblasts in mice and late-stage mature erythroblasts in humans.

the intracellular regulation shown in Figure 2.11 :

$$\frac{dz}{dt} = a_0, \tag{2.2.13}$$

64

$$\frac{du}{dt} = a_1 + b_1 z, \tag{2.2.14}$$

$$\frac{dv}{dt} = a_2 - b_2 zv, \tag{2.2.15}$$

$$\frac{dw}{dt} = a_3 - b_3 zw. \tag{2.2.16}$$

Here z is the concentration of activated glucocorticosteroid receptor (GR). The value of a_0 can depend on the extracellular concentration of GC. For a fixed concentration, it is a constant. Next, u is the concentration of activated BMPR4 receptor (BMP-R), which determines cell self-renewal and depends on the extracellular concentration of BMP4 provided by macrophages. Hence, a_1 depends on this concentration. The second summand in the right-hand side of equation (2.2.14) takes into account that self-renewal can be up-regulated by GR. Cell differentiation is determined by a relatively complex sub-scheme based on the transcription factor GATA-1. In order to simplify this regulation and to avoid introduction of additional parameters, we will keep only one variable v, which describes the concentration of GATA-1. The value of a_2 depends on the extracellular EPO concentration. Finally, w denotes the activated caspase concentration which determines cell apoptosis and depends on the intracellular Fas concentration which, in turn, depends upon the extracellular Fas-ligand concentration. Apoptosis is down-regulated by EPO (through a_3) and by GR taken into account through the last term in the right-hand side of equation (2.2.16). These are the main features of the regulatory mechanism. Some others are not taken into account in the simplified model because they are less essential but they can be easily introduced.

We suppose that cell fate is determined by the values of the variables u, v, w. Namely, if at some moment of time w (caspase) reaches its critical value w_{cr}, then the cell dies by apoptosis. The variables u (BMP4) and v (GATA-1) are compared at the end of the cell cycle. If $u > v$, then the cell divides and self-renews, otherwise it divides and differentiates.

Extracellular regulation. Intracellular regulation of erythroid progenitors is influenced by extracellular substances. Glucocorticosteroids (GC) and soluble growth factors (G) produced by the macrophage stimulate self-renewal. GC with a constant concentration

in the model, implicitly enters equation (2.2.13) through the right-hand side a_0 (the first relation in (3.1.5)) :

$$
\begin{aligned}
a_0 &= a_0^0 + a_0^1 GC, a_1 = a_1^0 + a_1^1 G, a_2 = a_2^0 + a_2^1 E, \\
a_3 &= a_3^0 + a_3^1 F.
\end{aligned} \tag{2.2.17}
$$

Growth factors enter equation (2.2.14) through a_1. EPO and Fas-ligand influence differentiation and apoptosis. They are taken into account in equations (2.2.15) and (2.2.16), respectively, by means of the coefficients a_2 and a_3. All dependencies in (3.1.5) are taken to be linear in order to simplify the model and to reduce the number of parameters. BMP4 at the surface of macrophage acts through the surface receptor BMP4-R to decrease cell cycle duration in those erythroid progenitors that are in contact with central macrophages.

Differentiated cells. Reticulocytes do not divide, but they stay in the bone marrow before entering the blood. Human mature erythroblasts, which give rise to the reticulocytes, are the major source of Fas-ligand that induces CFU-E/Pro-EB apoptosis by activating intracellular caspases by binding to the specific membrane receptor, Fas. In mice, the major source of Fas-ligand is the very early erythroblasts that are the immediate progeny of CFU-E/Pro-EBs.

If the concentration of Fas-ligand is sufficiently high, then the CFU-E/Pro-EBs die by apoptosis. In intermediate concentrations of Fas-ligand, the CFU-E/Pro-EBs differentiate into reticulocytes after three divisions. In low concentrations of Fas-ligand, the erythroblast progenitors proliferate without differentiation, i.e., they self-renew. Thus, the fate of erythroid progenitors is determined by the concentration of Fas-ligand or, in other words, by their spatial location with respect to the immature erythroblasts in mice and the mature erythroblasts in humans. Progenitors located close to Fas-ligand-producing erythroblasts die by apoptosis, those at an intermediate distance differentiate, and those located furthest from the Fas-ligand-producing erythroblasts proliferate without differentiation.

The numbers of differentiated cells and progenitors are strongly influenced by the values
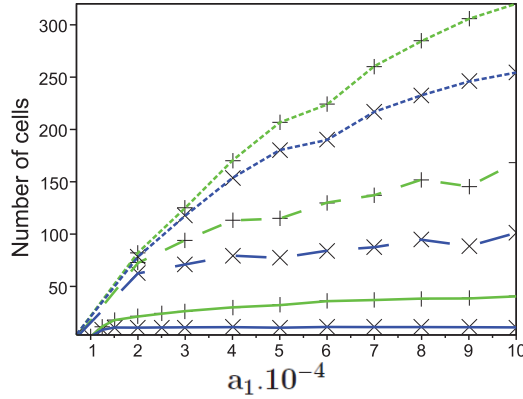
Figure 2.12: Average number of CFU-E/Pro-EBs and differentiating erythroblasts (green curves) and late-stage, pre-enucleation erythroblasts and reticulocytes (blue curves) in one erythroblastic island as a function of a_1 for different values of w_{cr} equal to 0.7 (upper pair of curves), 0.6 (middle pair of curves) and 0.509 (lower pair of curves), respectively. Fas-ligand produced by early stage erythroblasts. The average is taken with respect to time and with respect to 10 simulations.

of multiple parameters, but the total number of erythroid cells increases with greater values of w_{cr}, the critical variable of Fas-ligand which determines apoptosis of progenitors (Figure 2.12). Increased w_{cr} corresponds to greater values of EPO which stimulate survival of progenitors under the action of reduced Fas-ligand. Similarly, the number of erythroid cells also increases due to macrophages (parameter a_1) that stimulate self-renewal of CFU-E/Pro-EBs. In all cases, at steady state, CFU-E/Pro-EBs and differentiating erythroblasts outnumber the mature cells.

Results

Structure and function of erythroblastic islands. In our erythroblastic island model, macrophages produce various growth factors (G) including those, which stimulate proliferation without differentiation (self-renewal). Therefore, CFU-E/Pro-EBs located closest to and interacting most with the central macrophage proliferate without differentiation, while CFU-E/Pro-EBs located closest to Fas-ligand-producing erythroblasts die by Fas-mediated apoptosis. CFU-E/Pro-EBs located at intermediate distances between macrophages and

Fas-ligand-producing erythroblasts differentiate and provide new reticulocytes that replace those leaving the bone marrow by entering the circulating blood. Thus, normal CFU-E/Pro-EBs that do not interact directly with and are sufficiently far from the central macrophage will differentiate and cannot undergo unlimited proliferation. This organization of erythroblastic islands in the presence of a central macrophage appears to be very stable [70], and these erythroblastic islands can exist for an unlimited time with approximately constant size and a constant rate of reticulocyte production. However, this steady-state rate of erythropoiesis can be influenced by EPO, which downregulates apoptosis of CFU-E/Pro-EBs allowing their enhanced proliferation and differentiation in response to anemia.
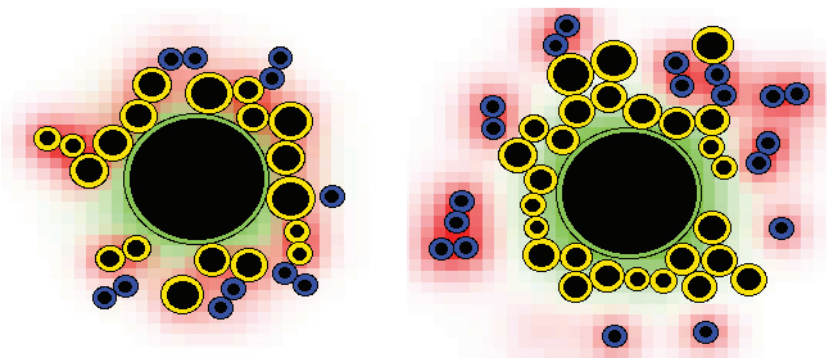
Figure 2.13: Typical structure of an erythroblastic island in the simulations : Fas-ligand produced by early-stage erythroblasts (left) or by late-stage erythroblasts (right). The large cell in the center is a macrophage, yellow cells - CFU-E/Pro-EBs and differentiating erythroblasts, blue - late-stage mature erythroblasts and reticulocytes, level of green - concentration of the growth factor (G) produced by the macrophage, level of red - concentration of Fas-ligand. Black circles inside cells show their incompressible parts.

The major source of Fas-ligand produced by erythroid cells is the late-stage erythroblasts in human [107] and the early-stage erythroblasts [100] in mice. Therefore, we considered models incorporating these two different sources of Fas-ligand and compared them. Figure 2.13 shows erythroblastic islands in which Fas-ligand is produced by early-stage erythroblasts (left) and by late-stage erythroblasts (right). If Fas-ligand is produced by late erythroblasts, then progenitors located closest to them die by apoptosis, so that these late erythroblasts are relatively isolated. If Fas-ligand is produced by early erythroblasts,

late erythroblasts can be close to but not surrounded by CFU-E/Pro-EBs. Otherwise, the quantity of Fas-ligand is high, resulting in apoptosis. In both cases, CFU-E/Pro-EBs are located closer to the central macrophage and mature erythroid cells are at the periphery of the island, i.e., the structure of the islands is similar in humans and mice.

The difference between human and murine erythroblastic islands appears in the quantitative analyses of the numbers of progenitors and of differentiated cells over time. In both cases the initial configuration is the same : several progenitors are located near the macrophage. In mice where Fas-ligand is produced by early erythroblasts (Figure 2.14, left) the number of erythroid cells grows faster than in human erythroblastic islands where they are produced by late erythroblasts (Figure 2.14, right). In mice, apoptosis of CFU-E/Pro-EBs occurs when their number becomes sufficiently large, and it does not influence their self-renewal in the beginning of the evolution of the island when their number is small. In humans, CFU-E/Pro-EB differentiation and apoptosis can occur from the very beginning, and together they slow down growth of cell number. This difference can play a role in stress erythropoiesis where the number of erythroblastic islands can greatly increase and new islands start their functioning with one or several CFU-E/Pro-EBs in the vicinity of a macrophage. The slower response in humans is consistant with experimental and clinical data (see Recovery from bleeding, Figure 2.17).

We considered next the dependence of the results on the concentration of EPO through the value of a_2. We compared the two cases where Fas-ligand is produced either by early-stage erythroblasts in mice or by late-stage erythroblasts in humans. In mice, the number of mature erythroblasts and reticulocytes was low for small values of a_2 and it increases slightly, while the number of progenitors remains almost constant (Figure 2.15, left). This behavior can be explained as follows. When a_2 is small, the value of the intracellular variable v also remains small and differentiation does not occur. CFU-E/Pro-EBs either self-renew, or they die by apoptosis, if the concentration of Fas-ligand is large enough. Increasing a_2 further increases the number of differentiated cells. For larger values of a_2, where differentiation begins to compete with self-renewal, the number of mature erythroblasts and reticulocytes
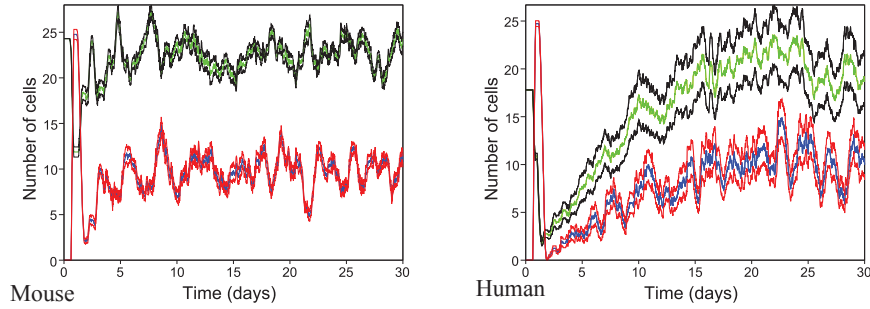
Figure 2.14: Number of CFU-E/Pro-EBs and differentiating erythroblasts (green curves) and mature erythroblasts and reticulocytes (blue curves) in one erythroblastic island as a function of time : Fas-ligand produced by early-stage erythroblasts (left) or by late-stage erythroblasts (right). Green and blue curves are mean values for 10 simulations. Black and red curves show the 95% confidence intervals (mean $\pm 1.96*$standard deviation$/\sqrt{n}$ ($n = 10$)). For the parameter values used, see Tables 6.3 and 6.4.

still increases but there is a significant decrease in the number of progenitors. For even larger values of a_2 the number of mature of erythroblasts and reticulocytes also decreases because of the decreased numbers of CFU-E/Pro-EBs.

This dependence is different in human erythroblastic islands where Fas-ligand is produced by late-stage erythroblasts (Figure 2.15, right). Surprisingly, increasing a_2 decreased the number of mature of erythroblasts and reticulocytes. Probably, this happened because the number of self-renewing progenitors decreased and the number of apoptotic cells increased. Since there were less progenitors, then the number of mature of erythroblasts and reticulocytes also decreased. As noted previously, CFU-E and differentiating erythroblasts outnumbered mature erythroblasts and reticulocytes, but the proportions remained about the same as the numbers of both decreased.

These results in Figure 2.15 show that the action of EPO on GATA-1 does not by itself increase the number of mature erythroid cells. EPO also acts on Fas receptors, downregulating apoptosis. Since we do not account explicitly for Fas receptors in the model, we described the action of EPO on apoptosis through the critical value of Fas-ligand. Figure 2.16 shows the average number of cells in the erythroblastic island for different values of w_{cr}. The qualitative behavior of the curves was similar in the cases where Fas-ligand was
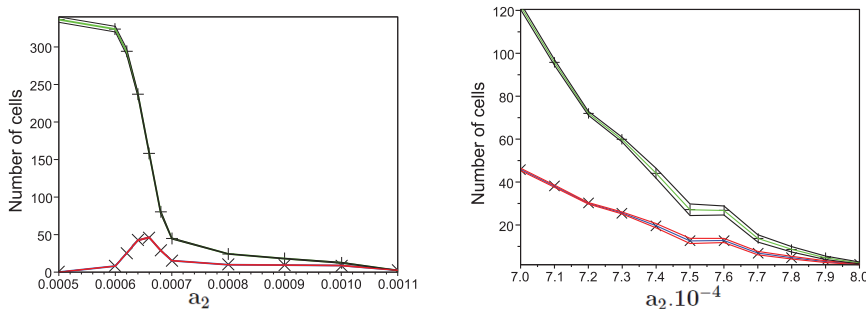
Figure 2.15: Average number of CFU-E/Pro-EBs and differentiating erythroblasts (green curve) and mature erythroblasts and reticulocytes (blue curve) in one erythroblastic island as a function of a_2. Black and red curves show the 95 % confidence intervals. Fas-ligand produced by early-stage erythroblasts (left) or by late-stage erythroblasts (right). The average is taken with respect to time and with respect to 10 simulations.
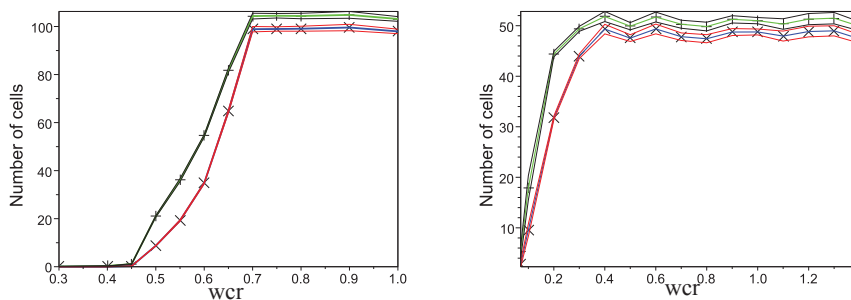
Figure 2.16: Average number of CFU-E/Pro-EBs and differentiating erythroblasts (green curve) and erythroblasts and reticulocytes (blue curve) in one erythroblastic island as a function of w_{cr}. Black and red curves show the 95 % confidence intervals. Fas-ligand produced by early-stage erythroblasts (left) or by late-stage erythroblasts (right). The average is taken with respect to time and with respect to 10 simulations.

produced by early-stage erythroblasts and by late-stage erythroblasts. However there was an essential difference between them for small values of w_{cr}. If Fas-ligand was produced by early-stage erythroblasts, they easily killed each other for small values of w_{cr} and the island disappeared. It was different if Fas-ligand was produced by late-stage erythroblasts. Progenitors had more time to expand before late-stage erythroblasts appeared and killed some of them by Fas-ligand production. Therefore, the island survived when late-stage erythroblasts were the source of Fas-ligand and values of w_{cr} were low.

Comparison with experiments and clinical data
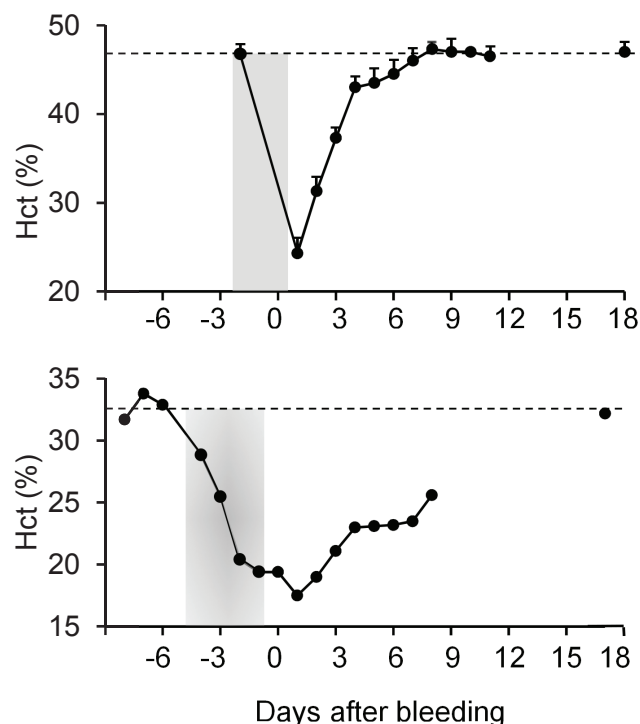
Figure 2.17: Recovery of hematocrits (Hct) after severe acute hemorrhage in mouse and human. In the upper panel, four healthy, adult mice were phlebotomized daily during the three days prior to monitoring recovery of Hcts. Data are means +1 S.D. of Hcts. The last phlebotomy was on Day 0. Day 1, with the nadir Hct, is the first day of recovery. For phlebotomy methods, see [92] and [124]. Shaded area shows the period of phlebotomies, and the dashed line indicates the mean baseline Hct of the mice prior to phlebotomies. In the lower panel, Hct of a patient who refused transfusion of blood during recovery from bleeding caused by anticoagulation administered during the 4-day period indicated by shading. The anticoagulation was last administered on Day -1. Day 1, with the nadir Hct, is the first day of recovery. The dashed line indicates the mean baseline Hct on Days -8 to -6, which were prior to the administration of anticoagulation.

Recovery from experimental bleeding in mice and in the clinical setting. Simulations of erythroblastic islands in Figure 2.14 predicted that mice with Fas-ligand provided mainly by early stage erythroblasts will have a more rapid erythrocyte production during stress erythropoiesis compared to humans with Fas-ligand provided mainly by late stage progenitors. Direct comparison of erythroblastic islands *in vivo* between mice and humans

is not feasible, but respective responses, in terms of recovery of circulating erythrocytes after severe blood loss, are shown in Figure 2.17. For this comparison, response to acute hemorrhage is measured in hematocrit (Hct), the percentage of the blood volume that is comprised of erythrocytes. Humans and mice have similar Hcts because mice have about twice as many erythrocytes per volume of blood as humans, but a mouse erythrocyte is about one-half the size of a human erythrocyte. In Figure 2.17, four normal mice are bled on three consecutive days such that their Hcts are reduced from 47 ± 1 % (mean ± 1 S.D.) to 24 ± 1 % on Day 1 of recovery, the day after the last bleeding. The human results are from a patient who bled for 3 to 4 days following anticoagulation therapy. His mean Hct of 33%, as measured on the 3 days prior to anticoagulation, decreased to a Hct of 17.5% on Day 1 of recovery. Despite his severe anemia, the patient refused the blood transfusions that would otherwise be given to a patient with such an acute anemia. The patient had a slight baseline anemia from chronic arthritis, but he did not have renal failure, adrenal failure or iron deficiency. When he refused blood transfusions, the patient received EPO (darbepoetin), corticosteroids, and intravenous iron, and he was monitored with daily Hct measurements.

In Figure 2.17, both the mice and the patient began their recovery after having lost about one-half of their baseline erythrocyte volume. However, the mice recover completely to their mean baseline Hct by Day 7 after bleeding, whereas the human patient, with a Hct of 26% on Day 8, only recovered about one-half the total erythrocyte volume that he had lost. During stress erythropoiesis, the size of individual islands increases because of more intensive self-renewal and downregulation of apoptosis, but the number of islands also grows. Thus, only a qualitative comparison is possible between the human data in Figure 2.17 and modeling in Figure 2.14 (right). In Figure 2.17, at some time between Day 9 and 17, when the patient had returned home and was not monitored daily, he recovered to his baseline Hct, while the simulations in Figure 2.14 indicate that, indeed, about two weeks is required for a human to return to a baseline Hct. The prolonged rate of recovery in the human patient compared to the mice is consistent with the simulation results in Figure

2.14 that predict that mice will respond more quickly than humans to a similar degree of acute blood loss. This prediction by our model indicates that the spatial constraints of the erythroblastic island structure coupled with the differences in Fas regulation patterns contribute to the prolonged recovery period after acute hemorrhage in humans compared to mice.

In vitro experiments on cell cultures. Since we cannot directly compare our models with erythroblastic island function *in vivo*, we also compared them with experimental results from cell cultures, which can be considered as good *in vitro* approximations.
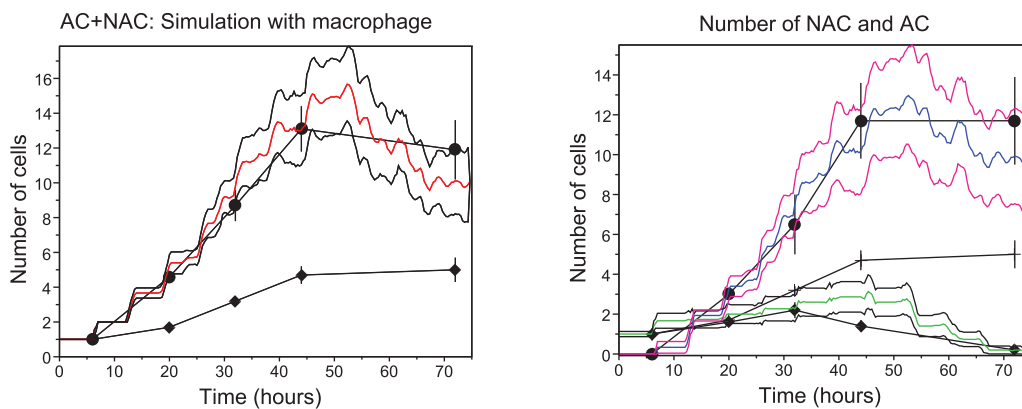
Figure 2.18: Comparison of *in vitro* experiments and numerical simulations with mouse cells. Left figure : the total number of erythroid cells in co-cultures (upper curve). The number erythroid cells in control cultures without macrophage (lower curve); black symbols - experiments, continuous curves - simulations. Three curves for each of the experiments represent mean value and confidence intervals for 10 simulations. Right figure : the number of cells adherent to macrophage in co-cultures (AC) - lower curve, nonadherent cells in co-cultures (NAC) - upper curve, and middle curve is control culture without macrophages. For a value of the parameters used, see Tables 3 and 4. Experimental data were originally reported in reference [124].

New features of the *in vitro* systems were added in the model. Since the duration of the cell cycle is different for erythroid cells adherent to macrophages (AC) in comparison with nonadherent erythroid cells (NAC), we introduced different cell types in the model: adherent progenitors and differentiated cells and nonadherent progenitors and differentiated cells. In the model, a cell is considered as adherent if at the moment of its birth the distance

74
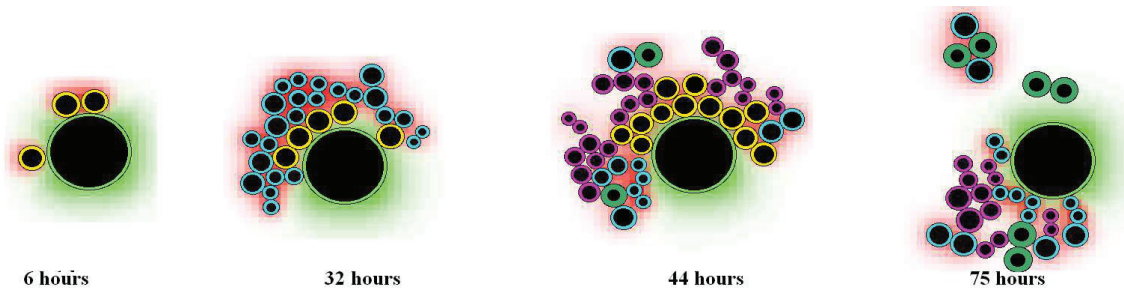
Figure 2.19: Simulation of one erythroblastic island *in vitro*. Large cell - macrophage, yellow cells - AC progenitors, blue - NAC progenitors, rose -NAC differentiated cells including reticulocytes, green - AC apoptotic cells. Fas-ligand is produced by early stage erythroblasts (yellow and light blue).
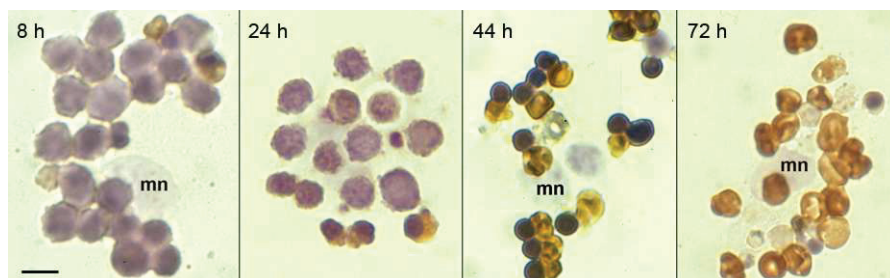
Figure 2.20: *In vitro* differentiation of erythroblasts in erythroblastic islands isolated from the spleens of mice in the erythroblastosis phase after infection with anemia-inducing strain of Friend virus. The erythroblastic islands were isolated as described previously [124], cultured with 4 units/mL of human EPO for 8, 24, 44, or 72 hours, fixed with glutaraldehyde, and stained with 3,3'-dimethoxybenzidine and hematoxylin. Hemoglobin-containing erythroid cells have orange-staining cytoplasm, while nuclei stain blue-violet. Examples of erythroblastic islands were selected at each time of culture to show morphological changes of terminal erythroid differentiation. Most 8 h cells that are have large nuclei and little hemoglobin content. At successive times, the differentiating erythroid cells show increasing hemoglobin accumulation and decreasing nuclear size with associated increases in chromatin condensation. In the 44 h island, most erythroblasts are mature with eccentrically located nuclei that characterize the pre-enucleation state. In the 72 h island most of the erythroid cells have enucleated, forming reticulocytes. Nuclei in various stages of degradation are also present. Bar equals 10 micrometers; mn designates macrophage nucleus.

from its center to the macrophage membrane is less than 1.5 of its radius. Parameters of intracellular regulation are the same for nonadherent cells and adherent cells. The difference between them is the duration of the cell cycle. In accordance with experimental estimates, we set the duration of cell cycle of adherent cells at 6 hours, and that of nonadherent cells at

16 hours. We add to these durations a random perturbation uniformly distributed between -90 and 90 minutes.

Moreover, we assumed in the model that differentiated cells can die by apoptosis, and that apoptotic cells are removed more slowly than they are *in vivo*. Without these assumptions we could not obtain a good description of the experimental data: the number of cells in the simulations continued to grow after 40 hours, while it decreased in the experiments (Figure 2.18). We note that modeling *in vivo* erythropoiesis (Section 2.2.4), we did not introduce apoptosis of differentiated cells assuming that they are promptly phagocytosed in the bone marrow. Likewise, reticulocytes, having completed differentiation in a period of hypoxic stress, egress promptly from the bone marrow into the circulating blood.

The results of numerical simulation are shown and compared to the experimental results in Figure 2.18. We obtained a very good approximation of the total number of cells and the number of adherent and nonadherent cells in the cultures with macrophages.

The total cell number in the cultures with macrophages grows faster than in the cultures without macrophages (see Figure 2.18 and [124]). This can be explained by the influence of macrophages on the duration of cell cycle of erythroid progenitors, most likely due to surface-displayed KL/SCF and locally produced by BMP4. Adherent cells (AC) located close to macrophage have shorter durations of cell cycle than nonadherent cells (NAC) located further from the macrophage (Figure 2.19, compare with Figure 2.20).

Progenitors located closer to the macrophage divide faster. Due to the increasing number of cells, they push each other further from the macrophage, resulting in slower division rates as they become further distanced from the macrophage. As the distances from the macrophage become even greater these erythroid progenitors differentiate or die by apoptosis.

Altogether, these comparisons allowed us to validate the model and to determine the parameters of intracellular regulation. Moreover, we could elucidate the influence of macrophages on the duration of the cell cycle.

Erythropoiesis is controlled by a complex regulation which is far from being completely

understood. The spatial organization of erythropoiesis in mammalian hematopoietic organs, including the fetal liver and spleen as well as the bone marrow, is based on a specific morphological structure, the erythroblastic island [40]. Our hybrid model is based on the erythroblastic island as a stable, functional unit that integrates its multiple microenvironmental influences with those of circulating regulators of erythropoiesis, such as EPO and glucocorticoids, that are produced at remote sites. As biological experiments incorporate the microenvironmental influences of erythroblastic islands on erythropoiesis, we argue that mathematical modeling should also incorporate them as well.

We have previously shown that one of the major roles of central macrophages was the stabilization of cell numbers in erythroblastic islands [70]. Simulations showed that islands without macrophages either grow exponentially or disappear after several cell cycles. We demonstrate here that central macrophages are also needed for an adequate response in stress situations, such as acute anemia, thereby reinforcing the need for proper spatial description in modeling of erythropoiesis. Simpler models based on ordinary differential equations, which implicitly assume a uniform cell distribution, cannot describe erythroblastic islands whose size and production of mature cells are determined by interaction of erythroid progenitors with reticulocytes and macrophages and, consequently, by their mutual locations.

In our hybrid model of erythropoiesis, we do not impose cell fate as a given parameter (deterministic or stochastic), as is conventionally done in cell population dynamics, but we describe the decision-making process at the cellular level as the function of its intracellular network. Indeed, the rates of self-renewal, differentiation and apoptosis cannot be considered as fixed parameters because they have strong variations for different cells inside the same island. Although the molecular network controlling this process had to be greatly simplified in Figure 2.11 compared to Figure 6.2, it nevertheless retained the essential characteristics that would be expected from such a network, and proved to be sufficient to derive the correct responses as a function of the cell's environment. One key issue is the parametrization of the model, since most parameters had to be fitted to obtain

the global expected behavior. A systematic parameter sweep was beyond the scope of the present work, but it could be performed to assess critical parameters, that would have to be measured.

Our modeling results were able to predict a more rapid recovery from acute anemia by mice compared to humans due to the more central location in murine erythroblastic islands of the main producers of Fas-ligand, the early stage-erythroblasts, as compared to the more peripheral location in human erythroblastic islands of the main producers of Fas-ligand, the late-stage erythroblasts. This prediction was confirmed by *in vivo* experimental evidence and clinical observations. A testable prediction of our model is that engineered mice that would express Fas-Ligand at later stages during the erythroid differentiation sequence would display a much slower recovery than wild-type mice. Whether this accelerated recovery from acute anemia by mice compared to humans might help explain the more rapid development of murine CFU-E into erythroid colonies *in vitro*, 2-3 days in mice [146, 112] versus 6-8 days in humans [134, 80], could also be addressed.

Furthermore, our results show that our model is consistent with experiments demonstrating enhanced proliferation *in vitro* of those erythroid cells that are most closely associated physically with central macrophages. It is interesting to note that in order to model the *in vitro* situation, two key assumptions had to be added: that differentiating cells can die by apoptosis, and that apoptotic cells are more slowly removed *in vitro* than *in vivo*. Although both assumptions stemmed as necessities for proper modeling, they were confirmed by experimental evidence [124].

In sum, our work demonstrates that a proper modeling of erythropoiesis requires departing from an average value for the decision-making rates, and to account for spatial organization of the cells, both for modeling *in vitro* and *in vivo* experiments.

2.2.5 Stability of multiple islands

Introduction

The stability of erythroblastic islands is studied with a model containing an intra- regulation by the two proteins Erk and Fas. It is known that macrophages influence surrounding cells in erythroblastic islands in many different ways [40, 124]. In our previous works we conjectured that one of its major roles can be to stabilize the island [24, 70]. Without a macrophage, a single island will unlimitedly grow or shrink and disappear after several cell cycles. *In vivo*, a big number of island interact with each other. So the question is whether this interaction can result in a stable production of red blood cells. In this work, we investigate a system of many islands. We begin with numerical simulations and then suggest and study a simplified analytical model. The main conclusion of this work is that feedback by erythropoietin can possibly stabilize a single island, but a system of many islands without macrophages is unstable. Maintenance of a constant level of erythrocytes in blood seems to be impossible to achieve with this model, and macrophages should be an important stabilizing factor.

Simulations of erythroblastic islands

Without feedback by erythropoietin. We first simulate a system of islands without feedback by erythropoietin. This means that α in equation (2.2.5) is constant. Two neighboring islands can interact mechanically (cells push each other) and biochemically through Fas-ligand. Figure 2.21 shows an example of 2D numerical simulations with a hybrid model for a system of nine islands. The initial configuration is shown in the left figure, and the same islands after some time in the right figure. We see that the islands can grow, merge or disappear. Their size and number change in time.

The number of erythroid progenitors in each island is shown in Figure 2.22 (left). During about ten cycles the islands remain approximately constant in size. After that, some of them exponentially grow (with time oscillations due to cell cycle), some other disappear.

Mature cells, reticulocytes leave the bone marrow into the blood and become erythro-

cytes. Figure 2.21 (left) shows the evolution of the number of erythrocytes in blood. It constantly grows and does not stabilize to a constant value, as it should be in accordance with biologically realistic behavior.
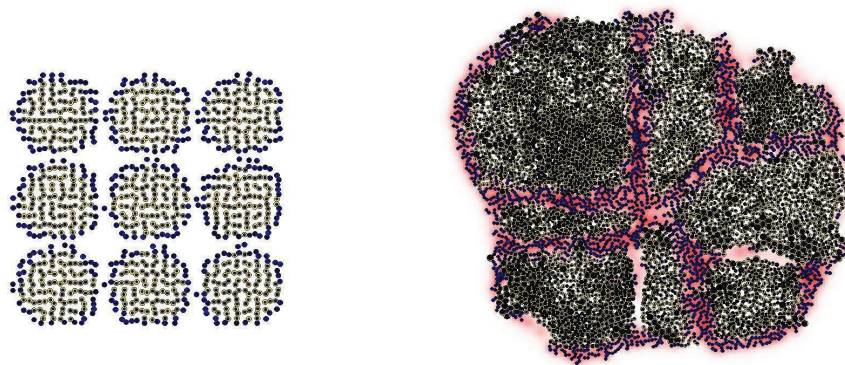
Figure 2.21: Simulation of erythroblastic islands. Initial configuration (left) and a snapshot of the islands after some time. Mature cells (reticulocytes) are shown in blue, immature cells (erythroid progenitors) are yellow and Fas-ligand is the red halo.
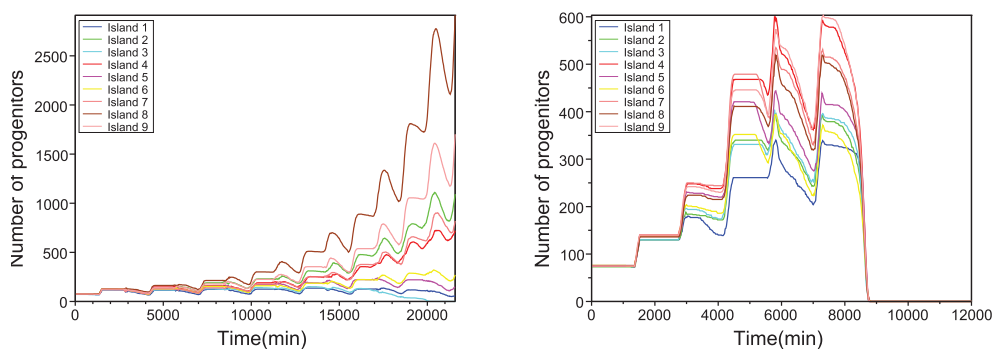
Figure 2.22: Number of progenitors in each island. Without feedback (left), some islands grow, some other disappear. In the case with feedback (right), after some time all islands disappear.

With feedback by erythropoietin. *In vivo*, the number of erythrocytes in blood determines the quantity of erythropoietin produced in the kidney [140]. This hormone comes to the bone marrow with blood flow and influences the fate of erythroid progenitors. On one

hand, it stimulates their self-renewal (function α in equation (2.2.5)), on the other hand, it downregulates apoptosis increasing the critical value of Fas, F_c. Both of the factors increase production of erythrocytes.

Denote by N the number of erythrocytes in blood and by N_0 its equilibrium value. Then the level of erythropoietin in blood depends on $N - N_0$. Hence α and F_c can also be considered as functions of $N - N_0$. For simplicity, we consider the linear dependencies:

$$\alpha = \alpha_0 + k_\alpha(N_0 - N), \qquad (2.2.18)$$

$$F_{cr} = F_0 + k_F(N_0 - N), \qquad (2.2.19)$$

where the parameters k_α and k_F should be chosen to stabilize the number of erythrocytes in blood.

However, varying these parameters we could not obtain this stabilization. The typical behavior of the system is shown in Figures 2.22 (right) and 2.23 (left). In the beginning, the number of progenitors and of reticulocytes (not shown) in the bone marrow grow. Consequently, the number of erythrocytes in blood also grow and exceeds the equilibrium value N_0. As a result, the concentration of erythropoietin drops, self-renewal of erythroid progenitors decreases, their apoptosis increases. The number of progenitors in the bone marrow and the number of erythrocytes in blood rapidly decay to zero, and the system cannot recover anymore. Thus, feedback by erythropoietin did not allow us to stabilize the number of erythrocytes in blood in the framework of the model under consideration.

Approximate analytical solution

In this section we consider a simplified model of erythropoiesis *in vivo* where we use a schematic geometric structure of erythroblastic islands. We assume that they keep a circular shape. Their global control is provided by the hormone erythropoietin whose quantity depends on the total number of erythrocytes produced by all islands. We will show that this system is unstable.
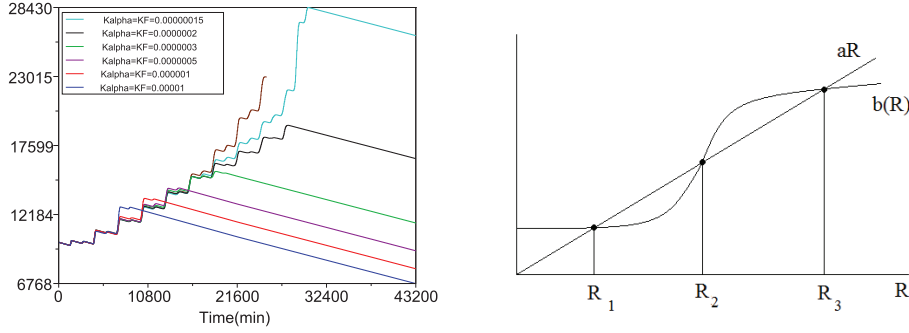
Figure 2.23: Left: number of erythrocytes in blood as a function of time for different values of feedback coefficients or without feedback (upper curve). Right: graphical solution of equation 2.2.21.

Single island. Simplifying the structure of an erythroblastic island, we suppose that erythroid progenitors fill a circle of radius R. Then the number n of progenitors in the island is proportional to its area $S = \pi R^2$: $n = \frac{\pi R^2}{\sigma}$, where σ is the area of a single progenitor cell. The rate of self-renewal of the progenitors is proportional to their number, that is to the area S of the circle. Reticulocytes are located at the boundary of the circle. Their number m is proportional to its length, $m = \frac{2\pi R}{d}$, where d is diameter of reticulocytes.

Since stimulation by Fas-ligand takes place at a small distance, we can suppose that only the progenitors located near the boundary die by apoptosis. Hence the apoptosis rate is proportional to $2\pi R$. We can now write the equation for the number of progenitors: $\frac{dn}{dt} = k_1 n - k_2 m$, where k_1 is determined by the duration of cell cycle, k_2 by the time during which the intracellular concentration of Fas reaches the critical level necessary to kill the cell. From the last equation we obtain:

$$\frac{dR}{dt} = aR - b, \qquad (2.2.20)$$

where $a = k_1/2$, $b = \sigma k_2/d$. This equation has a stationary solution, $R_0 = b/a$. It can be easily verified that it is unstable. If $R > R_0$, then the circle will indefinitely grow, if $R < R_0$ it will shrink. Thus, a single island in this model is unstable.

82

Stabilization by the apoptosis rate. The apoptosis rate b depends on the concentration of erythropoietin that depends, in its turn, on the number of erythrocytes N in blood. The number of erythrocytes depends on the number of reticulocytes. For the sake of simplicity, we suppose that this dependence is instantaneous, that is N is a function of m at the same moment of time. Then b can be considered as a function of R. Hence instead of equation (2.2.20) where b is a constant we obtain the equation

$$\frac{dR}{dt} = aR - b(R), \tag{2.2.21}$$

where $b(R)$ is some given function. According to its biological meaning, it is an increasing function. Dependance of apoptosis on erythropoietin concentration is specified in [55] on the basis of the data available in literature. Qualitatively, it has the S-shape shown in Figure 3 (right). Its exact form is not essential for what follows.

Equation (2.2.21) can have one or several stationary solutions. In the example, in Figure 3, there are three solutions. Only one of them is stable, $R = R_2$, since $b'(R_2) > a$. Two others are unstable. The solution of this equation with an initial condition $R(0) = R_0$ will converge to the stationary solution $R = R_2$ if $R_1 < R_0 < R_3$. If $R_0 < R_1$, the solution will decrease, and if $R(0) > R_3$, then it will grow.

System with more than one island. Let us return to a model similar to (2.2.21) when there are n islands with radii $R^1, ..., R^n$. Then we will have the system of equations

$$\frac{dR^j}{dt} = aR^j - b(S), \quad j = 1, ..., n, \tag{2.2.22}$$

where $S = \frac{1}{n}(R^1 + ... + R^n)$. The last term in equation (2.2.22) implies that erythropoietin production and apoptosis rate depend on the total (or average) erythrocyte concentration which is proportional to S.

Each stationary solution R_1, R_2, R_3 of equation (2.2.21) originates a stationary solution of system (2.2.22): $R^1 = ... = R^n = R_k$, $k = 1, 2, 3$. Let us show that solution R_2, which

is stable for equation (2.2.21), becomes unstable for system (2.2.22). We note first of all that taking a sum of all equations in (2.2.22) we obtain:

$$\frac{dS}{dt} = aS - b(S). \qquad (2.2.23)$$

As before, $S = R_2$ is a stationary solution of this equation. Therefore, the solution $S(t)$ of this equation with the initial condition $S(0) = R_2$ is identically equal to R_2. Let us now take initial conditions $R^j(0) = R_0^j$, $\quad j = 1, ..., n$ of system (2.2.22) in such a way that $\frac{1}{n}(R_0^1 + ... + R_0^n) = R_2$. Then $S(t) \equiv \frac{1}{n}(R^1(t) + ... + R^n(t)) \equiv R_2$. Hence system (2.2.22) can be written as

$$\frac{dR^j}{dt} = aR^j - b(R_2), \quad j = 1, ..., n. \qquad (2.2.24)$$

Hence all equations of this system are independent of each other. The functions $R^j(t)$ with the initial condition greater than R_2 exponentially grow, with the initial conditions less than R_2 exponentially decay till they become equal to 0. Since the solution is exponentially growing for a particular initial condition constructed above, then the matrix of the linearized system has a positive eigenvalue. Hence the dimension of the stable manifold is less than n. Therefore the solution with a generic initial condition, which does not belong to this manifold, will not converge to the stationary solution. Thus we have proved that stationary solutions of system (2.2.22) are unstable.

Chapter 3

Blood diseases

3.1 Multiple Myeloma

3.1.1 Biological background

Multiple myeloma (MM) is a relatively common disease that is characterized by bone marrow infiltration with malignant plasma cells and, very frequently has a malignancy-associated chronic anemia, i.e., a chronic decrease of circulating red blood cells. The degree of anemia is correlated with the degree of marrow infiltration [15] and with the proliferative rate of the myeloma cells, [71] both of which can be quantified before and after therapy. Many patients treated for MM respond with improved or resolved anemia. Thus, the marrow infiltration by MM can be examined from its most prevalent stage at diagnosis to its resolution or lowest degree of infiltration in those patients who respond to therapy, see Figure 3.1.

Among human diseases, the progression of chronic infections or metastatic tumor growth is variable, and infiltration of bone marrow by either process is rare when compared to infiltration by hematologic diseases. Some hematologic diseases such as lymphomas and leukemias often grow in the spleen as well as the bone marrow and, therefore, they can confound determinations of bone marrow involvement because the spleen, which enlarges and traps circulating cells will also reduce the numbers of circulating blood cells. Among the

various blood cell types, the red blood cells are the most accurate for determining decreased counts because they have a relatively narrow normal range compared to leukocytes and platelets, which can vary two-to-three fold and still remain in the normal range.

Erythropoiesis occurs in the bone marrow within small units of cells called erythroblastic islands. Erythroblastic islands consist of a central macrophage surrounded by erythroid cells beginning at the progenitor stage of colony-forming units-erythroid (CFU-Es) and extending through reticulocytes [40], [128]. CFU-Es have three possible fates: expansion of their numbers without differentiation, differentiation into reticulocytes, and death by apoptosis. CFU-E fate is determined by a very complex network of intracellular proteins.

Malignant cells of MM disrupt erythroblastic island function. MM cells produce two cytokines which be cytotoxic for erythroblasts: Fas-ligand (FL) and the tumor necrosis factor-related apoptosis-inducing ligand (TRAIL). Differentiating erythroblasts have receptors for both FL and TRAIL, and triggering the receptors activates apoptotic pathways in erythroblasts. If receptors of FL and TRAIL are activated, they induce apoptosis of erythroblasts. Abnormal up-regulation of apoptogenic receptors, including FL and TRAIL, by highly malignant myeloma cells is involved in the pathogenesis of the ineffective erythropoiesis and chronic exhaustion of the erythroid matrix, see Figure 3.2.

In addition, GATA-1 (a survival factor for erythroid precursors) was remarkably down-regulated in fresh erythroblasts from the severely anemic patients. These results indicate that progressive destruction of the erythroid matrix in aggressive MM is due to cytotoxic mechanisms based on the up-regulation in myeloma cells of FL, TRAIL, or both. It is conceivable that the altered regulation of these receptors defines a peculiar cytotoxic phenotype that drives the progression of aggressive MM [138].

Myeloma is treated with chemotherapies, which improves the patient's condition but does not heal the disease. Stem cell transplant are also used to try to cure patients. Anemia associated with myeloma is treated with erythropoietin (EPO) injections. This treatment rises patients life expectancy but, as chemotherapies, does not cure the disease.

In modeling of erythroblastic island function, immunoglobulin proteins produced by
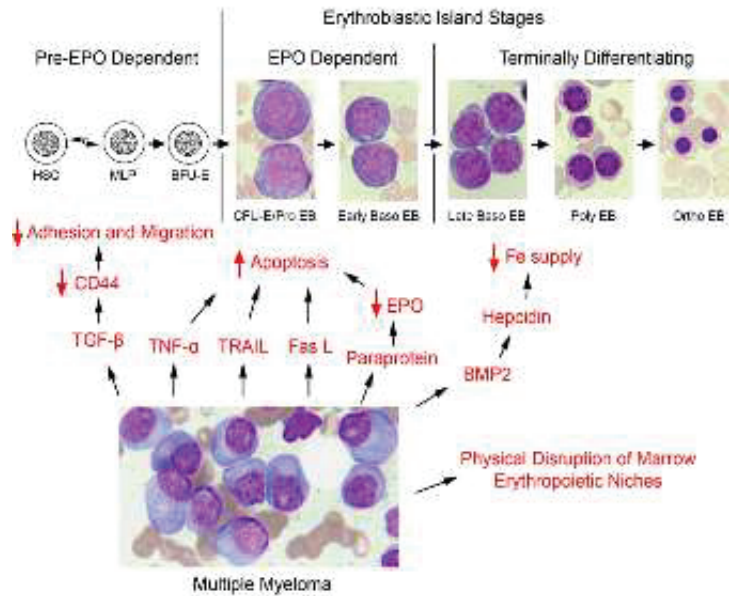
Figure 3.1: Effects of MM infiltration of the bone marrow that can lead to chronic anemia.

multiple myeloma can reduce renal function and, thereby, indirectly inhibit erythropoiesis via decreased EPO concentrations reaching the erythroblastic islands. Indeed, inappropriately low serum EPO concentrations have been reported in patients with multiple myeloma, and the degree of EPO deficiency is correlated with the amount of bone marrow infiltration and the proliferation rate of the multiple myeloma cells [15] and [71]. However, EPO concentrations can be corrected by successful treatment of the myeloma and/or administration of exogenous EPO. If the patients are successfully treated, the anemia resolves with the clearance of myeloma from the bone marrow.

3.1.2 Mathematical model

In this section we will model development of multiple myeloma in the bone marrow. At the first stage of this modeling, we will introduce erythroblastic islands in normal situation and will describe their functioning similar to the modeling presented in Section 2.2. We take into account here that some islands can extinct due to random perturbations in the dynamics
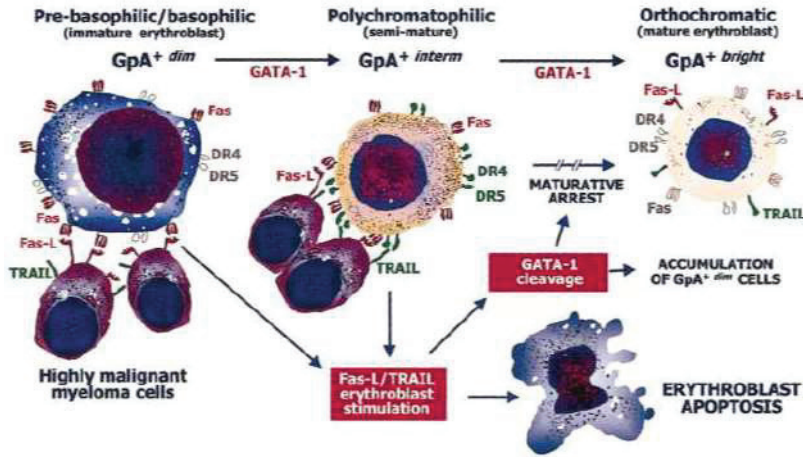
Figure 3.2: Schematic representation of defective erythropoiesis in MM from Blood [138].

of erythroid progenitors. In this case we reinitiate them introducing new progenitors. This corresponds to the action of colony forming units (CFU-E) cells that go around the bone marrow leaving erythroid progenitors (burst forming units, BFU-E) behind them.

After that, when we obtain a steady functioning of the system formed by a number of erythroblastic islands, we introduce multiple myeloma cells. They proliferate and form a tumor that grows and gradually fills the whole space. When it arrives to erythroblastic islands, it destroys them by the direct mechanical contact. Myeloma cells proliferate and push out normal erythroid cells. Moreover, malignant cells produce Fas-ligand and TRAIL protein which stimulate apoptosis of erythroid progenitors. Thus development of multiple myeloma leads to the destruction of erythroblastic islands and to severe anemia. It can be partially compensated by treatment with hormone erythropoietin (Epo) which downregulates apoptosis of erythroid progenitors.

Normal erythropoiesis

Cell dynamics is regulated by some proteins and growth factors that determine their self-renewal, differentiation and apoptosis. Their concentrations can be described by the system of ordinary introduced in Section 2.2.4:

88

$$\frac{dz}{dt} = a_0, \tag{3.1.1}$$

$$\frac{du}{dt} = a_1 + b_1 z, \tag{3.1.2}$$

$$\frac{dv}{dt} = a_2 - b_2 z v, \tag{3.1.3}$$

$$\frac{dw}{dt} = a_3 - b_3 z w. \tag{3.1.4}$$

Here u is the concentration of activated BMPR4 receptor (BMP-R), v is the concentration of GATA-1, w is the concentration of the activated caspase, z is the concentration of activated glucocorticosteroid receptor (GR). The parameters of the intracellular regulation depend on the extracellular regulation:

$$a_1 = a_1^0 + a_1^1 G, a_2 = a_2^0 + a_2^1 E, a_3 = a_3^0 + a_3^1 F. \tag{3.1.5}$$

Here G is the concentration of growth factor, E is the concentration of erythropoietin, F is the concentration of Fas-ligand.

After some time, reticulocytes leave the bone marrow in the blood flow where they become mature erythrocytes. In numerical simulation this time is taken equal one cell cycle, after which they are removed from the computational domain. Reticulocytes produce Fas-ligand. The distribution of its concentration is described by the equation:

$$\frac{\partial F}{\partial t} = D_F \Delta F + W_F - \sigma_F F, \tag{3.1.6}$$

where the first term in the right-hand side of this equation describes diffusion of Fas-ligand in the extracellular matrix, the second terms its production and the last terms its degradation. We should specify that Fas-ligand is a transmembranian protein which acts by direct cell-cell contact. Its description by the diffusion equation is a mathematical approximation. If the diffusion coefficient is sufficiently small, then it will be localized around the Fas-ligand

producing cells and act only on the neighboring cells. This approach allows us to avoid the detailed description of cell geometry. Let us also note that the production term is considered as a step-wise constant function with the support located at the area of Fas-ligand producing cells.

Let us recall that erythroblastic islands consist of erythroid progenitors and reticlocytes around central macrophages. During the development of multiple myeloma, malignant cells proliferate and push all other cells by the direct physical contact. This is one of the mechanisms which act on erythroblastic islands. Erythroid progenitors are small cells approximately of the same size as multiple myeloma cells.

Macrophages produce growth factor G which stimulated proliferation of erythroid progenitors. Its concentration is described by the reaction-diffusion equation

$$\frac{\partial G}{\partial t} = D_G \Delta G + W_G - \sigma_G G \tag{3.1.7}$$

which takes into account its diffusion, production and degradation.

Number of erythrocytes in blood. Anemia is one of the consequences of the disease, characterized by the low levels of healthy red blood cells (RBCs) and less than normal level of hemoglobin in blood.

Erythrocyte lifetime in blood for humans is 120 days. In order to accelerate the simulations, we reduce it to 40 day (as it is for mice). New erythrocytes are added when they leave the bone marrow (more precisely, reticulocytes become erythrocytes already in blood flow), and they are removed when their age reaches 40 days. Erythroblastic islands are shown in Figure 3.3 and the total number of erythrocytes produced by 8 islands in Figure 3.4. We can see that after about 20 days, the total number of erythrocytes reaches its steady level.

Disease

There are two mechanisms by which multiple myeloma cells invade the bone marrow. Cells of the tumor push out normal cells by pure mechanical interaction and cancer cells increase
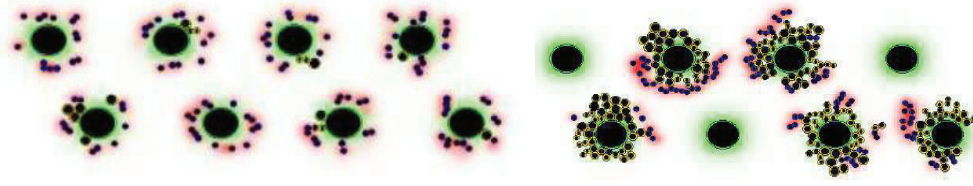
Figure 3.3: Numerical modeling of normal erythropoiesis with 8 erythroblastic islands. The initial cell distribution is shown in the left image, the same islands 5 days later in the right image. In some of the islands, erythroid progenitors disappear. In this case, they are added again due to the presence of CFU-E cells in the bone marrow. Fas-ligand produced by reticulocytes is shown in red and growth factor produced by macrophages in green.
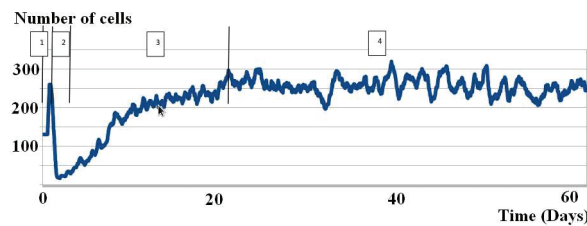
Figure 3.4: Total number of erythrocytes produced by 8 islands. After approximately 20 days it reaches a steady state level with some oscillations around it due to cell cycle.

apoptosis of erythroid progenitors by Fas-ligand and other biochemical signals. A comparative study of two cases of MM is conducted. We first studied MM with malignant cells acting only mechanically and then with cancer cells producing Fas-ligand and TRAIL. In both of them, the tumor does not spawn until the cells erythropoiesis reaches the stability phase. The objective is to study the impact of Fas-ligand on the evolution of different populations of cells. In other words, by comparing the populations of erythroid progenitors and reticulocytes, we establish the role of Fas-ligand secretion in the development of multiple myeloma.

Let us consider the case where malignant cells do not secrete Fas-ligand. We analyze the erythroid progenitors and reticulocytes populations. We notice that while in the stability phase, the progenitors' number is higher than the reticulocytes, the extinction of the progenitors takes place faster. This can only be explained by the Fas-ligand effect of the reticulocytes in the elimination of progenitors by triggering apoptosis. Nevertheless, because of the spatial organization and the location of macrophages, some of the progenitors

91

are surrounded by malignant cells. These cells are also pushed until they differentiate and either die or leave the bone marrow.

The same behavior of the populations can also be observed in the case of MM cells producing Fas-ligand. However, contrary to the case without Fas-ligand produced by MM cells, the difference between the time of extinction of progenitors and reticulocytes is not as important. In fact, if that difference is due to the Fas-ligand secreted by reticulocytes, the Fas-ligand secreted by the tumor overshadow the effect of the Fas-ligand of reticulocytes in the case of MM with Fas-ligand. This can be clearly noticed when analyzing qualitatively the maximal values of Fas-ligand in both cases. The result is that the same fate which is extinction is awaiting all cells whether they are progenitors or reticulocytes.

The first important effect of Fas-ligand does not take place until the few hours of the simulation. In fact, we have seen that the cells that are near the tumor disappear at a high rate when there is a secretion of Fas-ligand. While in the case of MM without Fas-ligand, the elimination of cells is primarily due the physical pushing of reticulocytes by the tumor against the progenitors. We have shown that while the difference in the apoptosis of progenitors in the two cases is not that significant, the reticulocytes difference is wider and clearer. In fact, the Fas-ligand protein is not only responsible of apoptosis, but also of differentiation. This is why the extinction of reticulocytes in the case of MM with Fas-ligand takes place earlier due to the early differentiation of a large number of progenitors. The progenitors late extinction is explained by the compensation of the Fas-ligand of the reticulocyte by the one of the MM.

Regulation by EPO

In the previous paragraph, we studied the development of multiple myeloma assuming that the concentration of erythropoietin was constant. However the number of erythrocytes in blood determines the quantity of erythropoietin produced in the kidney [140] and the number of erythrocytes depends on the quantity of EPO. Indeed, a feedback loop regulates the production of erythrocytes: if this number decreases, as in anemia, the amount of EPO
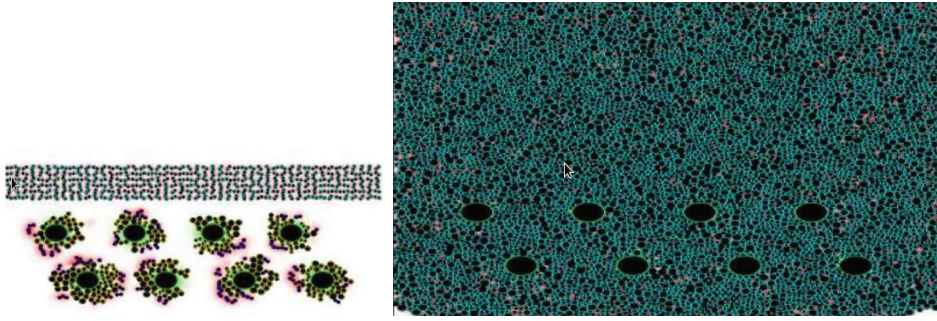
Figure 3.5: Left: appearance of the tumor (light blue cells in the top of the figure). Right: tumor invasion after 2 months.

(a) MM cells do not produce Fas-ligand and TRAIL

(b) MM cells produce Fas-ligand and TRAIL
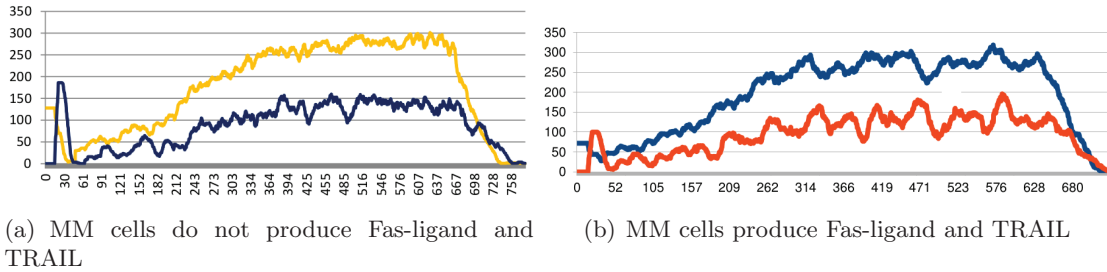
Figure 3.6: We can see the declining number of progenitors and of mature cells during the growth of tumors. Left: with cancer cells acting by mechanical actions (yellow curve - progenitors, blue curve - reticulocytes). Right: with cancer cells producing Fas-ligand and TRAIL (blue curve - progenitors, red curve - reticulocytes).

produced increases in order to stimulate erythropoiesis.

In the model of normal erythropoiesis developed in Section 2.2.4, apoptosis of erythroid progenitors is determined by the intracellular concentration of activated caspace (variable w in equation (2.2.16)). If this concentration exceeds some critical level w_{cr}, then the cell dies by apoptosis. The hormone erythropoietin produced in the kidney downregulates apoptosis of erythroid progenitors. In the model, we take this effect into account assuming that w_{cr} depends on the difference $N - N_0$ of the current number N or erythrocytes in blood and their number N_0 in normal conditions:

$$w_{cr} = w_{cr_0} - k(N - N_0) \tag{3.1.8}$$

Figure 3.7 shows the number of erythroid progenitors in the bone marrow and the number of erythrocytes in blood for fixed but different values of the critical value w_{cr}.
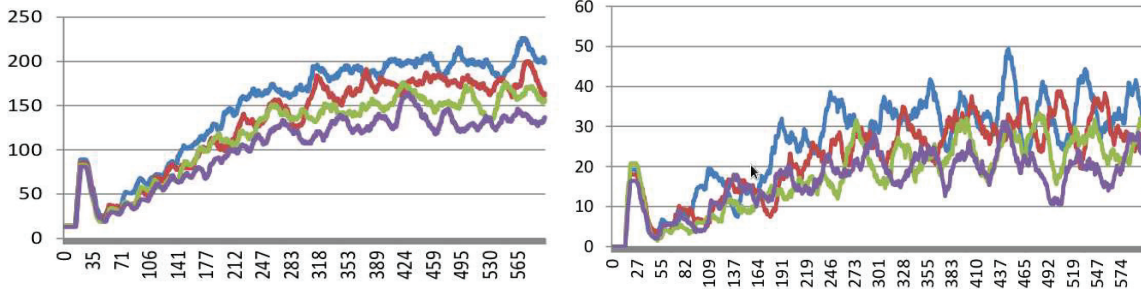
Figure 3.7: Purple curve: $w_{cr}=$ 0.08, green curve: $w_{cr}=$ 0.09, red curve: $w_{cr}=$ 0.1, blue curve: $w_{cr}=$ 0.11. Left: number of progenitors. Right: number of more mature cells, as functions of time.

The comparison of the both cases highlights the effect of EPO in regulating the population of cells. In fact, by increasing and decreasing the apoptosis rate, EPO manages to change the value to which the population converges.

Through these comparisons, we have shown that in the case of variable EPO, the population of normal cells takes a longer time to reach extinction than in the case of fixed variable. This can only explained by the variation of the threshold w_{cr}. Injection of EPO are used to treat myeloma. Treatment by exogenous EPO can be presented as an increasing of value of w_{cr}.

$$
w_{cr}(t) = \begin{cases} w_{cr_0} - k(N - N_0), t \leq T \\ \\ w_{cr_0} - k(N - N_0) + w_{cr_1}, t > T \end{cases} \tag{3.1.9}
$$

where T is the time of injection and w_{cr_1} describes the effect of exogenous EPO. In Figure 3.8, we can observe the increase of the number of erythrocytes, after an injection of EPO the population extinct with a delay.
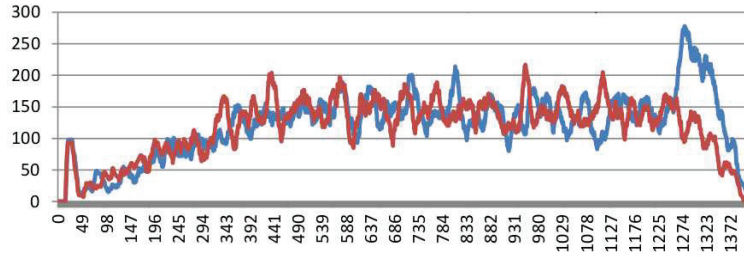
Figure 3.8: Blue curve: number of erythrocyte after injection of EPO. Red curve: number of erythrocyte without exogenous EPO.

3.1.3 Partial differentiation of myeloma cells

In Chapter 2 we presented two models of erythropoiesis with two different schemes of intracellular regulation. One of them was based on the interaction of Erk and Fas, another one on a more complete regulation with BMP4, Fas, GATA-1 and activated caspases. Though intracellular regulations are different, functioning of erythroblastic islands in these two cases is similar. The results on the development of multiple myeloma presented above are obtained for the second intracellular regulation (Section 2.2.4). We have also studied it in the case of the first intracellular regulation. The results obtained in this case are very similar to the other case, and we do not present them here.

We will study in this section how the rate of proliferation of multiple myeloma cells influences the tumor growth and anemia which accompany this blood disorder. We will consider this question in the case of the Erk-Fas intracellular regulation. We will suppose that at each cell cycle, a cancer cell has a probability p to divide into two daughters cells identical to the mother cell (self-renewal) and the probability $1 - p$ to divide into two differentiated cancer cells that stop their division after one cell cycle.

If $p = 1$, then all myeloma cells divide giving similar cells. This means that their number growth exponentially until they fill completely the whole computational domain (Figure 3.9). At the same time, erythroid progenitors and reticulocytes in the bone marrow rapidly disappear while the number of erythrocytes in blood gradually decay because their production in the bone marrow is stopped. If $p = 0.25$, then multiple myeloma cells stop

95
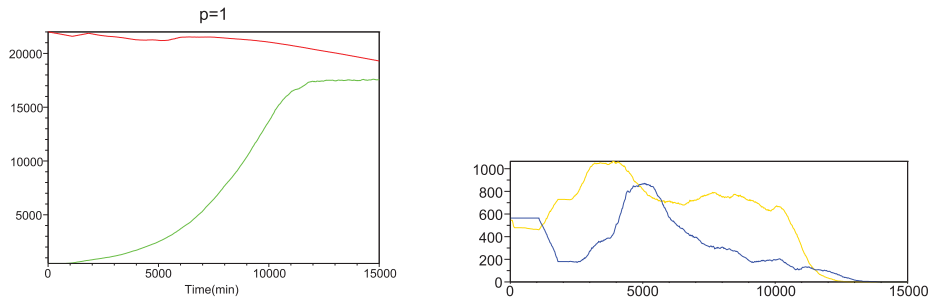
Figure 3.9: Figure 3.9: Cell number in time during multiple myeloma development: erythrocytes in blood (red), multiple myeloma cells (green), progenitors (yellow), mature cells (blue).

their proliferation after several cell cycles and erythropoiesis is almost normal. It is weakly influenced by the presence of non-diving myeloma cell in the bone marrow. The number of erythrocytes in blood for different values of p is shown in Figure 3.10. It rapidly decreases for $p > 0.5$ and it tends to its normal value for $p < 0.5$.
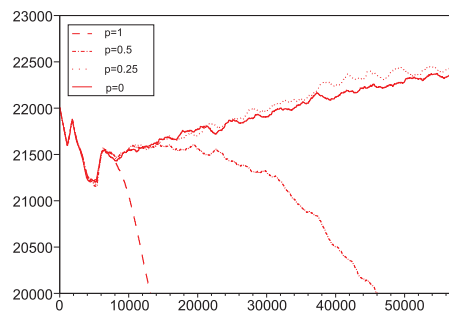
Figure 3.10: Number of erythrocytes in blood as a function of time for different values of the parameter p.

96

3.2 Lymphoma

3.2.1 Biological background

Healthy functioning thymus

Given the clinical presentation of the disease, the modeling assumes a tumor arising in the thymus. Therefore we begin by simulating the functioning of a healthy thymus. The thymus is an important organ in the formation of the immune system in very young childrens. Its action becomes negligible in adults. The thymus is composed of several lobules, containing a cortex and a medulla separated by a cortico medullary jontion. The thymus is the site of maturation, in particular the cortex [31], and education: selection process, of T lymphocytes. This area contains the three types of thymocytes studied: double negative (DN), double positive (DP) and single positive (SP). This classification depends on the expression of the receptors CD4 and CD8, DP: $CD4^+CD8^+$, DN: $CD4^-CD8^-$, SP: $CD4^+CD8^-$ or $CD4^-CD8^+$. Other thymic cells, such as nurse cells, cortical and medullary epithelial cells are involved in proliferation, differentiation and apoptosis of thymocytes.

During education process of thymic cells, stem cells located in the bone marrow can give rise to thymic precursors. Precursors will go through several stages of differentiation and proliferation to give rise to all the T cells. Precursors enter the thymus through blood vessels. During the early stages of T cell development precursors become DN1, which are multipotent cells able to differentiate into T lymphocyte, NK (Natural Killer) lymphocyte and dendritics cells. Pro T thymocytes (DN2) mature to become DP or NK. Finally, DP become SP and exit the thymus through blood vessels [86] (see Figures 3.11 and 3.12).

Education of T cells. Cancer cells appear when cells proliferate rather than differentiate, causing the emergence and development of a tumor. Control of maturation, migration, proliferation and differentiation of T cells ligneage is due to their interactions with other cells in the thymus, especially with epithelial cells, nurse cells and dendritic cells. For each new stage of differentiation and maturation, a transcription factor of a T cell, activated by
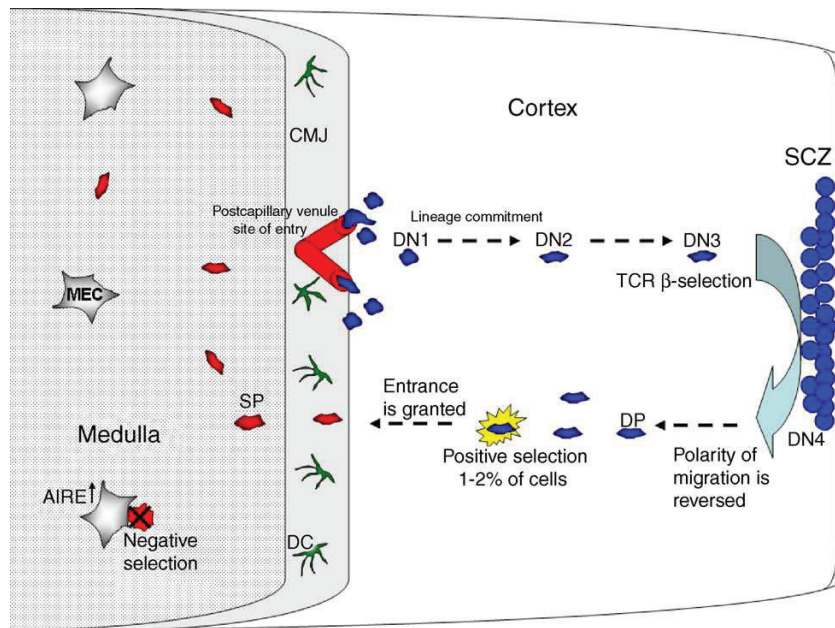
Figure 3.11: Intrathymic migration of developing thymocytes. T lineage precursors enter the thymus through post-capillary venules of the corticomedullary junction (CMJ) and then migrate outward to the subcapsulary zone (SCZ) where they undergo TCR beta chain rearrangement and selection. At this time polarity of migration is reversed and CD4+CD8+ (DP) thymocytes move back into the cortex for alpha chain rearrangement and for testing of nascent TCR through positive selection. Post-selected thymocytes are granted access to the medulla where they are screened for self-reactivity through negative selection. Pattern and legend from [166].

a signal from the microenvironment, is involved.

Selection. Each day 5.10^7 mature cells are produced but only 10^6 cells leave the thymus. 98% of the thymocytes die by apoptosis after three types of selections: β, positive and negative selections. During their development, lymphocytes express several receptors which allow cells to receive signals from their environment. Cells that fail to produce a functional pre-TCR (T cell receptor) are eliminated by apoptosis. This is called the β-selection. In positive selection, upon contact with cortical epithelial cells, lymphocytes DN receive a signal of life or death. In negative selection, upon contact with epithelial cells of medulla, surviving lymphocytes DP also receive this signal. More precisely, cells with a TCR (T cell membrane receptor) with sufficient affinity for self MHC (major histocompatibility complex)

molecules of epithelial cells, survive. In summary, the cells with too high or too low affinity with MHC die as a result of different selection processes.

Signal transmission. In the normal thymus, mature cells produce cytokines (soluble substances cell signaling). Cytokines may be interleukins, growth factors or inhibitory factors. They provide the biological support of proliferation, differentiation or death signal. There is a balance between cytokines families with antagonist roles.

Proliferation and differentiation of thymocytes is a response to epythelial cells (Figure 3.13). It is suggested that intracellular signals through different MAP (Mitogen-activated protein) kinase cascades selectively guide positive and negative selection of T lymphocytes [85].

MAPK acts during the signaling cascade that induces proliferation or differentiation. It is a regulator of the differentiation of immature thymocytes from double-negative to double-positive cell, most probably acting as a transducer of pre-T cell receptor signaling[56]. Signals through ERK signaling cascade and through p38 signaling cascade are critically involved in TCR signals inducing positive selection and negative selection, respectively [56]. Three proteins are mainly involved in the MAP cascade:

- ERK: activation of ERK by TCR promotes positive selection, differentiation of DN to DP and proliferation,

- p38: activation blocks differentiation. Inhibition of p38 MAP is necessary for differentiation and proliferation,

- JNK: activation of JNK is involved in negative selection.

Disease

Even if the disease begins in the thymus, it can also affect the bone marrow. The tumor and the action of treatment are not limited to the thymus and can reach the whole body through the blood vessels and also affect the bone marrow. The tumor appears due to the
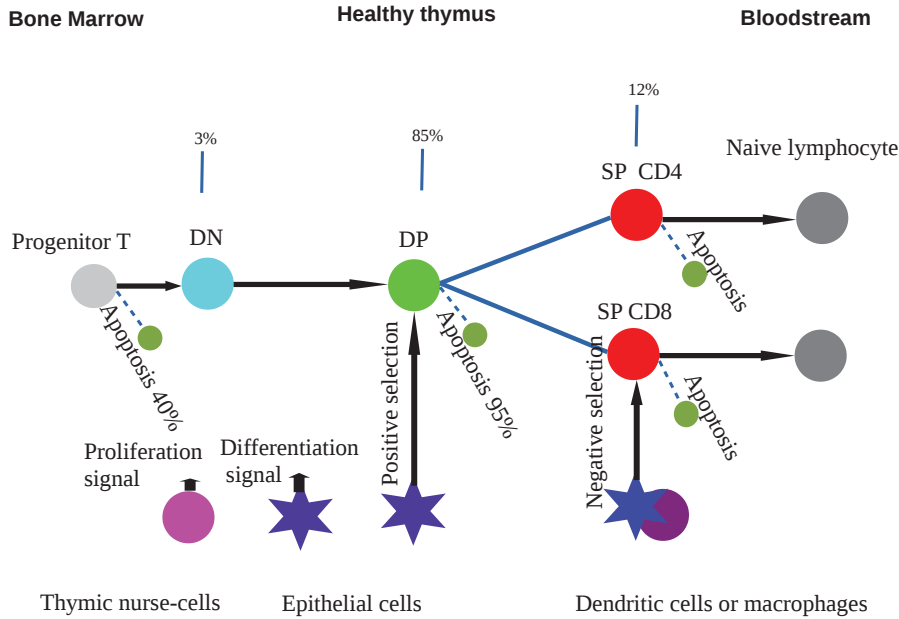
Figure 3.12: Differentiation pattern of normal cells.

malignant transformation of clonal abnormal progenitor cells capable of expansion with infinite self-renewal potential which occurs in thymus [102]. Such cells possess a genetic lesion that causes their proliferation and blocks their differentiation [47]. Genetic aberrations in leukemogenesis can affect transcription factor, protein-protein interaction, signal transduction, fate determination and cell cycle activator and differentiation [47]. The consequences of these genetic mutations are very complex and are not modeled in this study. In 90% of cases, lymphoma is caused by excessive proliferation of immature thymocytes [31].

3.2.2 Mathematical model

A hybrid model is used to model the education of T cells, the disease at a cellular level and the action of treatment. Healthy and cancer cells are modelled as discrete objects which interact with their environment. Intracellular proteins and extra-cellular regulation are described with continuous models, ordinary and partial differential equations [98, 69, 59, 6, 8, 9, 63]. Hybrid discrete-continuous models are widely used in the investigation of dynamics of cell populations in biological tissues and organisms that involve processes at

different scales.

Thymus modeling

The model of thymus considered in this work contains precursors, DN (3%), DP (85%) and SP (12%) cells (these values are taken from [90]). The proportions of cells remain approximately constant in a healthy individual. They provide a constant T cells production compensating apoptosis. Precursors are supposed to be committed to the T lineage by activation of their receptors *Notch*. Other lineages are not studied here. We only simulate the transformation of DN1 cells into DP and after that into SP.

Cell cycle duration is taken in average $T = 3$ days plus/minus random variation in time interval $[T - \delta, T + \delta]$, with a uniform distribution. At the end of cell cycle, the cell divides. Everywhere below we will set $\delta = 1$. At the moment of cell division, its choice between self-renewal, differentiation and apoptosis is specified. Early T cells are first located in a stromal cell niche [28]. They are exposed to stromal factors [28] which determine their proliferation and differentiation [56, 123]. Differentiation and self-renewal of T cells are controlled by signals emitted by their microenvironnement. Intracellular regulation which determines cell fate is described by ordinary differential equations (6.1.3), extracellular concentrations by partial differential equations (2.2.9). Apoptosis is modeled by probability distribution (cf. Paragraph "β-selection, negative and positive selections").

When cells become SP, they leave the thymus. In order to maintain a constant number of each type of cells, new cells are introduced in the computational domain by a periodic input of precursors. New cells are added if there is some space available for them. Consequently, if the number of lymphocytes in the thymus is sufficiently low, then new cells appear there. If the number of cells is high, for example in the case of tumor growth, there are no new cells. This is one of the reasons why during the progression of the disease, the thymus cannot perform its function.

To model the individual behavior of cells and also that of patients, parameters are assigned to each newly born cell. These parameters determine cell self-renewal capacity and

malignant potential. The parameters are the cell position, age, life expectancy, threshold of sensitivity to treatment, threshold of sensitivity to the external environment. These characteristics can be transmitted to daughter cells or they can be random variables.

Cell behavior depends on the intracellular and extracellular regulations described below. It also depends on its spatial location and on various cell specific parameters such as duration of cell cycle and sensitivity to treatment (Section 3.2).

Intracellular regulation

For each thymocyte we introduce an intracellular variable u which corresponds to the concentration of the proteins MAPK. Its evolution is described by the equation

$$\frac{du}{dt} = c_0 + kG, \qquad (3.2.10)$$

where c_0 is a positive constant and G is the concentration of extracellular growth factors. If u exceeds some critical value u_{crit} at the end of cell cycle, then the cell self-renews, otherwise it differentiates.

Extracellular regulation

Nurse cells produce growth factor G which promotes self-renewal of thymocytes. If they are close to nurse cells, then the intracellular concentration u will grow due to the presence of growth factor. It will reach the critical value and the cell will self-renew. The thymocytes located sufficiently far from the nurse cells will differentiate. Concentration of the growth factor G is described by the reaction-diffusion equation

$$\frac{\partial G}{\partial t} = D\Delta G + W - \gamma G, \qquad (3.2.11)$$

where D is the diffusion coefficient, W is the production rate, γ is the degradation rate. Nurse cells are considered as a constant source of growth factor. The last term in the right-hand side of this equation describes its degradation.

β-selection, negative and positive selections

Figure 3.13 shows the signal transduction responsible for different selections of T cells. Epithelial cells form a fibrous network in the thymus [31]. So we assume that they are numerous enough and uniformly distributed in space such that each T cell can receive their signals of life and death upon a cell to cell contact.

In simulations, apoptosis is modeled by a probability of remaining alive for each cell type. The probability of survival is equal to 60 % for precursors, 40 % for DN, 50 % for DP and 40 % for SP. After all maturation stages, a probability of 95 % of apoptosis for healthy cells is observed.

Regulation of the proliferation and differentiation of thymocytes by epithelial cells
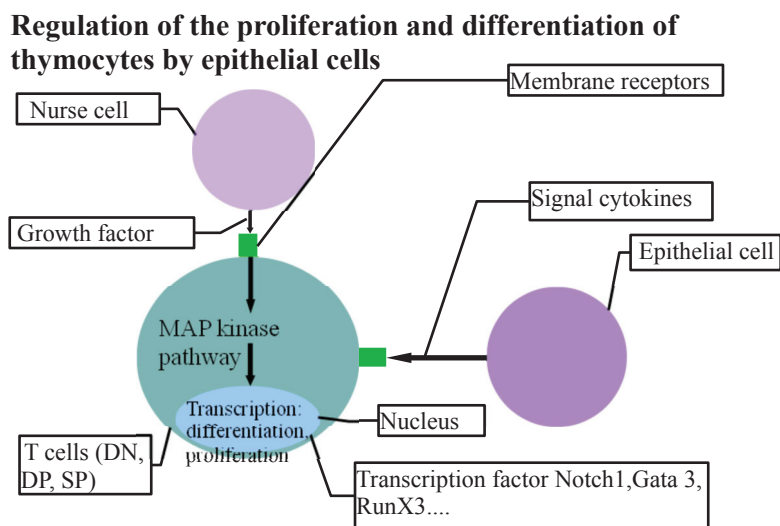
Figure 3.13: Simplified pattern of signals transduction. Each thymic cell receives signals from its microenvironnement. These signals determine the fate of cells by β, negative and positive selection.

Normal fonctioning of thymus

Spacial cell organization with different cell types is shown in Figure 3.15. Figure 3.14 shows the results of numerical simulations of healthy thymus which correspond to one year of real time. The number of different cell types is constant in average with some oscillations related to cell cycle. Proportions of DN, DP and SP cells are in agreement with their physiological

values in humans.
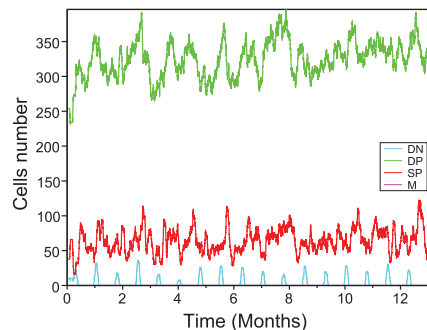
Figure 3.14: Numerical simulations of healthy thymus: a part of thymic cortex. The number of cells (DN (blue), DP (green), SP (red)) in a section of healthy thymus during one year.

3.2.3 Lymphoma development and treatment

Modeling of lymphoma

Appearance of tumor is caused by early thymocytes with excessive self-renewal and insufficient differentiation and apoptosis because of genetic mutations. In the model, we introduce a single mutated cell which begins to proliferate. Malignant cells self-renew at the end of each cell cycle with a given probability p. They have proliferating advantage compared to normal cells. They multiply and increase the volume of thymus. Gradually, the whole thymus is invaded by the tumor. Healthy cells can no longer develop normally. They disappear being replaced by malignant cells.

Figure 3.15 shows the development of tumor. It invades the thymus and destroys the spatial cell organization which is necessary for normal development of thymocytes. Therefore their number decreases. On the other hand, there is no enough space for new immature cells in the thymus. Therefore the influx of early thymocytes from the bone marrow (through the blood flow) also decreases. Both factors result in the decrease of the number of normal cells in the thymus (Figure 3.16).

104

(a) 3 days

(b) 10 days

(c) 27 days

(d) 45 days
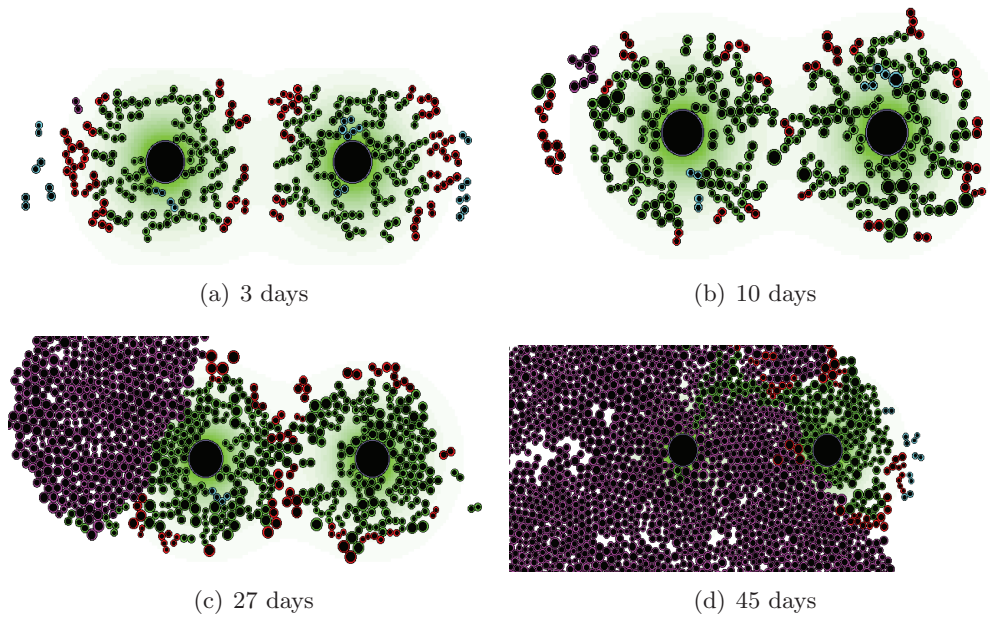
Figure 3.15: Development of tumor in the thymus. The number of malignant cells grows exponentially. They invade the thymus and push out normal cells. Cells shown in the figure: early thymocytes (gray), DN (blue), DP (green), SP (red), stromal cells (large purple cells), malignant cells (purple). Extracellular substances produced by nurse cells are shown as green halos.
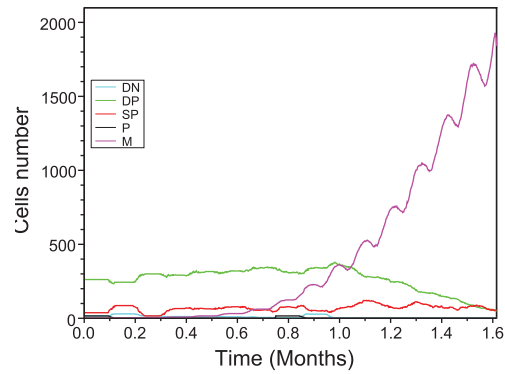
Figure 3.16: The number of cells before and during the development of tumor. The number of malignant cells grows exponentially, the number of normal cells decreases. The curve showing the number of malignant cells is purple, the corresponding curves for normal cells are blue, green and red.

Treatment

In this section we will study lymphoma treatment with chemotherapy. Medications used in the treatment represent a combination of drugs, mainly methotrexate and purinethol. Treatment consists of several phases: induction, consolidation, reinduction, maintenance [155]. We will take into account two phases: treatment of acute phase (induction) with the duration 1-1.5 months and maintenance treatment (up to 2 years after the beginning of of induction) [155]. Treatment doses for Mercaptopurine (plurimethol) are 50 mg/m^2 daily and for Methotrexate (PO) 20 mg/m^2 weekly.

The protocol of treatment is too complicated to be faithfully reproduced in the model. However the frequency of drug injection is sufficient to consider that its concentrations in the patient's body is constant during the treatment. We assume that cancer cells are exposed to the same quantity of treatment regardless of their location. Maintenance treatment begins after the complete or partial disappearance of the tumor.

<table>
<tr><td>(a) 46 days</td><td>(b) 48 days</td></tr>
<tr><td>(c) 65 days</td><td>(d) 66 days</td></tr>
</table>
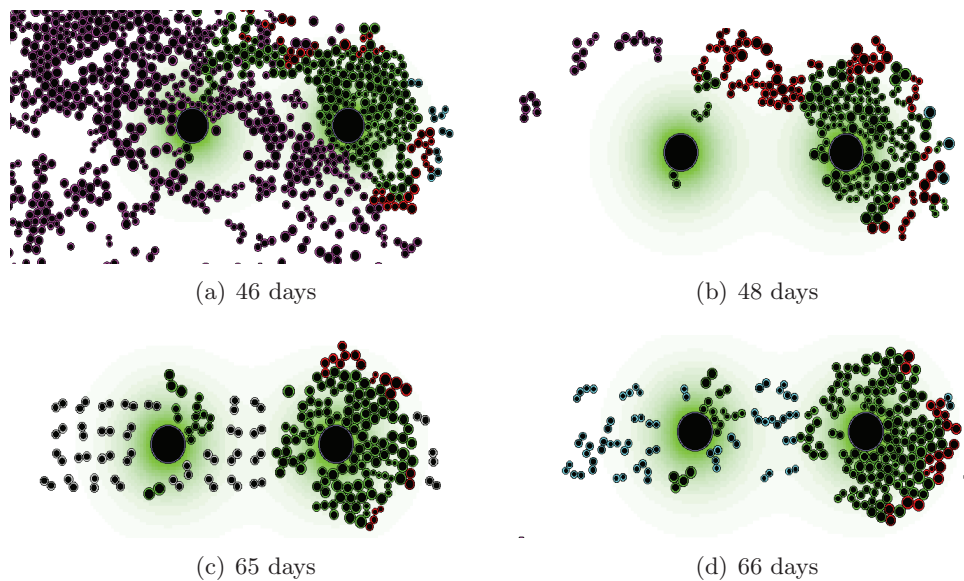
Figure 3.17: Simulations of lymphoma treatment by chemotherapy. When the tumor disappears, precursors enter the thymus and recreate its normal structure. Precursors (gray), DN (blue), DP (green), SP (red), stromal cells (large purple cells), epithelial cells (not shown, these cells form a fibrous network in the thymus), malignant cells (purple).
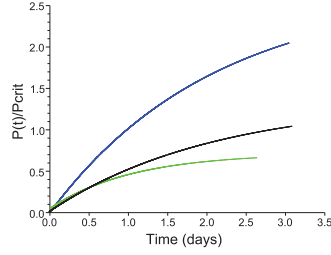
Figure 3.18: Ratio of intracellular drug concentration $p(t)$ and the threshold p_{crit} during cellular cycle for $k_+ = 2.10^{-3}$, $k_- = 10^{-3}$ (blue), $k_+ = k_- = 10^{-3}$ (black), $k_+ = 10^{-3}$, $k_- = 2.10^{-3}$ (green).

Physiologically based pharmacokinetic model (PBPK) for Methotrexate and Mercaptopurine comprises the following compartments: stomach, gut lumen, enterocyte, gut tissue, spleen, liver vascular, liver tissue, gall bladder, systemic plasma, red blood cells (RBC), kidney vascular, kidney tissue, skin, bone marrow, thymus, muscle and rest of the body [113]. All these tissues and organs were modelled using the standard flow limited equation:

$$V_T \frac{dC_T}{dt} = Q_T(C_P - \frac{C_T}{K_{p,T}}), \tag{3.2.12}$$

where V_T is the volume of tissue, C_T concentration of the drug, Q_T plasma flow, $K_{p,T}$ tissue/plasma concentration ratio for the tissues and C_P is the systemic plasma concentration [113]. We assume that a similar equation can be used at the cellular level:

$$\frac{dp}{dt} = k^+ p_0(t) - k^- p. \tag{3.2.13}$$

Here p is the intracellular drug concentration, p_0 is the concentration of drug in the thymus. The coefficient k^+ determines the ability of a cell to absorb the drug, k^- to remove it. When $p(t)$ reaches a critical value p_{crit}, the cell dies. The value p_{crit} can be different for different cells. It follows the normal distribution $N(p_{crit}, \sigma)$. The mean value is μ and σ, the standard deviation is equal to $10\%\mu$. The value of μ can be equal for all cells or can be inherited from

107

their mother cell. Cells have the ability to change their response to treatment by changing the value of p_{crit}. The intracellular drug concentration which is necessary to kill malignant cells is not known. We will vary the ratio $\frac{p_0}{p_{crit}}$ ($\frac{p_0}{p_{crit}} = 1.25$ in Figure 3.20).

Figure 3.18 shows intracellular drug concentration in time for various values of parameters. All cells for a given simulation follow the same dynamics of drug accumulation since, according to the assumptions of the model, the drug concentration is uniformly distributed inside the thymus and it does not depend on time. If the intracellular drug concentration reaches the critical level p_{crit} at the end of cell cycle, then the cell dies. Since cells differ by the duration of cell cycle and by the value p_{crit}, some cells can die while some other can survive the treatment.

The action of chemotherapy on thymus is illustrated in Figure 3.17. Malignant cells are gradually eliminated, new precursors enter the thymus and recreate its normal structure.

Duration of treatment from the data base EuroLB [60] is shown in Figure 3.19. Among 114 patients, 6 died from the disease. Data are available for three of them. They died 216, 477 and 594 days (7, 16 and 20 months) after the beginning of the maintenance treatment. Similar to the database EuroLB, we tested the durations of treatment in virtual patients at 6, 12, 18 and 24 months. As expected, the number of relapses decreases with a longer maintenance treatment (Figure 3.20).
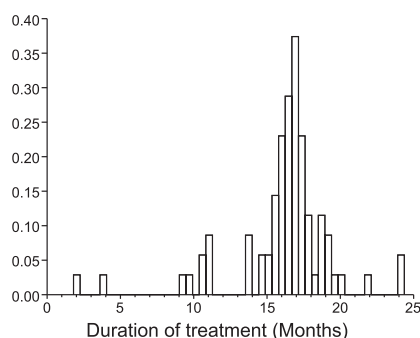
Figure 3.19: Histogram of the duration of maintenance treatment for 78 patients having T or B lymphome.
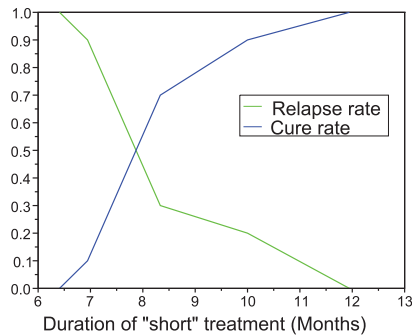
Figure 3.20: The number of relapses decreases (and number of healings increases) as a function of duration of short treatment for a constant ratio between p_{crit} and p_0, $p_{crit}=1.25p_0$.

Maintenance treatments

The criteria to monitor the evolution of the disease in virtual patients is the number of malignant cells. The number of cancer cells is observed for a period at most equal to two years (Figure 3.21). After treatment of the acute phase, the treatment of the maintenance phase begins at the same time for all patients. Statistical correlation between the duration of treatment, the relapse rate and the administered drug doses will be discussed in future studies. Figure 3.21 shows simulations of two years of treatment. During one month (time of acute phase of the disease), the number of cancer cells increases. One month after the beginning of treatment the number of cancer cells decreases and during the maintenance treatment it approaches zero. During the maintenance phase of treatment, all malignant cells die, or few cells survive and give rise to new cancer cells. Figures 3.21 (a) and (c) show a pair of cured patients, Figures 3.21 (b) and (d) show one patient completely cured and one patient who relapsed. The behavior of the two patient of a pair can be different for the same treatment (the same dose of drugs and the same duration of treatment).

Resistance to treatment

Cancer cells can develop resistance to treatment due selection and Darwinian evolution [152, 49]. The most resistant cells will survive and multiply while less resistant cells will

109
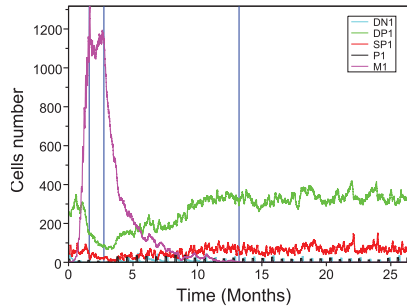
(a) Patient A: duration of maintenance treatment 24 months
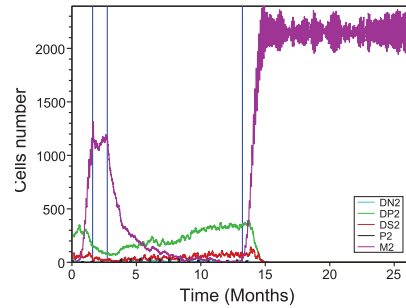
(b) Patient A: duration of maintenance treatment 12 months
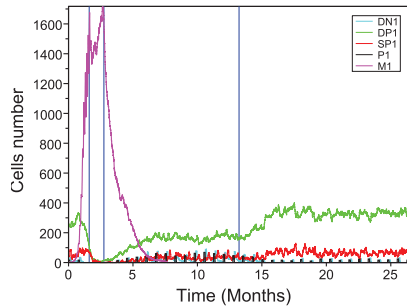
(c) Patient B: duration of maintenance treatment 24 months
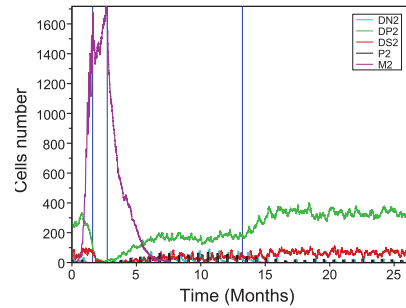
(d) Patient B: duration of maintenance treatment 12 months

Figure 3.21: Numerical simulation of lymphoma treatment. The first vertical line shows beginning of treatment of the acute phase, the second vertical line shows the end of treatment of the acute phase and beginning the maintenance treatment, the third vertical line shows the end of maintenance treatment for the patients in figures (b) and (d). One of them relapsed. Treatment is continued for patients in figures (a) and (c). Both of them are cured.

die. In order to model this effect, we introduce in the model variation of the critical value p_{crit}. Let us recall that when intracellular drug concentration reaches this value, the cell dies.

If this value is not reached by the end of cell cycle, the cell divides. The daughter cell will have the same critical value as the mother cell with a small random perturbation $p_{crit} \pm \epsilon$. We set $\epsilon = 10\% p_{crit}$. Hence we have diffusion of the critical value which leads to gradual appearance of more resistant cells. Since less resistant cells will be eliminated by
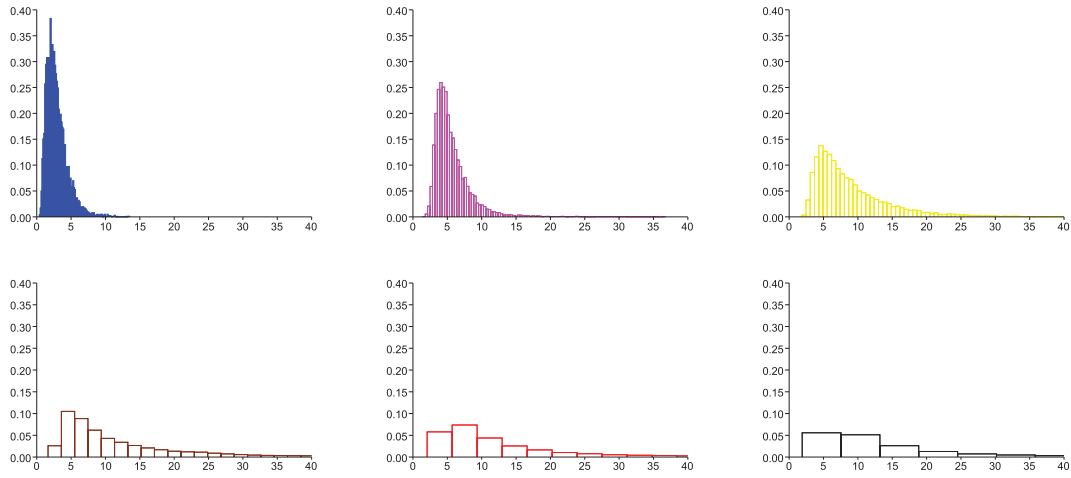
Figure 3.22: Cell distributions with respect to the values of p_{crit} after 1 (blue), 2 (pink), 4 (yellow), 9 (brown), 14 (red), 20 (black) months. After several months of treatment, the mean value of p_{crit} increases. We can observed a spreading of the gaussian distribution. Each histogram represents an average of 10 simulations.

treatment, the tumor will become more and more resistant to treatment. Figure 3.18 shows the quantity of drug inside a malignant cell during cell cycle. This quantity increases as a function of time.

Let us also note that the initial drug concentration in newly born cells are set zero because the drug molecules half-life time is very short.

Figures 2.4 and 3.22 show the evolution of cell distribution with respect to their critical values p_{crit}. We can conclude that these distributions move in the direction of large critical values resulting in appearance of cells resistant to treatment.

Chapter 4

Pulses in reaction-diffusion equations

4.1   Introduction

Biological cells can be characterized by their genotype. Cells of the same type have a localized density distribution in the space of genotypes. This distribution can evolve under the influence of various external factors. In particular cancer cells can adapt to chemotherapy treatment resulting in appearance of resistant clones. This process is called Darwinian evolution of cancer cells [27]. We studied above the emergence of resistance with hybrid discrete-continuous models in the case of lymphoma treatment. In this chapter we analyze this process with reaction-diffusion equations. We will consider the scalar reaction-diffusion equation

$$\frac{\partial u}{\partial t} = D \, \frac{\partial^2 u}{\partial x^2} + F(u, x),$$

(4.1.1)

on the whole axis. The typical example of the nonlinearity is given by the function

$$F(u, x) = u^k(1 - u) - \sigma(x)u,$$

(4.1.2)

where the first term describe the rate of cell birth and the second term the rate of their death. Let us note that the space variable x here corresponds to cell genotype, $u(x, t)$ is the cell density which depends on x and on time t. The diffusion term describe variation of genotype due to mutations, the mortality term depends on the space variable, that is on cell genotype. If $k = 1$ and $\sigma(x) = const$, then this equation does not have localized stationary solutions. In order to describe cell populations with localized genotype which correspond to certain cell type, we need to introduce space dependent mortality coefficients. This means that cells can survive only in a certain range of genotypes (survival gap). We will study the existence of stationary solutions of Equation 4.1.1 and will show that localized solutions (pulses) can exist under certain conditions of the function $\sigma(x)$. The method of proof is based on topological degree for elliptic problems in unbounded domains and on the Lerays-Schauder method. Consider now cell population dynamics if there are two survival gaps, that is two intervals of genotype where cells can survive. We will consider the model with global consumption of resources where all cells consume the same nutrients and their quantity is limited. Suppose that initially all cells are located in the first survival gap (Figure 4.2). If we increase the mortality coefficient there, then this cell population disappears. Instead of it, another cell population appears in the second gap. This behavior can be explained as follows. Cells located in the first survival gap consume all nutrients and do not allow cells in the second gap (which are present because of mutations) to proliferate. When cells from the first gap are removed, nutrients become available and cells in the second gap proliferate restoring a similar population with another genotype. This is one of possible mechanisms of emergence of cell clones resistant to chemotherapy in the process of treatment.

Existence of solutions of the semilinear elliptic equation

$$\Delta w + F(w, x) = 0 \tag{4.1.3}$$

in $\mathbb{R}^n$, $n \geq 1$ depends on the nonlinearity $F(w, x)$. It is studied in detail for polynomial

functions $F(w, x) = w^p$ where existence of solutions is determined by the values of n and p [37], [41], [42], [76], [77]. Another typical example is given by the nonlinearity $F(w, x) = -a(x)|w|^{p-2}w + \lambda b(x)|w|^{q-2}w$, where $a(x)$ and $b(x)$ are positive functions and λ is a positive parameter. Under some additional conditions it is proved that there exists a value of λ for which a nontrivial solution of this equation exists in the corresponding function space. In some cases it can be proved that this solution is radial ($n > 1$) and non-negative. The review of methods and results can be found in [7], [99].

In the second example considered above, the nonlinearity has variable sign and the trivial solution $w = 0$ can be stable. In this case, nontrivial solutions, if they exist, do not bifurcate from the trivial one. We can expect that they separate basins of attraction of the trivial solution and of some other solution or infinity (blow up solution). These properties can be clearly seen in the autonomous case, for example $F(w, x) = -aw + bw^2$, where a and b are some positive constants. In this case, equation (4.1.3) has a positive solution (pulse) which vanish at infinity [17]. It is unstable as a stationary solution of the corresponding parabolic equation. Solution of the Cauchy problem with a perturbed initial condition will converge either to 0 or grow to infinity. Moreover, such pulse solutions exist for any values of parameters a and b and not only for some values of parameters as in the example above. In the one-dimensional case, they can be easily found analytically.

In this work we will study existence of pulse solutions for a nonautonomous nonlinearity. We will consider the one-dimensional equation on the whole axis

$$w'' + F(w, x) = 0 \tag{4.1.4}$$

and we will look for its classical solutions with the limits

$$w(\pm\infty) = 0. \tag{4.1.5}$$

Similar to the example above, we will see that such solutions can separate basin of attraction of the trivial solution and of some other solution. In fact, existence of solutions of problem

114

(4.1.4), (4.1.5) will be determined by the properties of travelling waves for the corresponding autonomous equation with the limiting function $F_0(w) = \lim_{|x| \to \infty} F(w, x)$. The typical form of the function F considered in this work is given by the example from population dynamics

$$F(w, x) = w^2(1 - w) - \sigma(x)w, \tag{4.1.6}$$

where the first term in the right-hand side describes the reproduction of the population, the second term its mortality. The mortality rate $\sigma(x)$ is a positive function which depends on the space variable. We can consider the nonlinearity in a more general form. The conditions on it will be specified below.

We will use function (4.1.6) in order to explain the main features of this problem. Consider first the case where $\sigma(x) \equiv \sigma_0$ is a constant. Set

$$F_0(w) = w^2(1 - w) - \sigma_0 w.$$

Suppose that $0 < \sigma_0 < 1/4$ and consider the zeros of this function, $w_0 = 0$, w_1 and w_2 are solutions of the equation $w(1 - w) = \sigma_0$, $0 < w_1 < w_2$. If

$$\int_0^{w_2} F_0(w)dw > 0, \tag{4.1.7}$$

then the equation

$$w'' + F_0(w) = 0 \tag{4.1.8}$$

with the limits $w(\pm\infty) = 0$ has two solutions. The trivial solution $W_0(x) \equiv 0$ and a positive solution $W_1(x)$ which can be easily found analytically. Its explicit form is not essential for us. In the case of the inequality

$$\int_0^{w_2} F_0(w)dw < 0 \tag{4.1.9}$$

115

there exists only trivial solution. Finally, if

$$\int_0^{w_2} F_0(w)dw = 0, \tag{4.1.10}$$

then equation (4.1.8) does not have nontrivial solutions, which vanish at infinity, but there is a solution with the limits

$$w(-\infty) = w_2, \quad w(+\infty) = 0. \tag{4.1.11}$$

Let us note these three cases are related to the speed of travelling waves, that is solutions of the equation

$$w'' + cw' + F_0(w) = 0$$

with limits (4.1.11). Here c is the wave speed. Its sign can be determined multiplying the equation by w' and integrating from $-\infty$ to $+\infty$. If condition (4.1.7) is satisfied, then $c > 0$. If the inequality is opposite, then $c < 0$. Finally, in the case (4.1.10), $c = 0$. We will see that properties of solutions of problem (4.1.4), (4.1.5) depend on the sign of the wave speed.

Condition (4.1.7). In this case, the question about the existence of solution can be formulated in the following way. If we change the function $\sigma(x)$ by a continuous deformation starting from the constant σ_0, will the nontrivial solution persist? We will study this question by a Leray-Schauder method which is based on topological degree and a priori estimates of solutions. Topological degree in unbounded domains is defined in weighted spaces, in the space without weight it may not exist. Therefore the estimates should also be obtained in the weighted spaces. Usual estimates in Hölder or Sobolev spaces are not sufficient.

Let us explain in more detail what estimates we need in order to prove the existence of solutions and how they can be obtained. Consider equation (4.1.4) with the function $\sigma_\tau(x)$ which depends on a parameter τ. Suppose that there exists a limit $\sigma_0 = \lim_{x \to \pm\infty} \sigma_\tau(x)$.

Let $E = C_\mu^{2+\alpha}(\mathbb{R})$ be the weighted Hölder space with the norm $\|u\|_E = \|u\mu\|_{C^{2+\alpha}(\mathbb{R})}$, where $\mu(x) = \sqrt{1+x^2}$. If the usual Hölder norm $\|u\|_{E_0}$, $E_0 = C^{2+\alpha}(\mathbb{R})$ is bounded and the solution decays exponentially at infinity, then the weighted Hölder norm is also bounded. The E_0-norm of the solution can be estimated by the usual methods, exponential decay of solution at infinity follows from the assumption $F_0'(0) < 0$. However this is not sufficient for a uniform estimate in the weighted Hölder space. Consider a family of solutions u_τ which depends on a parameter τ. If the weighted norm $\|u\|_E$ tends to infinity as $\tau \to \tau_0$, then it can be verified that equation (4.1.8) has a nonzero solution, and u_τ converges to this solution. Under some additional conditions, we will prove that this convergence cannot occur and will obtain, by this, a priori estimates of solutions. We will use here monotonicity of solutions on the half-axis.

Condition (4.1.9). The situation is different in the case of condition (4.1.9). Equation (4.1.4) does not have nontrivial solutions vanishing at infinity. A nontrivial solution can bifurcate from the trivial solution. Condition (4.1.9) will allow us to obtain a priori estimates of nontrivial solutions in the weighted norm. Hence if the trivial solution becomes unstable, then we will obtain the existence of a nontrivial solution. Let us note that for function (4.1.6) the trivial solution becomes unstable if the function $\sigma(x)$ is negative for some x. This does not correspond to the biological meaning of this example. We consider this case in view of other possible applications and more general functions F.

Thus, equality (4.1.10) separates two cases where we prove existence of solutions. In the case where this equality is satisfied, the method to prove existence of solutions developed in this work is not applicable.

Nonlocal equations. Besides equation (4.1.4) we will also study the nonocal equation

$$w'' + F(w, x, I) = 0, \quad I(w) = \int_{-\infty}^{\infty} w(x) dx \qquad (4.1.12)$$

with the typical example of nonlinearity

$$F(w, x, I) = w^2(1 - I) - \sigma(x)w. \tag{4.1.13}$$

This case is quite similar to the previous one, and analysis of the existence of solutions is based on the previous results. However, due to the integral term, the number of solutions can change, and some of them can become stable [160]. Though we do not study stability of solutions in this work, this is an important justification for the investigation of pulse solutions.

Leray-Schauder method. Existence of solutions will be proved by the Leray-Schauder method based on the topological degree for elliptic problems in unbounded domains. Let us recall that the Leray-Schauder degree is not generally applicable in this case. It can be used under some special conditions on the coefficients which allow the reduction of the corresponding operator to the compact operator [99]. In our case this approach is not applicable. We will use the degree construction for Fredholm and proper operators with the zero index [159]. This construction requires the introduction of special weighted spaces. Therefore a priori estimates of solutions required for the Leray-Schauder method should also be obtained in the weighted spaces. This is a special type of estimates where the boundedness of the solution and of its derivatives is not sufficient. These estimates will be obtained for monotone solutions and will require separation of monotone and non-monotone solutions (explained below). This approach is inspired by the method of proof of travelling waves for monotone and locally monotone systems [158].

In the next section we will introduce function spaces and operators, we will obtain a priori estimates of solutions and prove the main existence result (Theorem 2.7). It corresponds to the case (4.1.7) in the example considered above. In Section 4.3 we will discuss another possible case which correspond to inequality (4.1.10). Nonlocal equations will be considered in Section 4.4.

4.2 Monotone solutions on the half-axis

We begin with the problem on the half-axis. We consider equation (4.1.4) for $x > 0$ with the Neumann boundary condition and look for a solution decaying at infinity:

$$w'(0) = 0, \quad w(+\infty) = 0. \tag{4.2.1}$$

This problem can be extended to the whole axis by symmetry. We will assume that

$$F(0, x) = 0, \quad x \geq 0; \quad \frac{\partial F(w, x)}{\partial x} < 0, \quad w > 0, \quad x \geq 0 \tag{4.2.2}$$

and for some $\epsilon > 0$

$$F'_w(0, x) \leq -\epsilon, \quad \forall x \geq 0. \tag{4.2.3}$$

Moreover, there exists $w_+ > 0$ such that

$$F(w, x) < 0, \quad \forall x \geq 0, w > w_+. \tag{4.2.4}$$

4.2.1 Operators and spaces

We will use the Leray-Schauder method to prove the existence of solutions. We need to introduce the operators, function spaces, construct a continuous deformation of the operator and obtain a priori estimates of solutions. Operators and spaces should be defined in such a way that the topological degree exists for them. We suppose that the function $F(w, x)$ is sufficiently smooth with respect to both variables. We can assume for simplicity that it is infinitely differentiable with all derivatives bounded. Consider the operator

$$A(w) = w'' + F(w, x)$$

acting from the space

$$E_1 = \{u \in C_\mu^{2+\alpha}(\mathbb{R}_+), \ u'(0) = 0\}$$

into the space $E_2 = C_\mu^\alpha(\mathbb{R}_+)$. Here $C_\mu^{k+\alpha}(\mathbb{R}_+)$ is a weighted Hölder space with the norm

$$\|u\|_{C_\mu^{k+\alpha}(\mathbb{R}_+)} = \|u\mu\|_{C^{k+\alpha}(\mathbb{R}_+)},$$

where $\mu(x)$ is a weight function. We will set $\mu(x) = \sqrt{1+x^2}$. Construction of the topological degree for such spaces and operators can be found in [159].

4.2.2 Separation of monotone solutions

We will obtain a priori estimates of solutions for monotonically decreasing solutions. Therefore we need to separate them from non-monotone solutions. We understand this separation in the following sense. Consider a solution $w_\tau(x) \not\equiv 0$ which depends on parameter τ. The dependence on τ is continuous in the norm $C^1(\mathbb{R}_+)$. Suppose that the solution $w_\tau(x)$ is monotonically decreasing for $\tau < \tau_0$ and it is not monotonically decreasing for $\tau > \tau_0$. We will prove that this assumption leads to a contradiction.

We proceed by contradiction. Then there is a sequence $\tau_n \to \tau_0$ and the sequence of solutions $w_n(x) = w_{\tau_n}(x)$ such that these functions are not monotone and the function $w_0(x) = w_{\tau_0}(x)$ is monotone. Therefore there exists a sequence x_n such that $w_n'(x_n) = 0$. Without loss of generality, we can suppose that $x_n \to x_0$, where one of the following three cases takes place: $0 < x_0 < \infty$, $x_0 = \infty$, $x_0 = 0$. We will show that all of them lead to contradiction.

Finite value of x_0. Consider first the case where $0 < x_0 < \infty$. Then $w_0'(x_0) = 0$ and $w_0'(x) \leq 0$ for all $x \geq 0$. Set $u(x) = -w_0'(x)$. Differentiating equation (4.1.4), we get

$$u'' + F_w'(w_0, x)u - F_x'(w_0, x) = 0. \tag{4.2.5}$$

Since $u(x) \geq 0$ for all $x \geq 0$, $u(x_0) = 0$, $F_x' < 0$, then we obtain a contradiction in signs in the last equation. If the inequality in (4.2.2) is not strict, that is $F_x' \leq 0$, then the last equation contradicts the maximum principle.

Let us consider one more generalization. We will suppose that

$$F(w, x) = 0 \quad \Rightarrow \quad F_x'(w, x) < 0, \quad w > 0, \quad x \geq 0. \tag{4.2.6}$$

Therefore the derivative F_x' is negative not everywhere as in condition (4.2.2) but only at zero lines of the function F.

Since $w_0''(x_0) = 0$, then $F(w_0(x_0), x_0) = 0$. By virtue of condition (4.2.6), we have $F_x'(w_0(x_0), x_0) < 0$. Differentiating equation (4.1.4) and taking into account that $w_0'(x_0) = 0$, we obtain

$$w_0'''(x_0) = -F_x'(w_0(x_0), x_0) > 0. \tag{4.2.7}$$

Hence $w_0'(x) > 0$ in some neighborhood of the point x_0. This contradicts the assumption that $w_0'(x) \leq 0$.

Infinite value of x_0. We consider now the case where $x_n \to \infty$. Since $w_n(x) \to w_0(x)$ in $C^1(\mathbb{R}_+)$ and $w_0(x) \to 0$ as $x \to \infty$, then $w_n(x_n) \to 0$ as $n \to \infty$. If $w_n(x_n) > 0$, then $F(w_n(x_n), x_n) < 0$ and $w_n''(x_n) > 0$. Hence any positive extremum of the functions $w_n(x)$ is a minimum. Therefore they cannot converge to zero at infinity. Similarly, if $w_n(x_n) < 0$, then it is a maximum and, as before, the function cannot converge to zero at infinity. Finally, if $w_n(x_n) = 0$, then by virtue of condition (4.2.2) we have that $F(w_n(x_n), x_n) = 0$, $w_n''(x_n) = 0$. Therefore $w_n(x) \equiv 0$. This contradicts our assumption that all solutions $w_\tau(x)$ are nontrivial.

Zero value of x_0. Let us consider the last case where $x_n \to x_0 = 0$. We note that $F(w_0(0), 0) > 0$. Indeed, if $F(w_0(0), 0) < 0$, then $w_0''(0) > 0$. Since $w_0'(0) = 0$, then this function cannot be monotonically decreasing.

If $F(w_0(0), 0) = 0$, then $w_0''(0) = 0$. The function $u(x) = -w_0'(x)$ satisfies equation (4.2.5) where $F_x' < 0$. Since $u(x) \geq 0$ for all $x \geq 0$, $u(0) = 0$ and $u'(0) = 0$, then we obtain a contradiction with the Hopf lemma which affirms that $u'(0) > 0$. In the case of the generalized condition (4.2.6), we get inequality (4.2.7). It contradicts the assumption that the function $w_0(x)$ is decreasing.

Thus, we proved that $F(w_0(0), 0) > 0$. Therefore the same inequality holds in some neighborhood of $x = 0$. Since $w_n(x)$ converges uniformly to $w_0(x)$, then $w_n''(x) < 0$ in the interval $0 < x < \delta$ with some positive δ independent of n. This assertion contradicts the assumption that $w_n'(x_n) = 0$ and $x_n \to 0$ as $n \to \infty$. We proved the following theorem.

Theorem 2.1 (Separation of monotone solutions.) *There exists a positive number r such that for any solution of problem (4.2.8), (4.2.9), which depends on a parameter τ, such that*

$$\|w_M - w_N\|_{E_1} \geq r$$

for any monotone solution w_M and any nonmonotone solution w_N of this problem. This estimate does not depend on τ.

4.2.3 A priori estimates of monotone solutions

We consider the equation

$$w'' + F_\tau(w, x) = 0 \tag{4.2.8}$$

on the half-axis $x > 0$ with the Neumann boundary condition:

$$w'(0) = 0. \tag{4.2.9}$$

We will look for its solution decaying at infinity, $w(+\infty) = 0$. In order to simplify the presentation, we suppose that the function $F_\tau(w, x)$ is infinitely differentiable with respect

to all variables w, x, τ,

$$F_\tau(0, x) = 0, \quad x \geq 0; \quad \frac{\partial F_\tau(w, x)}{\partial x} < 0, \quad w > 0, \quad x \geq 0 \qquad (4.2.10)$$

and

$$\frac{\partial F_\tau(0, x)}{\partial w} \leq -\epsilon, \quad x \geq 0, \ \tau \in [0, 1] \qquad (4.2.11)$$

for some $\epsilon > 0$. Moreover, there exists $w_+ > 0$ such that

$$F_\tau(w, x) < 0, \quad \forall w > w_+, \ x \geq 0, \ \tau \in [0, 1] \qquad (4.2.12)$$

Let $w_\tau(x)$ be positive solutions of problem (4.2.8), (4.2.9) decaying at infinity. From condition (4.2.12) it follows that $w_\tau(x) \leq w_+$ for all x and τ. Indeed, since we consider montonically decreasing solutions, it is sufficient to verify that $w_\tau(0) \leq w_+$. If the opposite inequality holds, then, by virtue of the equation, $w_\tau''(0) > 0$, and this function is not decreasing.

Since the function $F_\tau(w, x)$ is sufficiently smooth with respect to w, x and τ, then solutions are uniformly bounded in $C^2(\mathbb{R}_+)$ and the dependence on τ is continuous in $C^1(\mathbb{R}_+)$. In order to prove that solutions are uniformly bounded in the weighted Hölder norm, it is sufficient to verify that the weighted norm

$$\|w_\tau\|_\mu = \|w\mu\|_{C(\mathbb{R}_+)}$$

of these solutions is uniformly bounded. Here $\mu(x) = \sqrt{1 + x^2}$.

Let $\epsilon > 0$ be sufficiently small such that $F_\tau(w, x) < 0$ for $0 < w < \epsilon$ and all $x \geq 0$. Such ϵ exists by virtue of condition (4.2.11). Since $w_\tau(x)$ is a decreasing function and, obviously, $w_\tau(0) > \epsilon$ (otherwise $F_\tau(w_\tau(0), 0) < 0$ and $w_\tau''(0) > 0$), then there exists a unique solution of the equation $w_\tau(x) = \epsilon$. Denote it by x_τ.

The solutions $w_\tau(x)$ admit a uniform exponential estimate for $x > x_\tau$. Therefore if x_τ

is uniformly bounded, then we obtain a uniform estimate of the norm $\|w_\tau\|_\mu$.

Suppose that the values x_τ are not uniformly bounded. Then there exists a sequence τ_n for which $x_n = x_{\tau_n} \to \infty$. Without loss of generality we can assume that $\tau_n \to \tau_0$ for some $\tau_0 \in [0, 1]$. We will consider the corresponding sequence of solutions $w_n(x) = w_{\tau_n}(x)$. It has a subsequence locally convergent to a solution $w_0(x)$ such that $w_0'(0) = 0$ and $w_0(\infty) > 0$. The latter follows from the equality $w_n(x_n) = \epsilon$ and convergence of the sequence x_n to infinity.

Let us also consider the sequence $v_n(x) = w_n(x + x_n)$ of shifted solutions. Obviously, $v_n(0) = \epsilon$. It has a subsequence locally convergent to a monotone solution $v_0(x)$ of equation

$$v'' + F_+(v) = 0 \tag{4.2.13}$$

defined on the whole axis and such that $v_0(+\infty) = 0, v_0(-\infty) > \epsilon$. Here

$$F_+(v) = \lim_{x \to \infty} F_{\tau_0}(v, x).$$

This limit exists by virtue of the condition on the derivative in (4.2.10).

Set $v_- = v(-\infty)$. Then $F_+(v_-) = 0$. Multiplying equation (4.2.13) by v' and integrating, we obtain

$$\int_0^{v_-} F_+(u)du = 0.$$

Thus, the assumption that x_τ is not uniformly bounded leads to the conclusion that there exists a zero v_- of the function F_+ such that the previous equality holds.

Condition 2.2. For any $v > 0$, if $F_+(v) = 0$, then $\int_0^v F_+(u)du \neq 0$.

If this condition is satisfied, then the values x_τ are uniformly bounded. Hence the norm $\|w_\tau\|_\mu$ is also uniformly bounded.

4.2.4 Model problem

Consider the function $F(w, x)$, which satisfies conditions (4.2.2)-(4.2.4), and the limit function

$$F_+(w) = \lim_{x \to +\infty} F(w, x).$$

We suppose that it satisfies the following conditions:

$$F'_+(0) < 0, \quad F_+(w) < 0 \text{ for } w > w_+ \tag{4.2.14}$$

with some $w_+ > 0$. Moreover there exists $w_0 \in (0, w_+)$ such that $F_+(w_0) \neq 0$,

$$\int_0^{w_0} F_+(u) du = 0, \quad \int_0^w F_+(u) du \neq 0 \;\; \forall w \in (0, w_+), w \neq w_0. \tag{4.2.15}$$

Then problem

$$w'' + F_+(w) = 0, \quad w'(0) = 0, \quad w(+\infty) = 0$$

has a unique positive solution $w_0(x)$, and $w_0(0) = w_0$ is its maximal value. This solution can be easily found analytically.

We will find the index of this solution, that is the value of the degree with respect to small sphere around this solution. It is given by the following expression:

$$\mathrm{ind}(w_0) = (-1)^\nu,$$

where ν is the number of positive eigenvalues (with their multiplicities) of the linearized operator

$$Lu = u'' + F'_+(w_0(x))u$$

acting on functions $C^2(\mathbb{R}_+)$.

Lemma 2.5. *The eigenvalue problem*

$$u'' + F'_+(w_0(x))u = \lambda u, \quad u'(0) = 0, \quad u(\infty) = 0 \tag{4.2.16}$$

does not have a zero eigenvalue.

Proof. Let us note first of all that the essential spectrum of this problem lies in the left-half plane since $F'_+(0) < 0$. Suppose that the assertion of the lemma does not hold and problem (4.2.16) has a nontrivial solution $u_0(x)$ for $\lambda = 0$. Then this solution cannot be positive for all x. Indeed, if $u_0(x) > 0$ for $0 \le x < \infty$, then the function $v_0(x) = u_0(|x|)$ defined on the whole axis is a positive solution of the equation

$$v'' + F'_+(w_1(x))v = 0, \quad x \in \mathbb{R},$$

where the function $w_1(x)$ is an extension on the whole axis of the function $w_0(x)$ by symmetry. Since the function $v_0(x)$ is positive, then $\lambda = 0$ is the principal eigenvalue of the operator

$$Lv = v'' + F'_+(w_1(x))v,$$

and this eigenvalue is simple [158]. On the other hand, $v_1(x) = w'_1(x)$ is an eigenfunction of this operator corresponding to the zero eigenvalue, and

$$v_1(x) = -w'_0(-x) > 0, \quad -\infty < x < 0, \quad v_1(x) = w'_0(x) < 0, \ 0 < x < \infty.$$

Hence this eigenfunction is not positive, and it is different from the eigenfunction $v_0(x)$. We obtain a contradiction with simplicity of the principal eigenvalue.

Thus, the function $u_0(x)$ has variable sign. Since it is determined up to a factor, we can assume that $u_0(0) < 0$. Then it has positive values for some $x > 0$ and it decays at infinity since $F'_+(0) < 0$.

Next, the function $u_1(x) = -w'_0(x)$ is a solution of the problem

$$u'' + F'_+(w_0(x))u = 0, \quad u(0) = 0, \quad u(\infty) = 0,$$

which differs from problem (4.2.16) considered for $\lambda = 0$ by the boundary condition. This function is positive for all $x > 0$. We will use this function to prove that the solution $u_0(x)$ cannot exist. Set $\omega(x) = tu_1(x) - u_0(x)$, where t is a positive number. This function satisfies the equation

$$\omega'' + F'_+(w_0(x))\omega = 0. \tag{4.2.17}$$

Let x_0 be such that

$$F'_+(w_0(x)) < 0, \quad x_0 \leq x < \infty.$$

Since $u_1(x)$ is a positive function, we can choose t for which $\omega(x_0) > 0$. We can verify that

$$\omega(x) > 0, \quad x_0 \leq x < \infty. \tag{4.2.18}$$

Indeed, if $\omega(x_1) < 0$ for some $x_1 > x_0$, then this function has a negative minimum since it converges to 0 at infinity. We obtain a contradiction in signs in equation (4.2.17) at the point of minimum. If $\omega(x_1) = 0$, then we get a contradiction with the maximum principle. Indeed, since $\omega(x) \geq 0$ for $x \geq x_0$, then this function is either everywhere positive or identically zero for such x. The latter contradicts the assumption that $\omega(x_0) > 0$.

Let us recall that $u_0(0) < 0$. Therefore $\omega(0) > 0$ for any $t > 0$. Moreover, (4.2.18) holds for t large enough. Hence for t sufficiently large, the function $\omega(x)$ is positive for all $x \geq 0$. If $t = 0$, then it has negative values since $u_0(x)$ has positive values. Let t_0 be the infimum of all t for which $\omega(x)$ is positive for all $x \geq 0$. Then there exists a value $x_2 \in [0, x_0]$ for which $\omega(x_2) = 0$. Indeed, if $\omega(x)$ is positive in this interval, then t can be decreased in such a way that it remains positive there. Since $\omega(x_0) > 0$, then (4.2.18) holds, and $\omega(x)$ is positive for all x. This contradicts the definition of t_0.

Thus, $\omega(x) \geq 0$ for all $x \geq 0$ and $\omega(x_2) = 0$. But this is not possible by virtue of the

maximum principle. Hence problem (4.2.16) cannot have nontrivial solution for $\lambda = 0$.

$\square$

Remark 2.6. The principal eigenvalue λ_0 of problem (4.2.16) is positive. Indeed, if it is non-positive, then, since the corresponding eigenfunction is positive, we will obtain a contradiction with the fact that the function $-w_0'(x)$ is a positive (for $x > 0$) solution of the equation $Lu = 0$ (cf. the proof of the lemma). We proved in Lemma 2.5 that this problem does not have a zero eigenvalue. We can verify that any real $\lambda \in (0, \lambda_0)$ is not an eigenvalue of this problem. Indeed, suppose that there is an eigenvalue $\lambda^* \in (0, \lambda_0)$. The corresponding eigenfunction $u^*(x)$ cannot be positive because only the principal eigenvalue has a positive eigenfunction. As in the proof of the lemma, we introduce the function $\omega = tu_1 - u^*$. It satisfies the equation

$$\omega'' + F_+'(w_0(x))\omega + \phi(x) = \lambda^*\omega,$$

where $\phi(x) = \lambda^* t u_1$. As above, we choose $t > 0$ in such a way that $\omega(x) \geq 0$ for all x and $\omega(x_2) = 0$ for some $x_2 > 0$. Since $\phi(x) > 0$ for all $x > 0$, then we obtain a contradiction in signs in the last equation at $x = x_2$.

4.2.5 Existence theorem

We can now prove the main theorem of this section.

Theorem 2.7. *If the function $F(w, x)$ satisfies conditions (4.2.2)-(4.2.4) and the function $F_+(w)$ satisfies conditions (4.2.14), (4.2.15), then problem*

$$w'' + F(w, x) = 0, \tag{4.2.19}$$

$$w'(0) = 0 \tag{4.2.20}$$

on the half-axis $x > 0$ has a positive monotonically decreasing solution vanishing at infinity.

It belongs to the weighted Hölder space E_1.

Proof. We will consider the homotopy

$$F_\tau(w, x) = \tau F(w, x) + (1 - \tau)F_+(w).$$

Let us recall Condition 2.2, which follows from (4.2.14), (4.2.15), and assumption that solutions are uniformly bounded are used for a priori estimates of monotone solutions. The latter can follow from the maximum principle or from the estimates. Conditions (4.2.14) and (4.2.15) provide existence of solutions for the model problem; conditions (4.2.10) and (4.2.11), which follow from (4.2.2)-(4.2.4) and the definition of the function $F_\tau(w, x)$, provide separation of monotone solutions.

For $\tau = 0$ this equation has a unique strictly decreasing solution $w_0(x)$. Let us find its index, that is the degree with respect to a small ball which contains only this solution and no other solutions. Such small ball exists because the operator linearized about this solution is invertible (Lemma 2.5). By virtue of Lemma 2.5 and Remark 2.6

$$\text{ind } (w_0) = (-1)^\nu = -1,$$

where ν is the number of positive eigenvalues of the operator linearized about this solution together with their multiplicities [159].

Let us recall that the operator $A_\tau : E_1 \times [0, 1] \to E_2$,

$$A_\tau(w) = w'' + F_\tau(w, x)$$

is proper on closed bounded sets. This means that for any compact set $G \subset E_2$ and any closed bounded set $M \subset E_1 \times [0, 1]$, the set $A_\tau^{-1}(G) \cap M$ is compact. Therefore the set of solutions of equation (4.2.8) for all $\tau \in [0, 1]$ is compact. By virtue of a priori estimates of monotone solutions, there is a bounded ball $B \subset E_1$ which contains all such solutions. Next, because of the separation of monotone and non-monotone solutions, we can construct

a domain $D \subset B$ such that it contains all monotone solutions, and it does not contain non-monotone solutions.

Next, monotone solutions of problem (4.2.8) cannot approach the trivial solution $w \equiv 0$ in the norm of the function space. Indeed, if $w(0)$ is sufficiently small, then $w''(0) = -F_\tau(w(0), 0) > 0$ and the solution is not monotone since it grows for small x and vanishes at infinity.

Thus, the domain D can be constructed in such a way that it does not contain the trivial solution either. Therefore by virtue of homotopy invariance of the degree $\gamma(A_\tau, D)$ we get

$$\gamma(A_1, D) = \gamma(A_0, D) = -1.$$

Hence equation (4.2.8) has a positive decaying solution from the space E_1 for $\tau = 1$. The theorem is proved.

$\square$

Remark 2.8. If we consider equation (4.2.19) on the whole axis with a function $F(w, x)$ even with respect to x for each w, then we can use the result of Theorem 2.7 and extend the solution from the half-axis to the whole axis by symmetry.

4.2.6   Examples

Example 2.9. Consider the function

$$F(w, x) = aw^2(1 - w) - \sigma(x)w,$$

where $a > 0$ is a constant, $\sigma(x)$ is a positive bounded increasing function, $\sigma_+ = \sigma(+\infty)$. If problem (4.2.8), (4.2.9) has a positive solution, then the estimate $\sup_x w(x) \leq 1$ holds. Indeed, otherwise at the point of maximum we obtain a contradiction in signs in the equation.

Let $a > 4\sigma_+$. Then equation $aw(1 - w) = \sigma_+$ has two positive solutions. Denote the maximal of them by v_-. If

$$v_-\left(1 - \frac{3}{4} v_-\right) > \frac{3\sigma_+}{2a},$$

then $\int_0^{v_-} F_+(u)du > 0$, and Condition 2.2 is satisfied. In this case we can apply the result on the existence of solutions. If the integral is negative, the solution may not exist since condition (4.2.15) is not satisfied.

Example 2.10. Consider, next, the function

$$F(w, x) = aw^2 - \sigma(x)w.$$

Condition 2.2 is obviously satisfied in this case. However we need to estimate the maximum of the solution. It does not follow in this case from the maximum principle since the function $F(w, x)$ is not negative for large w. We multiply the equation

$$w'' + aw^2 - \sigma(x)w = 0$$

by w' and integrate from 0 to ∞. Taking into account that $w'(0) = 0$ and $w'(x) < 0$ for all $x > 0$, we get

$$\frac{a}{3} w^3(0) = -\int_0^\infty \sigma(x)ww'dx < \frac{1}{2} \sigma_+ w^2(0).$$

Hence $\sup_x w(x) = w(0) < 3\sigma_+/2a$. Thus we can obtain a priori estimates and prove existence of solutions by the Leray-Schauder method.

Remark about upper and lower functions. Let us consider as example the function F given by equality (4.1.6). The condition (4.2.2) implies that $\sigma'(x) > 0$. Set

$$F_-(w) = w^2(1 - w) - \sigma(0)w, \quad F_+(w) = w^2(1 - w) - \sigma(+\infty)w.$$

Suppose that problems

$$w'' + F_\pm(w) = 0, \quad w'(0) = 0, \quad w(+\infty) = 0$$

have solutions and denote them by $w_-(x)$ and $w_+(x)$, respectively. Their existence depends on the values of $\sigma(0)$ and $\sigma(+\infty)$, and it can be easily verified. Then $w_-(x)$ is an upper function and $w_+(x)$ is a lower function. If $w_+(x) \leq w_-(x)$ for all $x \geq 0$, then we can use the method of upper and lower functions to prove the existence of solutions of the problem under consideration. However, this inequality does not hold, and this method is not applicable. The function $w_-(x)$ is positive. It can be considered as an upper function. Then the corresponding solution will decay in time and uniformly converge to the trivial solution $w = 0$ but not to the pulse solution.

4.3 Solutions on the half-axis without monotonicity condition

In the previous section we proved existence of monotone solutions on the half-axis using separation of monotone and non-monotone solutions and a priori estimates of monotone solutions. In this section we will study the case without separation of monotone and non-monotone solutions. In this case we need to obtain a priori estimates of solutions which may not be monotone. We consider problem (4.2.8), (4.2.9) on the half-axis assuming that condition (4.2.11) is satisfied. We do not assume here condition (4.2.10).

We consider the equation

$$w'' + F_\tau(w, x) = 0 \tag{4.3.1}$$

on the half-axis $x > 0$ with the boundary condition

$$w'(0) = 0. \tag{4.3.2}$$

We will look for solutions decaying at infinity. Here

$$F_\tau(w, x) = \tau F(w, x) + (1 - \tau)F_+(w),$$

where

$$F_+(w) = \lim_{x \to \infty} F(w, x).$$

The function $F_\tau(w, x)$ depends on the parameter $\tau \in [0, 1]$. We suppose that it is infinitely differentiable with respect to the variables w, x, τ and

$$F_\tau(0, x) = 0, \quad F_\tau(w, x) < 0, \quad \forall w > w_+, \ x \geq 0, \ \tau \in [0, 1]. \tag{4.3.3}$$

We will also assume that

$$F_+(0) = 0, \ F'_+(0) < 0 \ \text{ and } \ \int_0^w F_+(u)du < 0, \quad \forall w \in (0, w_+). \tag{4.3.4}$$

Proceeding as in Section 4.2.3, we estimate the values x_τ. If they are not uniformly bounded, then the equation

$$w'' + F_+(w) = 0 \tag{4.3.5}$$

has a bounded solution $w_0(x)$ on the whole axis such that $w_0(+\infty) = 0$. Then $0 \leq w_0(x) \leq w_0$ for all $x \in \mathbb{R}$. Moreover either $w_0(x)$ is a monotonically decreasing solution with some limit w_0 at $-\infty$ or it is a pulse solution vanishing at $\pm\infty$ and some maximal value w_0. In both cases, $\int_0^{w_0} F_+(u)du = 0$. We obtain a contradiction with inequality (4.3.4). Thus, we can formulate the following theorem.

Theorem 3.1. *If conditions (4.3.3) and (4.3.4) are satisfied, then solutions of problem (4.3.1), (4.3.2) are uniformly bounded in the norm $C_\mu^{2+\alpha}(\mathbb{R}_+)$.*

If $\tau = 0$, then equation (4.3.1) coincides with equation (4.3.5). It has only the trivial solution. The value of the degree with respect to any bounded set in the space E_1 equals

133

1. If $F(0, x) \equiv 0$ for all x, then problem (4.3.1), (4.3.2) also has the trivial solution. If a simple real eigenvalue of the problem linearized about the trivial solution crosses the origin, then this solution becomes unstable and nontrivial solutions bifurcate from it. This is not only a local bifurcation. There is a continuous branch of solutions starting from the trivial solution.

4.4 Existence of pulses in the case of global consumption

We consider the equation

$$w'' + F(w, x, I(w)) = 0 \tag{4.4.1}$$

on the whole axis. It describes evolution of biological species with global consumption of resources [27], [160]. Here

$$F(w, x, I) = aw^2(1 - I(w)) - \sigma(x)w, \quad I(w) = \int_{-\infty}^{\infty} w(x)dx.$$

We look for a positive solution decaying at infinity. Set

$$c = 1 - I(w) \tag{4.4.2}$$

and $w = u/(ac)$. Then we get the equation

$$u'' + u^2 - \sigma(x)u = 0 \tag{4.4.3}$$

which we studied in Section 4.2.5. If $\sigma(x)$ is a positive even function bounded and increasing for $x > 0$, then it has a positive decaying at infinity solution (Example 2.10). Then from (4.4.2)

$$c^2 - c + \frac{1}{a} I(u) = 0. \tag{4.4.4}$$

This equation has two real solutions if $I(u) < a/4$, one solution in the case of equality, and no solutions if the inequality is opposite. Hence equation (4.4.1) has pulse solutions if the reproduction rate coefficient a is sufficiently large.

Example 4.1. In the case when $\sigma(x) = \sigma_0 > 0$ is a constant, assuming $u'(0) = 0$ we can find the analytic solution:

$$u(x) = \frac{3\sigma_0}{2\cosh^2\left(\frac{\sqrt{\sigma_0}}{2}x\right)}$$

and the value of the integral $I(u) = 6\sqrt{\sigma_0}$. Therefore, in the case of $a > 24\sqrt{\sigma_0}$ we have the two pulse solutions given by the formula

$$w_{1,2}(x) = \frac{3\sigma_0}{2ac_{1,2}\cosh^2\left(\frac{\sqrt{\sigma_0}}{2}x\right)} \quad , \quad c_{1,2} = \frac{1 \pm \sqrt{1 - \frac{24}{a}\sqrt{\sigma_0}}}{2} .$$

When $a = 24\sqrt{\sigma_0}$, there is a single pulse

$$w(x) = \frac{3\sigma_0}{a\cosh^2\left(\frac{\sqrt{\sigma_0}}{2}x\right)} .$$

Finally, for $0 < a < 24\sqrt{\sigma_0}$, we have no real valued pulse solutions.

4.5 Mathematical model of the development of the resistance to chemotherapy

It is known that cancer treatment by chemotherapy can result in the emergence of cell lines resistant to treatment. We will consider a mathematical model which describes this effect.

4.5.1 Model

We consider a cell population with the density $u(x, t)$ which depends on its genotype x and on time t. Genotype x is considered as a continuous one-dimensional variable. When cells divide, their genotype can change due to small random mutations. The evolution of the cell density is described by the equation

$$\frac{\partial u}{\partial t} = d \, \frac{\partial^2 u}{\partial x^2} + W_b - W_d, \qquad (4.5.1)$$

where W_b is the rate of cell birth and W_d the rate of death. We will suppose that x takes all real values though we can also consider a bounded interval. Next, we assume that all cells consume the same nutrients independently of their genotype, and that the rate of cell birth depends on available nutrient:

$$W_b = au(b - cI(u)), \quad I(u) = \int_{-\infty}^{\infty} u(y, t)dy.$$

Finally, the death rate depends on the genotype:

$$W_d = \sigma(x)u.$$

We will look for positive solutions of this equation which decay at infinity assuming that the integral $I(u)$ is well defined.

4.5.2 Stationary solution

Existence of stationary solutions

Let us begin with the following example. If the mortality coefficient is constant $\sigma(x) \equiv$ const, then integrating equation (4.5.1), we obtain

$$I' = aI(b - cI). \tag{4.5.1}$$

Hence $I(t)$ converges exponentially to $I(\infty) = b/c$. Though the integral of solution converges to a positive constant, it can be proved that $u(x, t)$ converges uniformly to zero. This, the only stationary solution of equation (4.5.1) is the trivial solution $u \equiv 0$.

In order to get nontrivial solutions of this equation, we will consider the death rate coefficient depending on genotype x. We will consider the following model example

$$\sigma(x) = \begin{cases} \sigma_0 & , \quad |x| \geq L \\ \sigma_1 & , \quad |x| < L \end{cases}, \tag{4.5.2}$$

where L is a positive constant. Without loss of generality we can set $\sigma_1 = 0$. Otherwise we can take it into account in the constant b. We will find a stationary solution of equation (4.5.1) analytically. Put $k = a(b - cI(u))$. Then for $|x| \leq L$ we have the equation:

$$dw'' + kw = 0$$

which we consider on the half-axis $x > 0$ with the boundary condition $w'(0) = 0$. Then

$$w(x) = c_1 \cos(\lambda x),$$

where $\lambda = \sqrt{k/d}$, c_1 is an arbitrary constant.

If $x > 0$, then the equation becomes

$$dw'' + (k - \sigma_0)w = 0.$$

Hence

$$w(x) = c_2 e^{\mu x} ,$$

where $\mu = \sqrt{(\sigma_0 - k)/d}$, c_2 is an arbitrary constant.

From the conditions

$$w(-L) = w(+L), \quad w'(-L) = w'(L)$$

we get the equalities:

$$c_1 \cos(\lambda L) = c_2 e^{-\mu L} , \quad -c_1 \lambda \sin(\lambda L) = -c_2 \mu e^{-\mu L} .$$

This system has a nontrivial solution if the determinant equals zero. It gives the equation

$$\tan(\lambda L) = \frac{\mu}{\lambda} .$$

It can be written as equation with respect to k:

$$\tan\left(\sqrt{\frac{k}{d}} L\right) = \sqrt{\frac{\sigma_0}{k} - 1} . \tag{4.5.3}$$

This equation has one or more solutions in the interval $0 < k < \sigma_0$. It is interesting to note that this solution depends only on d, L and σ_0 and it is independent of a, b and c, that is of parameters which determine the rate of cell birth.

When we find the value of k, we can determine, next, the ratio

$$\tau = \frac{c_2}{c_1} = \cos(\lambda L) \, e^{\mu L} ,$$

the solution $w(x) = c_1 w_0(x)$, where

$$w_0(x) = \begin{cases} \cos(\lambda L) & , \quad 0 < x \le L \\ \tau \exp(-\mu x) & , \quad \quad x > L \end{cases} .$$

Finally, the constant c_1 can be found from the equation

$$k = a \left(b - 2c \, c_1 \int_0^\infty w_0(x) dx \right) .$$

4.5.3   Cell population with multiple survival gaps

Local and global consumption of resources

In the model example considered in the previous section, the mortality coefficient $\sigma(x)$ has a small or zero value in some interval $|x| < L$ and a high value outside this interval. In this case, the cell population is basically localized inside this interval. Its density exponentially decays outside it because of cell death. From the biological point of view, this means that cells survive with some given genotype and do not survive for other genotypes. We will call this interval of genotypes survival gap.

Let us now consider the case with several survival gaps, that is with several intervals of genotype with zero death rate,

$$\sigma(x) = \begin{cases} 0 & , \quad y_i < x < z_i, \;\; y_i < x < z_i \\ \sigma_0 & , \quad \quad \text{otherwise} \end{cases} .$$

We will begin with the equation

$$\frac{\partial u}{\partial t} = d \, \frac{\partial^2 u}{\partial x^2} + au(b - cu) - \sigma(x)u. \tag{4.5.1}$$

It differs from equation (4.5.1) by the birth rate. Instead of the global consumption which depends on the integral $I(u)$ we consider local consumption which depends on u. This model implies that each cell type (genotype) consumes its own nutrients.

Figure 4.1 shows the results of numerical simulations for equation (4.5.1). The initial
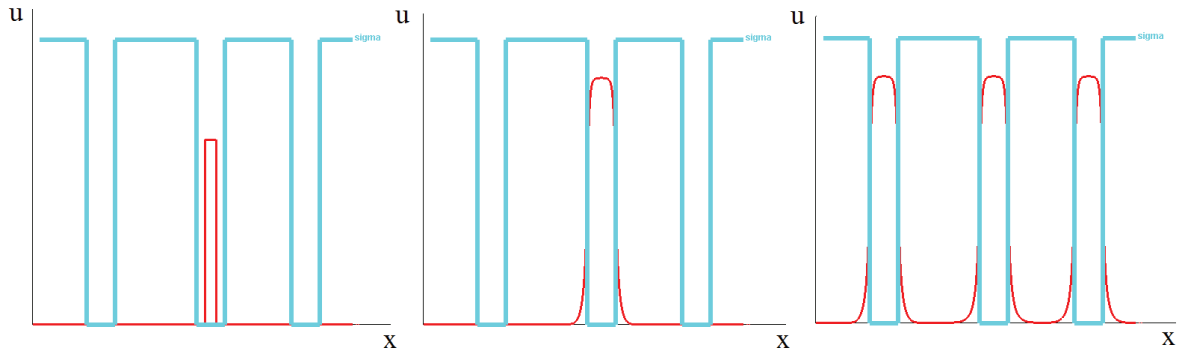
Figure 4.1: Initial condition and the snapshot of solution of equation (4.5.1) for $t = 10$ and $t = 70$.

condition is localized in the central survival gap. After some time cell subpopulations appear also in two other gaps. This is possible because they have resources independently of cells in the central gap.
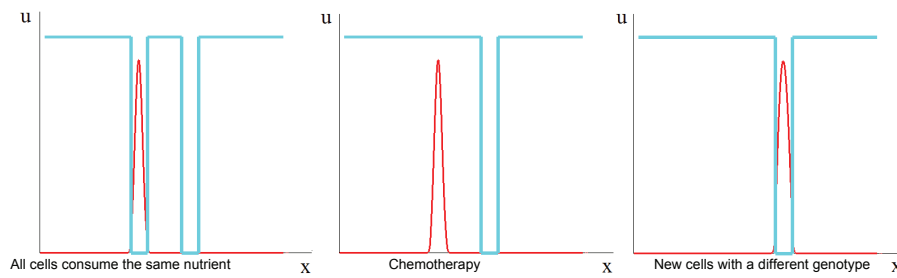
Figure 4.2: Cell population is localized in the first survival gap (left). If the mortality coefficient there is increased (middle), then this cell population disappears. Instead of it, cells appear in the second survival gap (right).

The situation is different if all cells consume the same nutrients. The corresponding example is shown in Figure 4.2. Cell population is localized in the first gap. If we increase the mortality coefficient there and, by this, remove this gap, then this cell population disappears. Instead of it, another cell population appears in the second gap.

4.5.4 Cancer treatment

One of possible reasons of relapse in cancer treatment by chemotherapy is emergence of new lineages of malignant cells resistant to treatment. These cells can appear due to secondary

140

mutations from the existing malignant cells in the tumor. Some of them can get in another survival gap. However they will not proliferate because they do not have enough nutrients. If the original population of cancer cells is removed by chemotherapy, nutrients will be available and these other cells will start proliferating.

The model presented above describes this process. It also allows us to estimate the time of relapse. Let a cell population be located in the first survival gap, and l be the distance from it to the second survival gap. Then from the stationary solution presented in Section 3.1 we estimate the number of cells in the second survival gap as $w(l) = c_2 \exp(-\mu l)$. When cells in the first survival gap are removed by chemotherapy, the integral $I(u)$ rapidly decreases and can be approximated by 0. From the equation we obtain the growth rate of cell population in the second survival gap:

$$u(l, t) = w(l)e^{abt} \ .$$

The product ab is determined by the duration of cell cycle and can be found experimentally for each cell lineage. The value $w(l)$ is the probability of cells in the first survival gap to have mutation which will put them in the second survival gap. In fact, diffusion in the space of genotypes should be understood in terms of such probabilities. If it can be estimated, then we find how cell population grows in time.

Let us note that in this estimate, the first cell population is removed by treatment instantaneously. More precise estimates can be obtained if we take into account its decay rate.

Chapter 5

Conclusions

Cette thèse est consacrée aux modèles hybrides discret-continus appliqués à la modélisation de l'hématopoïèse et de maladies du sang, telles que le myélome multiple et le lymphome lymphoblastique à cellules T, ainsi qu'à l'analyse des solutions d'équations de réaction-diffusion permettant de décrire l'évolution darwinienne de cellules malignes.

Modèles hybrides. Les modèles hybrides permettent de décrire le comportement des cellules sanguines (apoptose, prolifération et différenciation) en couplant l'aspect continu des équations différentielles ordinaires pour la régulation intracellulaire ainsi que des équations aux dérivées partielles pour la régulation extracellulaire avec une représentation discrète des cellules considérées comme des sphères, auxquelles sont attribués des paramètres.

Choix de lignage. Les modèles hybrides sont utilisés pour simuler l'hématopoïèse. Ils permettent, en considérant uniquement une régulation intracellulaire de simuler le choix de lignage du progéniteur MEP, l'une des premières étapes de la cascade de différenciations aboutissant à la formation des cellules sanguines.

Erythropoïèse. Plusieurs régulations intracellulaires mettant en jeux la compétition entre plusieurs protéines auxquelles s'ajoute une régulation extracellulaire permettent de simuler l'érythropoïèse. En comparant les résultats obtenus avec des données biologiques,

nous constatons que le modèle permet de reproduire assez fidèlement les processus biologiques, en particulier les mécanismes permettant d'adapter le nombre de globules rouges produits à un stress subi par l'organisme, par exemple dans le cas d'une hémorragie.

Myélome multiple. Ces modèles ont été ensuite utilisés pour simuler deux maladies du sang. Le myélome multiple est une maladie invasive du sang, qui peut induire une grave anémie. En effet, le développement de tumeurs détruit la structure des îlots érythroblastiques en les écrasant et en produisant une substance cytotoxique: le Fas-ligand. La modélisation de l'action mécanique et de la production de Fas-ligand ont permis de simuler l'apparition de l'anémie.

Lymphome lymphoblastique à cellules T. Le lymphome lymphoblastique à cellules T provoque l'apparition de tumeurs dans le thymus et est traité pendant deux ans. Les résultats montrent qu'il semble possible de réduire la durée du traitement d'entretien sans augmenter le nombre de rechute. Cette hypothèse va être testée sur une population virtuelle créée avec ce modèle, permettant de représenter le thymus dans son fonctionnement normal ou altéré par la maladie. La variable permettant de suivre l'état du malade, rémission ou rechute, est le nombre de cellules cancéreuses.

Évolution darwinienne des cellules. La modélisation du traitement du lymphome a également permis de simuler l'apparition d'une résistance aux médicaments utilisés pendant la chimiothérapie grâce aux modèles hybrides. D'autres formes de modélisation sont envisageables. Il est possible de modéliser l'apparition d'une résistance aux traitement en considérant la distribution du phénotype des cellules malignes. Elle peut être étudiée comme étant la solution d'une équation de réaction-diffusion, dont les paramètres dépendent des nutriments disponibles et consommés par les cellules malignes. La résistance est alors due à une forme de sélection et à l'évolution darwinnienne des cellules.

Bibliography

[1] M. Abromowitch, R. Sposto, S. Perkins, D. Zwick, S. Siegel, J. Finlay, M.S. Cairo. *Children's Oncology Group. Shortened intensified multi-agent chemotherapy and non-cross resistant maintenance therapy for advanced lymphoblastic lymphoma in children and adolescents: report from the Children's Oncology Group.* Br J Haematol., 143 (2) (2008), 261–7.

[2] A.S. Ackleh, K. Deng, C.E. Cole, H.T. Tran. *Existence-uniqueness and monotone approximation for an erythropoiesis age-structured model.* J Math Anal Appl., 289 (2004), 530–544.

[3] A.S. Ackleh, K. Deng, K. Ito, J. Thibodeaux. *A structured erythropoiesis model with nonlinear cell maturation velocity and hormone decay rate.* Math Biosci., 204 (2006), 21–48.

[4] E. Afenya, S. Mundle. *Hematologic disorders and bone marrow-peripheral blood dynamics.* Math. Model. Nat. Phenom., 5 no. 3 (2010), 15–27.

[5] G.R. Aispuru, M.V. Aguirre, J.A. Aquino-Esperanza, C.N. Lettieri, J.A. Juaristi, N.C. Brandan. *Erythroid expansion and survival in response to acute anemia stress: the role of EPO receptor, GATA-1, Bcl-xL and caspase-3.* Cell Biol. Int., 32 (8) (2008) 966–78.

[6] T. Alarcón, H.M. Byrneb, P.K. Mainia. *A cellular automaton model for tumour growth in inhomogeneous environment.* J. Theor. Biol., 225 (2003), 257–274.

[7] A. Ambrosetti, A. Malchiodi. Nonlinear analysis and semilinear elliptic problems. Cambridge Univ. Press, Cambridge, 2007.

[8] A.R.A. Anderson, M.A.J. Chaplain, K.A. Rejniak. *The cellular Potts model and its variants.* Single-Cell-Based Models in Biology and Medicine, (2007).

[9] A.R.A. Anderson, M.A.J. Chaplain. *Continuous and discrete mathematical models of tumor-induced angiogenesis.* Bull. Math. Biol., 60 (5) (1998), 857–99.

[10] A.R.A. Anderson, M. Chaplain, K.A. Rejniak. *Single cell based models in biology and medicine.* Mathematics and Biosciences in Interaction, (2007).

[11] A.R.A. Anderson, K.A. Rejniaka, P. Gerleea, V. Quaranta. *Modelling of Cancer Growth, Evolution and Invasion: Bridging Scales and Models.* Math. Model. Nat. Phenom., 2 (3) (2007), 1–29.

[12] R. Apostu, M.C. Mackey. *Understanding cyclical thrombocytopenia: A mathematical modeling approach.* J. Theor. Biol., 251 (2008), 297–316.

[13] S. Balea, A. Halanay, D. Jardan, M. Neamtu. *Stability analysis of a feedback model for the action of the immune system in leukemia.* Math. Model. Nat. Phenom., 9 no. 1 (2014), 108–132.

[14] A. Bauer, F. Tronche, O. Wessely, C. Kellendonk, H.M. Reichardt, P. Steinlein, G. Schutz, H. Beug. *The glucocorticoid receptor is required for stress erythropoiesis.* Genes Dev., 13 no. 22 (1999), 2996–3002.

[15] Y. Beguin, M. Yerna, M. Loo, M. Weber, G. Fillet. *Erythropoiesis in multiple myeloma: defective red cell production due to inappropriate erythropoietin production.* Br J Haematol (1992), 82, 648-53.

[16] J. Bélair, M.C. Mackey, J.M. Mahaffy. *Age-structured and two-delay models for erythropoiesis.* Math Biosci., 128 (1995), 317–346.

[17] H. Berestycki, P.L. Lions, L.A. Peletier. *An ODE approach to the existence of positive solutions for semilinear problems in* $\mathbb{R}^N$. Indiana Univ. Math. J., 30 (1981), no.1, 141–157.

[18] S. Bernard , J. Bélair, M.C. Mackey. *Oscillations in cyclical neutropenia: New evidence based on mathematical modeling.* J. Theor. Biol., 223 (2003), 283–298.

[19] N. Bessonov, F. Crauste, I. Demin, V. Volpert. *Dynamics of Erythroid Progenitors and Erythroleukemia.* Math Model Nat Phenom., 4 (2009) 210–232.

[20] N. Bessonov, F. Crauste, S. Fischer, P. Kurbatova, V. Volpert. *Application of Hybrid Models to Blood Cell Production in the Bone Marrow.* In press Math. Model. Nat. Phenom

[21] N. Bessonov, I. Demin, P. Kurbatova, L. Pujo-Menjouet, V.Volpert. *Multi-agent systems and blood cell formation.* In: Multi-Agent Systems - Modeling, Interactions, Simulations and Case Studies, F. Alkhateeb, E. Al Maghayreh, I. A. Doush, Editors, (2011), 395–424.

[22] N. Bessonov, I. Demin, L. Pujo-Menjouet, V. Volpert. *A multi-agent model describing self-renewal of differentiation effects on the blood cell population.* Mathematical and computer modelling, 49 (2009), 2116–2127.

[23] N. Bessonov, N. Eymard, P. Kurbatova, V. Volpert. *Mathematical modeling of erythropoiesis in vivo with multiple erythroblastic islands.* Applied Mathematics Letters, 25 (2012), 1217–1221.

[24] N. Bessonov, P. Kurbatova, V. Volpert. *Particle dynamics modelling of cell populations.* Proc. Conf. JANO, Mohhamadia, 2008. Math. Model. Nat. Phenom., 5 7 (2010), 42–47.

[25] N. Bessonov, P. Kurbatova, V. Volpert. *Pattern Formation in Hybrid Models of Cell Populations.* V. Capasso et al. (eds.), Pattern Formation in Morphogenesis, Springer Proceedings in Mathematics 15, Springer-Verlag Berlin Heidelberg, (2013), 107–119.

146

[26] N. Bessonov, L. Pujo-Menjouet, V. Volpert. *Cell modelling of hematopoiesis.* Math. Model. Nat. Phenom., 1 no. 2 (2006), 81–103.

[27] N. Bessonov, N. Reinberg, V. Volpert. *Mathematics of Darwin's diagram.* Math. Model. Nat. Phenom., 9 (2014), no. 3, in press.

[28] T. Boehm. *Self-renewal of thymocytes in the absence of competitive precursor replenishment.* J. Exp. Med. Vol., 209 No. 8 (2012), 1397-1400.

[29] B.R. Bonn, M. Rohde, M. Zimmermann, D. Krieger, I. Oschlies, F. Niggli, G. Wrobel, A. Attarbaschi, G. Escherich, W. Klapper, A. Reiter, B. Burkhardt. *Incidence and prognostic relevance of genetic variations in T-cell lymphoblastic lymphoma in childhood and adolescence.* Blood, 121(16) (2013), 3153–60.

[30] F. Bouilloux, G. Juban, N. Cohet, D. Buet, B. Guyot, W. Vainchenker, F. Louache, F. Morle. *EKLF restricts megakaryocytic differentiation at the benefit of erythrocytic differentiation.* Blood, 1 112 (3) (2008), 576-84.

[31] N. Brousse *Lymphome Lymphoblastique T enfant et adulte* (2009).

[32] L. Brugières, V. Minard, C. Patte. *Lymphomas in children and adolescents.* Rev Prat., 62 (4) (2012), 453–8.

[33] B. Burkhardt, M. Zimmermann, I. Oschlies, F. Niggli, G. Mann, R. Parwaresch, H. Riehm, M. Schrappe, A. Reiter, BFM Group. *The impact of age and gender on biology, clinical features and treatment outcome of non-Hodgkin lymphoma in childhood and adolescence.* Br J Haematol., 131 (1) (2005), 39–49.

[34] B. Burkhardt, W. Woessmann, M. Zimmermann, U. Kontny, J. Vormoor, W. Doerffel, G. Mann, G. Henze, F. Niggli, W.D. Ludwig, D. Janssen, H. Riehm, M. Schrappe, A; Reiter. *Impact of cranial radiotherapy on central nervous system prophylaxis in children and adolescents with central nervous system-negative stage III or IV lymphoblastic lymphoma.* J Clin Oncol., 20 24 (3) (2006), 491–9.

[35] M. Buyse, S. Michiels, D.J. Sargent, A. Grothey, A. Matheson, A. de Gramont. *Integrating biomarkers in clinical trials.* Expert Rev Mol Diagn., 11 (2) (2011), 171–182.

[36] A.Q. Cai, K.A. Landman, B.D. Hughes, C.M. Witt. *T cell development in the thymus: from periodic seeding to constant output.* J Theor Biol., 249 (2) (2007), 384–94.

[37] L.A. Caffarelli, B. Gidas, J. Spruck. *Asymptotic symmetry and local behavior of semilinear elliptic equations with critical Sobolev growth.* Comm. Pure Appl. Math., 42 (1989), no. 3, 271–297.

[38] A.B. Cantor, S.H. Orkin. *Transcriptional regulation of erythropoiesis: an affair involving multiple partners.* Oncogene, 21 (21) (2002), 3368–3376.

[39] S. Chari, S. Winandy *Ikaros Regulates Notch Target Gene Expression in Developing Thymocytes.* The Journal of Immunology, 181 (2008), 6265–6274.

[40] J.A. Chasis, N. Mohandas. *Erythroblastic islands: niches for erythropoiesis.* Blood, 112 (2008).

[41] W.X. Chen, C. Li. *Classification of solutions of some nonlinear elliptic equations.* Duke Math. J., 63 (1991), no. 3, 615–622.

[42] W.X. Chen, C. Li. *Qualitative properties of solutions to some nonlinear elliptic equations in R^2.* Duke Math. J., 71 (1993), no. 2, 427–439.

[43] K. Chen, J. Liu, S. Heck, J.A. Chasis, X. An, N. Mohandas. *Resolving the distinct stages in erythroid differentiation based on dynamic changes in membrane protein expression during erythropoiesis.* Proc Natl Acad Sci U S A, 106 (2009), 17413–174138.

[44] R. Cheong, A. Bergmann, S.L. Werner, J. Regal, A. Hoffmann, A. Levchenko. *Transient IkappaB kinase activity mediates temporal NF-kappaB dynamics in response to a wide range of tumor necrosis factor-alpha doses.* J. Biol. Chem., 281 (2006), 2945–2950.

[45] R. Cheong, A. Bergmann, S.L. Werner, J. Regal, A. Hoffmann, A. Levchenko. *Transient IkappaB kinase activity mediates temporal NF-kappaB dynamics in response to a wide range of tumor necrosis factor-alpha doses.* J. Biol. Chem., 281 (2006), 2945–2950.

[46] S. Cherukuria, N. A. Tripoulasa, S. Nurkoc, P. L. Foxa. *Anemia and impaired stress-induced erythropoiesis in aceruloplasminemic mice.* Blood Cells, Molecules, and Diseases, Volume 33 (2004), 346–355.

[47] S. Chiaretti, R. Foà. *T-cell acute lymphoblastic leukemia.* Haematologica, 94 (2), (2009).

[48] A. Chow, M. Huggins, J. Ahmed, D. Hashimoto, D. Lucas, Y. Kunisaki, S. Pinho, M. Leboeuf, C. Noizat, N. van Rooijen, M. Tanaka, Z.J. Zhao, A. Bergman, M. Merad, P.S. Frenette. *CD169(+) macrophages provide a niche promoting erythropoiesis under homeostasis and stress.* Nat Med., 19 (2013), 429–436.

[49] J. Clairambault, P. Magal, V. Volpert. *Cancer as evolutionary process.* European Communications in Mathematical and Theoretical Biology 2013, No. 16.

[50] C. Colijn, M.C. Mackey. *A mathematical model of hematopoiesis – I. Periodic chronic myelogenous leukemia.* J. Theor. Biol., 237, (2005), 117–132.

[51] C. Colijn, M.C. Mackey. *A mathematical model of hematopoiesis – II. Cyclical neutropenia.* J. Theor. Biol., 237 (2005), 133–146.

[52] S. Cortelazzo, M. Ponzoni, A.J. Ferreri, D. Hoelzer. *Lymphoblastic lymphoma.* Crit Rev Oncol Hematol., 79 (3) (2011), 330–43.

[53] C. Cornu, B. Kassai, R. Fisch, C. Chiron, C. Alberti, R. Guerrini, A. Rosati, G. Pons, H. Tiddens, S. Chabaud, D. Caudri, C. Ballot, P. Kurbatova, A. Castellan, A. Bajard, P. Nony; CRESim & Epi-CRESim Project Groups. *Experimental designs for small randomised clinical trials: an algorithm for choice.* Orphanet J Rare Dis., 8:48. doi: 10.1186/1750-1172-8-48. Review (2013).

[54] E. Coustan-Smith, M. Abromowitz, J.T. Sandlund, D. Campana. *A novel approach for minimal residual disease detection in childhood T-cell lymphoblastic lymphoma (T-LL): a children ś oncology group report.* Blood (ASH Annual Meeting Abstracts), 110 3564, (2007).

[55] F. Crauste, I. Demin, O. Gandrillon, V. Volpert. *Mathematical study of feedback control roles and relevance in stress erythropoiesis.* J. Theor. Biology, 263 (2010), 303–316.

[56] T. Crompton, K.C. Gilmour, M.J. Owen. *The MAP Kinase Pathway Controls Differentiation from Double-Negative to Double-Positive Thymocyte.* Cell, Volume 86, Issue 2, (1996), 243–251.

[57] F. Crauste, L. Pujo-Menjouet, S. Génieys, C. Molina, O.Gandrillon. *Adding Self-Renewal in Committed Erythroid Progenitors Improves the Biological Relevance of a Mathematical Model of Erythropoiesis.* J. Theor. Biology, Volume 250 (2008), 322–338.

[58] C.H. Dai, S.B. Krantz, K.M. Zsebo.*Human burst-forming units-erythroid need direct interaction with stem cell factor for further development.* Blood, 78 (1991), 2493–4977.

[59] J.C. Dallon. *Models with lattice-free center-based cells interacting with continuum environment variables.* Single Cell Based Models in Biology and Medicine. Mathematics and Biosciences in Interaction, III (2007), 197–219.

[60] Database EuroLB. Protocole Euro LB-02/LMT2004. Etude Européenne de traitement des Lymphomes Lymphoblastiques de l'enfant. Coordonnateur National : Yves Bertrand (SFCE), Coordination Internationale : Alfred Reiter (Giessen). ClinInfo.

[61] S. Dazy, F. Damiola, N. Parisey, H. Beug, O. Gandrillon. *The MEK-1/ERKs signaling pathway is differentially involved in the self-renewal of early and late avian erythroid progenitor cells.* Oncogene, 22 (2003), 9205–9216.

[62] I. Demin, F. Crauste, O. Gandrillon, V. Volpert. *A multi-scale model of erythropoiesis.* J Biol Dyn., 4 (2010), 59–70.

[63] A. Deutsch. *Lattice-gas cellular automaton modeling of developing cell systems.* Single-Cell-Based Models in Biology and Medicine, Mathematics and Biosciences in Interaction, (2007), 29–51.

[64] R. Dillon, M. Owen, K. Painter. *A single-cell-based model of multicellular growth using the immersed boundary method.* AMS Contemp. Math., 466 (2008), 1–15.

[65] W.A. Dik, K. Pike-Overzet, F. Weerkamp, D. de Ridder, E.F.E. de Haas, M.R.M. Baert, P. van der Spek, E.E.L. Koster, M.J.T. Reinders, J.J.M. van Dongen, A.W. Langerak, F.J.T. Staal. *New insights on human T cell development by quantitative T cell receptor gene rearrangement studies and gene expression profiling.* JEM. Vol., 201 No. 11 (2005), 1715–1723.

[66] S. Dormann, A. Deutsch. *Modeling of self-organized avascular tumor growth with a hybrid cellular automaton.* In Silico Biol., (2002), 393–406,.

[67] J. Eller , I. Gyori, M. Zollei, F. Krizsa. *Modelling Thrombopoiesis Regulation - I Model description and simulation results.* Comput. Math. Appli., 14 (1987), 841–848.

[68] N. Eymard, P. Kurbatova. *Hybrid models in hematopoiesis.* submitted.

[69] N. Eymard, N. Bessonov, O. Gandrillon, M.J. Koury, V. Volpert. *The role of spatial organisation of cells in erythropoiesis.* Journal of Mathematical Biology, (2014).

[70] S. Fischer, P. Kurbatova, N. Bessonov, O. Gandrillon, V. Volpert, F. Crauste. *Modelling erythroblastic islands: using a hybrid model to assess the function of central macrophage.* Journal of Theoretical Biology, 298 (2012), 92–106.

[71] A. Fossa, D. Brandhorst, JH. Myklebust, S. Seeber, MR. Nowrousian. *Relation between S-phase fraction of myeloma cells and anemia in patients with multiple myeloma.* Exp Hematol, (1999), 27, 1621-6.

[72] P. Frontelo, D. Manwani, M. Galdass, H. Karsunky, F. Lohmann, P.G. Gallagher, J.J. Bieker. *Novel role for EKLF in megakaryocyte lineage commitment.* Blood, 110 (12) (2007), 3871–3880.

[73] O. Gandrillon. *The v-erbA oncogene. Assessing its differentiation-blocking ability using normal chicken erythrocytic progenitor cells.* Methods Mol. Biol., 202 (2002), 91–107.

[74] O. Gandrillon, J. Samarut. *Role of the different RAR isoforms in controlling the erythrocytic differentiation sequence. Interference with the v-erbA and p135gag-myb-ets nuclear oncogenes.* Oncogene, Volume 16 No. 5 (1998), 563–574.

[75] O. Gandrillon , U. Schmidt, H. Beug, J. Samarut. *TGF-beta cooperates with TGF-alpha to induce the self-renewal of normal erythrocytic progenitors: evidence for an autocrine mechanism.* Embo J., 18 (1999), 2764–2781.

[76] B. Gidas, J. Spruck. *Global and local behavior of positive solutions of nonlinear elliptic equations.* Comm. Pure Appl. Math., 34 (1981), no. 4, 525–598.

[77] B. Gidas, J. Spruck. *A priori bounds for positive solutions of nonlinear elliptic equations.* Comm. Partial Differential Equations, 6 (1981), no. 8, 883–901.

[78] C. Giverso, M. Scianna, L. Preziosi, N. Lo Buono, A. Funaro. *Individual Cell-Based Model for In-Vitro Mesothelial Invasion of Ovarian Cancer*, Math. Model. Nat. Phenom., 5 (1) (2010), 203–223.

[79] A. Golubev. *Random discrete competing events vs. dynamic bistable switches in cell proliferation in differentiation.* J. Theor. Biol., 267 (3) (2010), 341–354.

[80] C.J. Gregory, A.C. Eaves. *Human marrow cells capable of erythropoietic differentiation in vitro: definition of three erythroid colony responses.* Blood, 49 (1977), 855–864.

[81] T. Gregory, C. Yu, A. Ma, S.H. Orkin, G.A. Blobel, M.J. Weiss. *GATA-1 and erythropoietin cooperate to promote erythroid cell survival by regulating bcl-xL expression.* Blood, 94 (1999), 87–96.

[82] A. Halanay. *Periodic solutions in a mathematical model for the treatment of chronic myelogenous leukemia.* Math. Model. Nat. Phenom., 7 no. 1 (2012), 235–244.

[83] A. Halanay, D. Candea, I.R. Radulescu. *Existence and stability of limit cycles in a two-delays model of hematopoiesis including asymmetric division.* Math. Model. Nat. Phenom., 9 no. 1 (2014), 58–78.

[84] J. Hochberg, M.S. Cairo. *Childhood and adolescent lymphoblastic lymphoma: end of the beginning and future directions.* Pediatr Blood Cancer, 53 (6) (2009), 917–9.

[85] D. Hoelzer, N. Gokbuget. *T-cell lymphoblastic lymphoma and T-cell acute lymphoblastic leukemia: a separate entity?* Clin Lymphoma Myeloma, 9(Suppl. (3)) (2009), S214–21.

[86] C.A. Janeway et Al. *Immunobiology* 6 th. edition Garland Science.

[87] J. Jeon, V. Quaranta, P.T. Cummings. *An Off-Lattice Hybrid Discrete-Continuum Model of Tumor Growth and Invasion.* Biophys. J., 98 (1) (2010), 37–47.

[88] Y. Jiang, J. Pjesivac-Grbovic, C. Cantrell, J.P. Freyer. *A Multiscale Model for Avascular Tumor Growth.* Biophys J., 289 (6) (2005), 3884–3894.

[89] M. Karttunen, I. Vattulainen, A.Lukkarinen. A novel methods in soft matter simulations. Springer, Berlin, (2004).

[90] U. Koch, F. Radtke. *Mechanisms of T Cell Development and Transformation* Annu. Rev. Cell Dev. Biol., 27 (2011), 539–62

[91] M. Koulnis, Y. Liu, K. Hallstrom, M. Socolovsky. *Negative autoregulation by Fas stabilizes adult erythropoiesis and accelerates its stress response.* PLoS One, (2011).

[92] M.J. Koury, M.C. Bondurant. *Erythropoietin retards DNA breakdown and prevents programmed death in erythroid progenitor cells.* Science, 248 (1990), 378–381.

[93] M.J. Koury. *Erythropoietin: the story of hypoxia and a finely regulated hematopoietic hormone.* Exp Hematol., 33 (2005), 1263–1270.

[94] S.T. Koury, M.J. Koury, M.C. Bondurant, J. Caro, S.E. Graber. *Quantitation of erythropoietin-producing cells in kidneys of mice by in situ hybridization: correlation with hematocrit, renal erythropoietin mRNA, and serum erythropoietin concentration.* Blood, Volume 74 No. 2 (1989), 645–651.

[95] A. Krinner, I. Roeder, M. Loeffler, M. Scholz. *Merging concepts - coupling an agent-based model of hematopoietic stem cells with an ODE model of granulopoiesis.* BMC Systems Biology, 7:117 (2013).

[96] P. Kurbatova. Modélisation hybride de l'érythropoïese et des maladies sanguines. [Hybrid modeling of erythropoiesis and blood diseases]. PhD thesis, University Lyon 1 (2011). French.

[97] P. Kurbatova, S. Bernard, N. Bessonov, F. Crauste, I. Demin, C. Dumontet, S. Fischer, V. Volpert. *Hybrid Model of Erythropoiesis and Leukemia Treatment with Cytosine Arabinoside.* 2011, SIAM J. Appl. Math, Volume 71, Issue 6 (2011), 2246–2268.

[98] P. Kurbatova, N. Eymard, V. Volpert. *Hybrid model of erythropoiesis.* Acta Biotheoretica, Volume 61, Issue 3 (2013), 305-315.

[99] I. Kuzin, S. Pohozaev. Entire solutions of semilinear elliptic equations. Birkhäuser, Basel, 1997.

[100] Y. Liu, R. Pop, C. Sadegh, C. Brugnara, V.H Haase, M. Socolovsky. *Suppression of Fas-FasL coexpression by erythropoietin mediates erythroblast expansion during the erythropoietic stress response in vivo.* Blood, 108 (2006), 123–133.

[101] H. Ludwig, E. Fritz, H. Kotzman, P.Hocker, H.Gisslinger, U. Barnas. *Erythropoietin treatment of anemia associted with multiple myeloma.* The new england journal of medecine, vol. 322,(1990) no. 24, 1693–9.

[102] F. Ma, A. Manabe, D. Wang, M. Ito, A. Kikuchi, M. Wada, M. Ito, A. Ohara, R. Hosoya, S. Asano, K. Tsuji. *Growth of human T cell acute lymphoblastic leukemia lymphoblasts in NOD/SCID mouse fetal thymus organ culture.* Leukemia, 16 (2002), 1541–1548.

[103] M.C. Mackey. *Unified hypothesis of the origin of aplastic anaemia and periodic hematopoïesis.* Blood, 51 (1978), 941–956.

[104] M.C Mackey. *Dynamic hematological disorders of stem cell origin.* In: G. Vassileva-Popova and E. V. Jensen, Editors. Biophysical and Biochemical Information Transfer in Recognition, Plenum Press, New York, (1979), 373–409.

[105] M.C. Mackey, R. Rudnicki. *A new criterion for the global stability of simultaneous cell replication and maturation processes.* J. Math. Biol., 38 (1999), 195–219.

[106] J.M. Mahaffy, J. Belair, M.C. Mackey. *Hematopoietic model with moving boundary condition and state dependent delay: applications in erythropoiesis.* J. Theor. Biol., 190 (1998), 135–146.

[107] R. De Maria, U. Testa, L. Luchetti, A. Zeuner, G. Stassi, E. Pelosi, R. Riccioni, N. Felli, P. Samoggia, C. Peschle. *Apoptotic Role of Fas/Fas Ligand System in the Regulation of Erythropoiesis.* Blood, 93 (1999), 796–803.

[108] S.R. McDougall, A.R.A. Anderson, M.A.J. Chaplain, J.A. Sherratt. *Mathematical modelling of flow through vascular networks: Implications for tumour-induced angiogenesis and chemotherapy strategies.* Bulletin of Mathematical Biology, 64 (4) (2002), 673–702.

[109] R. Mehr, A.S. Perelson, M. Fridkis-Hareli, A. Globerson. *Feedback regulation of T cell development in the thymus* J Theor Biol., 181 (2) (1996), 157–67.

[110] S. Millot, V. Andrieu, P. Letteron, S. Lyoumi, M. Hurtado-Nedelec, Z. Karim, O. Thibaudeau, S. Bennada, J.L. Charrier, S. Lasocki, C. Beaumont. *Erythropoietin stim-*

ulates spleen BMP4-dependent stress erythropoiesis and partially corrects anemia in a mouse model of generalized inflammation. Blood, 116 (2010), 6072–6081.

[111] S.B. Murphy. *Classification, staging and end results of treatment of childhood non-Hodgkin's lymphomas: dissimilarities from lymphomas in adults.* Semin Oncol., 7 (1980), 332–339.

[112] W. Nijhof, P.K. Wierenga. *Isolation and characterization of the erythroid progenitor cell: CFU-E.* J Cell Biol., 96 (1983), 386–392.

[113] K. Ogungbenro. *Physiologically based pharmacokinetic modelling of methotrexate and 6-mercaptopurine in adults and children* submitted.

[114] J.M. Osborne, A. Walter, S.K. Kershaw, G.R. Mirams, A.G. Fletcher, P. Pathmanathan, D. Gavaghan, O.E. Jensen, P.K. Maini, H.M. Byrne. *A hybrid approach to multi-scale modelling of cancer.* Phil. Trans. R. Soc. A, 368 (2010), 5013–5028.

[115] H. Ozbay, C. Bonnet, H. Benjelloun, J. Clairambault. *Stability analysis of cell dynamics in leukemia.* Math. Model. Nat. Phenom., 7 (2012), no. 1, 203–234.

[116] B. Panzenböck, P. Bartunek, M.Y. Mapara, M. Zenke. *Growth and differentiation of human stem cell factor/erythropoietin-dependent erythroid progenitor cells in vitro.* Blood, 92 (1998), 3658–3668.

[117] T. Papayannopoulou, A.R. Migliaccio, J.L. Abkowitz, A.D. D'Andrea. *Biology of erythropoiesis, erythroid differentiation, and maturation.* In Hematology: Basic Principles and Practice, 5th Edition, (2009), 276-294, Hoffman R, Benz EJ Jr, Shattil SJ, Furie B, Silberstein LE, McGlave P and Heslop HE, Editors, Churchill Livingstone, Elsevier, Inc., Philadelphia.

[118] A.A. Patel, E.T. Gawlinsky, S.K. Lemieux, R.A. Gatenby. *A Cellular Automaton Model of Early Tumor Growth and Invasion: The Effects of Native Tissue Vascularity and Increased Anaerobic Tumor Metabolism.* J. Theor. Biol., 213 (2001), 315–331.

156

[119] R.F. Paulson, L. Shi, D.C. Wu. *Stress erythropoiesis: new signals and new stress progenitor cells.* Curr Opin Hematol., 18 (2011), 139–145.

[120] I. Ramis-Conde, D. Drasdo, A.R.A. Anderson, M.A.J. Chaplain. *Modeling the Influence of the E-Cadherin-β-Catenin Pathway in Cancer Cell Invasion: A Multiscale Approach.* Biophys. J., 95 (1) (2008), 155–165.

[121] P. Ramos, C. Casu, S. Gardenghi, L. Breda, B.J. Crielaard, E. Guy, M.F. Marongiu, R. Gupta, R.L. Levine, O. Abdel-Wahab, B.L. Ebert, N. Van Rooijen, S. Ghaffari, R.W. Grady, P.J. Giardina, S. Rivella. *Macrophages support pathological erythropoiesis in polycythemia vera and β-thalassemia.* Nat Med., 19 (2013), 437–445.

[122] M. Reth, T. Brummer. *Feedback regulation of lymphocyte signalling.* Nat Rev Immunol, (4) (2004), 269–77.

[123] M. Rincon, R.A. Flavell, R.J. Davis. *Signal transduction by MAP kinases in T lymphocytes.* Oncogene, Volume 20, Number 19, (2001), 2490–2497.

[124] M.M. Rhodes, P. Kopsombut, M.C. Bondurant, J.O. Price, M.J. Koury. *Adherence to macrophages in erythroblastic islands enhances erythroblast proliferation and increases erythrocyte production by a different mechanism than erythropoietin.* Blood, 111 (2008).

[125] I. Roeder. *Quantitative stem cell biology: computational studies in the hematopoietic system.* Curr. Opin. Hematol., 13 (2006), 222–228.

[126] I. Roeder, I. Glauche. *Towards an understanding of lineage specification in hematopoietic stem cells: A mathematical model for the interaction of transcription factors GATA-1 and PU.1.* Journal of Theoretical Biology, 241 (2006), 852–865.

[127] E.V. Rothenberg, T. Taghon. *Molecular genetics of T cell development.* Annu. Rev. Immunol., 23 (2005), 601–49.

157

[128] C. Rubiolo, D. Piazzolla, K. Meissl, H. Beug, J.C. Huber, A. Kolbus, M. Baccarini. *A balance between Raf-1 and Fas expression sets the pace of erythroid differentiation.* Blood, 108 (2006), 152–159.

[129] Y. Sadahira, H. Wada, T. Manabe, Y. Yawata. *Immunohistochemical assessment of human bone marrow macrophages in hematologic disorders.* Pathology international, (1999), 49, 626-32.

[130] Y. Sadahira, T. Yasuda, T. Yoshino, T. Manabe, T. Takeishi, Y. Kobayashi, Y. Ebe, M. Naito. *Impaired splenic erythropoiesis in phlebotomized mice injected with CL2MDP-liposome: an experimental model for studying the role of stromal macrophages in erythropoiesis.* J Leukoc Biol., 68 (2000), 464–470.

[131] J.T. Sandlund, C.H. Pui, Y. Zhou, F.G. Behm, M. Onciu, B.I. Razzouk, N. Hijiya, D. Campana, M.M. Hudson, R.C. Ribeiro. *Effective treatment of advanced-stage childhood lymphoblastic lymphoma without prophylactic cranial irradiation: results of St Jude NHL13 study.* Leukemia, 23(6) (2009), 1127–30.

[132] M. Santillan, J.M. Mahaffy, J. Belair, M.C. Mackey. *Regulation of platelet production: The normal response to perturbation and cyclical platelet disease.* J. Theor. Biol., 206 (2000), 585–603.

[133] N.J. Savill, W. Chadwick, S.E. Reece. *Quantitative analysis of mechanisms that govern red blood cell age structure and dynamics during an aemia.* PLoS Comput Biol., (2009), 5:e1000416.

[134] K. Sawada, S.B. Krantz, J.S. Kans, E.N. Dessypris, S. Sawyer, A.D. Glick, C.I. Civin. *Purification of human erythroid colony-forming units and demonstration of specific binding of erythropoietin.* J Clin Invest. 80 (1987), 357–366.

[135] S.T. Sawyer, S.M. Jacobs-Helber. *Unraveling distinct intracellular signals that promote survival and proliferation: study of erythropoietin, stem cell factor, and constitutive signaling in leukemic cells.* J. Hematother. Stem Cell Res. 9, (2000) 21–29.

[136] M. Scianna, R.M.H. Merks, L. Preziosi, E. Medico. *Individual cell-based models of cell scatter of ARO and MLP-29 cells in response to hepatocyte growth factor.* J. Theor. Biol., 260 (1) (2009), 151–160.

[137] E. Schmidt, B. Burkhardt. *Lymphoblastic lymphoma in childhood and adolescence.* Pediatr Hematol Oncol., 30 (6) (2013), 484–508.

[138] F. Silvestris, P. Cafforio, M. Tucci, F. Dammacco. *Negative regulation of erythroblast maturation by Fas-L1/TRAIL1 highly malignant plasma cells: a major pathogenetic mechanism of anemia in multiple myeloma.* Blood, 99 (2002), no. 4, 1305–1313.

[139] R.V. Sionov, S. Kfir-Erenfeld, R. Spokoini, E. Yefenof. *A Role for Bcl-2 in Notch1-Dependent Transcription in Thymic Lymphoma Cells.* Advances in Hematology. Article ID 435241, (2012).

[140] M. Socolovsky. *Molecular insights into stress erythropoiesis.* Current opinion in hematology, 14 (2007).

[141] M. Socolovsky, H. Nam, M.D. Fleming, V.H. Haase, C. Brugnara, H.F. Lodish. *Ineffective erythropoiesis in Stat5a(-/-)5b(-/-) mice due to decreased survival of early erythroblasts.* Blood, 98 (2001), 3261–3273.

[142] F.J. Staal, F. Weerkamp, A.W. Langerak, R.W. Hendriks, H.C. Clevers. *Transcriptional control of T lymphocyte differentiation.* Stem Cells, 19 (2001), 165–179.

[143] B. Stark, S. Avigad, D. Luria, S. Manor, T. Reshef-Ronen, G. Avrahami, I. Yaniv. *Bone marrow minimal disseminated disease (MDD) and minimal residual disease (MRD) in childhood T-cell lymphoblastic lymphoma stage III, detected by flow cytometry (FC) and real-time quantitative polymerase chain reaction (RQ-PCR).* Pediatr Blood Cancer, 52 (1) (2009), 20–5, .

[144] J. Starck, M. Weiss-Gayet, C. Gonnet, B. Guyot, J.M. Vicat, F. Morlé. *Inducible Fli-1 gene deletion in adult mice modifies several myeloid lineage commitment decisions*

and accelerates proliferation arrest and terminal erythrocytic differentiation. Blood, 116 (23) (2010), 4795–805.

[145] A. Stéphanou, S.R. McDougall, A.R.A. Anderson, M.A.J. Chaplain. *Mathematical modelling of flow in 2D and 3D vascular networks: Applications to anti-angiogenic and chemotherapeutic drug strategies.* Mathematical and Computer Modelling, 41 (10) (2005), 1137–1156.

[146] J.R.Stephenson, A.A. Axelrad, D.L. McLeod, M.M. Shreeve. *Induction of colonies of hemoglobin-synthesizing cells by erythropoietin in vitro.* Proc Natl Acad Sci U S A, 68 (1971), 1542–1546.

[147] T. Stiehl, A. Marciniak-Czochra. *Mathematical modeling of leukemogenesis and cancer stem cell dynamics.* Math. Model. Nat. Phenom., 7 (2012), no. 1, 166–202.

[148] T. Sugawara, T. Moriguchi, E. Nishida, Y. Takahama. *Differential Roles of ERK and p38 MAP Kinase Pathways in Positive and Negative Selection of T Lymphocytes.* Immunity, Vol. 9 (1998), 565–574.

[149] S.H. Swerdlow. Cancer IAFRO, World Health Organization. *WHO Classification of Tumours of Haematopoietic and Lymphoid Tissues.* World Health Organization. 2008.

[150] M.R. Tallack, A.C. Perkins.*Megakaryocyte-erythroid lineage promiscuity in EKLF null mouse blood.* Haematologica, 95 (1) (2010), 144–147.

[151] A.M. Termuhlem, L.M. Smith, S.L. Perkins, M. Lones, J.L. Finlay, H. Weinstein, T.G. Gross, M. Abromowitch. *Disseminated lymphoblastic lymphoma in children and adolescents: results of the COG A5971 trial: a report from the Children's Oncology Group.* Br J Haematol., 162 (6) (2013), 792–801.

[152] F. Thomas, D. Fisher, P. Fort, J-P Marie, S. Daoust, B. Roche, C. Grunau, C. Cosseau, G. Mitta, S.Baghdiguian, F. Rousset, P. Lassus, E. Assenat, D. Grégoire, D. Missé , A. Lorz, F. Billy, W. Vainchenker, F. Delhommeau, S. Koscielny, R. Itzykson,

R. Tang, F. Fava, A. Ballesta, T. Lepoutre, L. Krasinska, V. Dulic, P. Raynaud, P. Blache, C. Quittau-Prevostel, E. Vignal, H. Trauchessec, B. Perthame, J. Clairambault, V. Volpert, E. Solary, U. Hibner, M. E. Hochberg. *Applying ecological and evolutionary theory to cancer: a long and winding road.* Evolutionary Applications, 6 (1), ISSN 1752-4571 (2013), 1–10.

[153] D.G. Tubergen, M.D. Krailo, A.T. Meadows, J. Rosenstock, M. Kadin, M. Morse, D. King, P.G. Steinherz, J.H. Kersey. *Comparison of treatment regimens for pediatric lymphoblastic non-Hodgkin's lymphoma: a Childrens Cancer Group study.* J Clin Oncol., 13 (6) (1995), 1368–76.

[154] A.S. Tsiftsoglou, I.S. Vizirianakis, J. Strouboulis. *Erythropoiesis: model systems, molecular regulators, and developmental programs.* IUBMB Life., 61 (8) (2009), 800–830.

[155] A. Uyttebroeck, S. Suciu, G. Laureys, A. Robert, H. Pacquement, A. Ferster, G. Marguerite, F. Mazingue, M. Renard, P. Lutz, X. Rialland, F. Mechinaud, H. Cavé, L. Baila, Y. Bertrand. *Treatment of childhood T-cell lymphoblastic lymphoma according to the strategy for acute lymphoblastic leukaemia, without radiotherapy: Long term results of the EORTC CLG 58881 trial.* Europeen journal of cancer, 44 (2008), 840–846.

[156] L. Varricchio, V. Tirelli, E. Masselli, B. Ghinassi, N. Saha, P. Besmer, A.R. Migliaccio. *The expression of the glucocorticoid receptor in human erythroblasts is uniquely regulated by KIT ligand: implications for stress erythropoiesis.* Stem Cells Dev., 21 (2012), 2852–2865.

[157] V. Volpert. Elliptic partial differential equations. Volume 2. Reaction-diffusion equations. Birkhäuser, 2014.

[158] A.I. Volpert, V. Volpert, V.A. Volpert. *Traveling wave solutions of parabolic systems.* Translation of Mathematical Monographs, Vol.140, AMS, Providence, 1994.

[159] V. Volpert. Elliptic partial differential equations. Volume 1. Fredholm theory of elliptic problems in unbounded domains. Birkhäuser, 2011.

[160] V. Volpert. Elliptic partial differential equations. Volume 2. Reaction-diffusion equations. Birkhäuser, 2014.

[161] M. von Lindern, W. Zauner, G. Mellitzer, P. Steinlein, G. Fritsch, K. Huber, B. Löwenberg, H. Beug. *The glucocorticoid receptor cooperates with the erythropoietin receptor and c-Kit to enhance and sustain proliferation of erythroid progenitors in vitro.* Blood, 94 (1999), 550–559.

[162] M. von Lindern, U. Schmidt, H. Beug. *Control of erythropoiesis by erythropoietin and stem cell factor: a novel role for Bruton's tyrosine kinase.* Cell Cycle, 3 (2004), 876–879.

[163] H.E. Wichmann, M.D. Gerhardts, H. SPechtmeyer, R. Gross. *A mathematical model of thrombopoiesis in rats.* Cell Tissue Kinet., 12 (1979), 551–567.

[164] H.E. Wichmann, M. Loeffler. *Mathematical Modeling of Cell Proliferation.* Volume 1, Model description, Irradiation, Erythropoietic Stimulation, (1985) Editor H. E Wichman CRC, Boca Raton, FLorida.

[165] H.E. Wichmann, M. Loeffler, K. Pantel, H. Wulff. *A mathematical model of erythropoiesis in mice and rats. Part 2: Stimulated erythropoiesis.* Cell Tissue Kinet., 22 (1989), 31–49.

[166] C.M. Witt, E.A. Robey. *Thymopoiesis in 4 dimensions.* Seminars in Immunology. 17 (2005), 95–102.

[167] H. Wu, X. Liu, R. Jaenisch, H.F. Lodish. *Generation of committed erythroid BFU-E and CFU-E progenitors does not require erythropoietin or the erythropoietin receptor.* Cell, 83 (1995) 59–67.

[168] H. Wulff, H.E. Wichmann, K. Pantel, M. Loeffler. *A mathematical model of erythropoiesis in mice and rats. Part 3: Suppressed erythropoiesis.* Cell Tissue Kinet., 22 (1989), 51–61.

[169] J. Zhu, S.G. Emerson. *Hematopoietic cytokines, transcription factors and lineage commitment.* Oncogene, 21 (2002), 3295–3313.

Chapter 6

Appendix

6.1 Numerical implementation

6.1.1 Resolution of reaction-diffusion equations

Concentrations evolution of a substance U is described with the following reaction-diffusion equations,

$$\frac{\partial U}{\partial t} = D\Delta U + W - \sigma U, \tag{6.1.1}$$

where W is a constant source term, σ is degradation rate and D is diffusion rate.

In a two dimensional space,

$$\begin{cases} \dfrac{\partial U}{\partial t} = D(\dfrac{\partial^2 U}{\partial^2 x} + \dfrac{\partial^2 U}{\partial^2 y}) + W - \sigma U, 0 \leq x, y \leq L, 0 \leq t \leq T \\[2mm] \qquad\qquad U(x, y, 0) = \psi(x, y), 0 \leq x, y \leq L \\[2mm] \qquad\qquad\qquad U(x, y, t)|_D = G \end{cases} \tag{6.1.2}$$

We use a finite difference scheme in the square domain $0 \leq x, y \leq L, 0 \leq t \leq T$ with the boundary D. We choose the grid $(x_i, y_j, t_n) = (ih_x, jh_y, n\Delta t)$, with i $= 1, 2, ..., N_x$ and $h_x = \frac{1}{N_x}$, j $= 1, 2, ..., N_y$ and $h_y = \frac{1}{N_y}$.

Equations can be written in the following form and solved by alternating direction implicit method.

$$
\begin{cases}
\dfrac{u_{i,j}^{n+1/2} - u_{i,j}^{n}}{\Delta t/2} = D\dfrac{u_{i+1,j}^{n+1/2} - 2u_{i,j}^{n+1/2} + u_{i-1,j}^{n+1/2}}{h_x^2} + \\
\qquad\qquad D\dfrac{u_{i,j+1}^{n} - 2u_{i,j}^{n} + u_{i,j-1}^{n}}{h_y^2} + W_{i,j} - \sigma u_{i,j}^{n+1/2} \\[4pt]
\dfrac{u_{i,j}^{n+1} - u_{i,j}^{n+1/2}}{\Delta t/2} = D\dfrac{u_{i+1,j}^{n+1/2} - 2u_{i,j}^{n+1/2} + u_{i-1,j}^{n+1/2}}{h_x^2} + \\
\qquad\qquad D\dfrac{u_{i,j+1}^{n+1} - 2u_{i,j}^{n+1} + u_{i,j-1}^{n+1}}{h_y^2} + W_{i,j} - \sigma u_{i,j}^{n+1}
\end{cases}
\tag{6.1.3}
$$

With boundary conditions, $u_{i,0}^{n} = u_{0,j}^{n} = 0$ and $u_{i,N_y-1}^{n} = u_{N_x-1,j}^{n} = 0$.

$$
-\underbrace{\left(\frac{2}{\Delta t} + \frac{2D}{h_x^2} + \frac{\sigma}{2}\right)}_{c_i} u_{i,j}^{n+1/2} + \underbrace{\frac{D}{h_x^2}}_{b_i} u_{i+1,j}^{n+1/2} + \underbrace{\frac{D}{h_x^2}}_{a_i} u_{i-1,j}^{n+1/2} =
$$

$$
\underbrace{-\left(\frac{2}{\Delta t} - \frac{2D}{h_y^2}\right)u_{i,j}^{n} - \frac{D}{h_y^2}u_{i,j+1}^{n} - \frac{D}{h_y^2}u_{i,j-1}^{n} + W_{i,j}}_{f_i}
$$

$$
-c_i u_{i,j}^{n+1/2} + b_i u_{i+1,j}^{n+1/2} + a_i u_{i-1,j}^{n+1/2} = f_i
$$

With simplified notations $u_{i,j}^{n+1/2} = u_i$, we get

$$
\begin{aligned}
u_{i-1} &= \alpha_i u_i + \beta_i \\
\alpha_i &= \frac{b_{i-1}}{c_{i-1} - a_{i-1}\alpha_{i-1}} \\
\beta_i &= \alpha_i \beta_{i-1} - \frac{f_{i-1}\alpha_i}{b_{i-1}}
\end{aligned}
$$

$$- \ (\underbrace{\frac{2}{\Delta t} + \frac{2D}{h_y^2} + \frac{\sigma}{2}}_{C_j})u_{i,j}^{n+1} + \underbrace{\frac{D}{h_y^2}}_{B_j}u_{i,j+1}^{n+1} + \underbrace{\frac{D}{h_y^2}}_{A_j}u_{i,j-1}^{n+1} =$$

$$\underbrace{-(\frac{2}{\Delta t} - \frac{2D}{h_x^2})u_{i,j}^{n+1/2} - \frac{D}{h_x^2}u_{i+1,j}^{n+1/2} - \frac{D}{h_x^2}u_{i-1,j}^{n+1/2} + W_{i,j}}_{F_j}$$

$$-C_i u_{i,j}^{n+1} + B_i u_{i,j+1}^{n+1} + A_i u_{i,j-1}^{n+1} = F_i$$

With simplified notations $u_{i,j}^{n+1} = u_j$, we get

$$u_{j-1} = \gamma_j u_j + \kappa_j$$

$$\gamma_j = \frac{B_{j-1}}{C_{j-1} - A_{j-1}\gamma_{j-1}}$$

$$\kappa_j = \gamma_j \kappa_{j-1} - \frac{F_{j-1}\kappa_j}{B_{j-1}}$$

The Thomas algorithm consists of calculating $u_{i,j}^{n+1/2}$ and $u_{i,j}^n$ (which approximate $U(x_i, y_j, t_{n+1/2})$ and $U(x_i, y_j, t_n)$) with the previous recurrent formulas.

6.1.2 Implementation of numerical algorithms

The software used for the simulation of hematopoiesis is written in C^{++}, with operating system Ubuntu. The computations are carried out in dimensionless length units in such a way that the initial cell diameter corresponds to one unit. The computation domain is a square with the side equal 100 length units. In dimensional variables we consider cell diameters to be 10 microns.

The structure of the software is as follow:

- Creation of a cell culture (list of cells) and of the computation domain. For each cell:

166

Initialization cells parameters

Updated

Calculation of forces between cells

Calculation of intra and extra cellular concentrations

Age of cell
>
cell cycle

Yes　　　　　　No

Cell growth

Cancerous cell

Yes　　　　No

Intracellular treatment
>
Treatment threshold

Yes　　　No

Selection
(probability of death)

Yes　　　No

Death

Self renewal

Death

Intracellular
concentration
<
Threshold

Yes　　　No

Differentiation

Self renewal

Figure 6.1: Simplification of the algorithm describing the fate of cells.

- − Initialization of parameters. Birth of the healthy cells of a section of thymus and of one cancer cell. Each cell has a duration of life, coordinates, and intracellular concentrations.

- − Forces between cells and coordinate of cells are calculated, movement is due to Newton's second law.

- − Intracellular and extracellular concentrations are calculated.

- • Application of the rules governing healthy cell divisions.

- Every time step, age of cell is evaluated. While the age of the cell is less than or equal to the cell cycle, the cell grows.

- If a cell survives to the three selections, it self-renews or it differentiates according to the intracellular concentration.

- Application of the rules governing cancer cell divisions

  - If the age of a cancer cell is equal or exceeds cell cycle duration and if the quantity of treatment is less than a threshold, the cell divides. Otherwise the cell dies.

- Treatment of the disease based of the date.

- Updated of the cell culture.

Parameters of intracellular regulation are not known from the experiments. We choose them in such a way that: 1. the bistable dynamics is preserved, 2. the hybrid system shows qualitatively correct and robust behavior with a correct proportion of cells of different types, 3. the results of the simulations fit the experimental curves. The values of parameters are given in the following tables.

6.2   Values of parameters for lineage choice

	day 0	day 2	day 3	day 4	day 6
number of cells	210^5	6.610^5	11.910^5	16.510^5	
ratio of differentiated cells (%)	0	40		80	97

Table 6.1: Biological data for Section 2.2.2.

Parameter	Value	Unit
Cell cycle length	720	min
Cell cycle variation	420	min
α	0.000358	h^{-1}
β	0.05	$h^{-1}.NU^{-1}$
a	0.0041	h^{-1}
b	0.0139	$h^{-1}.NU^{-1}$
c	0.00139	h^{-1}
d	0.00011	h^{-1}
kg	0.0002	$h^{-1}.NU^{-2}$
E_{cr}	0.8	NU
F_{cr}	0.19	NU
E_0 Value of initial quantity E	0.015	NU
F_0 Value of initial quantity F	0.01	NU

Table 6.2: Intracellular parameters. Data for Section 2.2.2.

Parameter	Value	Unit
Cells cycle length T	18	h
Cells cycle variation	3	h
a_0^0	0.001	
a_0^1	0	
a_1^1	0.0001	
a_1^0	0.0000005	
a_2^1	0	
a_2^0	0.00077	
a_3^1	0.0001	
a_3^0	0.000001	
b_1	0.0004	
b_2	0.0045	
b_3	0.43	
w_{cr}	0.09	NU

Table 6.3: Values of intracellular parameters. figure 2.14 (right).

Parameter	Value	Unit
Cells cycle length T	18	h
Cells cycle variation	3	h
a_0^0	0.001	
a_0^1	0	
a_1^1	0.00025	
a_1^0	0.0000005	
a_2^1	0	
a_2^0	0.000825	
a_3^1	0.0001	
a_3^0	0.000001	
b_1	0.0004	
b_2	0.0045	
b_3	0.51	
w_{cr}	0.509	NU

Table 6.4: Values of intracellular parameters. figure 2.14 (left).

Parameter	Value	Unit
AC Cells cycle length	6.5	h
Cells cycle variation	0.5	h
a_0^0	0.001	
a_0^1	0	
a_1^1	0.000035	
a_1^0	0.000035	
a_2^1	0	
a_2^0	0.00035	
a_3^1	0.0001	
a_3^0	0.000001	
b_1	0.0004	
b_2	0.0045	
b_3	0.4	
w_{cr}	0.5	NU

Table 6.5: Values of intracellular parameters for AC. figure 2.18.

Parameter	Value	Unit
NAC Cells cycle length	16	h
Cells cycle variation	0.5	h
a_0^0	0.001	
a_0^1	0	
a_1^1	0.00003	
a_1^0	0.0000005	
a_2^1	0	
a_2^0	0.00044	
a_3^1	0.0001	
a_3^0	0.000001	
b_1	0.0004	
b_2	0.0045	
b_3	0.4	
w_{cr}	0.485	NU

Table 6.6: Values of intracellular parameters for NAC. figure 2.18.

Parameter	Value	Unit
Cell cycle length	720	min
Cell cycle variation	420	min
α	0.000358	h^{-1}
β	0.05	$h^{-1}.NU^{-1}$
a	0.0041	h^{-1}
b	0.0139	$h^{-1}.NU^{-1}$
c	0.00139	h^{-1}
d	0.00011	h^{-1}
kg	0.0002	$h^{-1}.NU^{-2}$
E_{cr}	0.8	NU
F_{cr}	0.19	NU
E_0 Value of initial quantity E	0.015	NU
F_0 Value of initial quantity F	0.01	NU

Table 6.7: Intracellular parameters (Section 2.2.2).

Parameter	Value	Unit
r_0	0.01	L
m	1	M
μ	6.10^5	h^{-1}
K	$0.9.10^6$	$M.h^{-2}$
D_{F_L}	3.10^{-4}	$L^2.h^{-1}$
k_{F_L}	3.10^{-3}	F_L molecules / reticulocyte / h
σ_{F_L}	0.6	h^{-1}

Table 6.8: Extracellular parameters (Section 2.2.2).

6.3 Appendix 1. Intracellular regulation of erythroid progenitors

In the derivation of the variables used in the model in Figure 2.11, we considered intracellular regulation of erythroid progenitors where each of three possible cell fates (self-renewal, terminal differentiation, or apoptosis) is determined by the concentration or activity of specific proteins. Figure 6.2 shows a biological scheme summarizing known intracellular regulatory events in erythroid progenitors at the CFU-E/Pro-EB stage of differentiation, including the spatial interactions of the erythroid progenitors with the central macrophage, other erythroid cells in an erythroblastic island, and the general microenvironment in the bone marrow.

In Figure 6.2, human fetal erythroid progenitors have been proposed to have an intracellular network comprised of opposing and antagonistic functions that can be represented by two proteins. One protein, ERK, is a kinase within the Ras/Raf/ERK signal transduction pathway of growth factors and hematopoietic cytokines that can stimulate self-renewal in CFU-E/Pro-EBs [128, 61]. In erythroid progenitors, ERK concentrations are increased by activated glucocorticosteroid receptors that, in turn, are directly related to the extracellular concentration of glucocorticosteroid hormones produced in the adrenals [116, 161]. Stress erythropoiesis requires functional glucocorticosteroid receptors [14]. EPO and KL/-SCF also increase intracelluar ERK concentrations [162]. Activated ERK, in turn, increases glucocorticosteroid receptor expression [156]. The second protein is Fas, a member of the

tumor necrosis factor receptor family that can activate specific caspases, a series of intracellular proteolytic enzymes that promote apoptosis [128]. At high levels of activation, Fas stimulates erythroid progenitor apoptosis [107, 100], while at lower activities it promotes terminal erythroid differentiation [128] that is mediated through the activity of the transcription factor GATA-1 on the expression of many erythroid-specific genes. Activated Fas concentrations are directly related to extracellular Fas-ligand concentrations, which in human hematopoietic tissues are produced mainly by the most mature erythroblasts [107] and in mouse hematopoietic tissues are produced mainly by early stage erythroblasts [100].

The intracellular concentration of activated Fas is a key factor in the decisions made by the erythroid progenitor in Figure 2.10. When a specific threshold of intracellular Fas-mediated caspase activity is present, the erythroid progenitor dies by apoptosis. If the intracellular concentration of activated Fas is not sufficient to reach the apoptosis threshold, then the erythroid progenitor makes the second decision based on a competition between ERK-mediated self-renewal and Fas-mediated terminal differentiation [128]. The major regulator of Fas activity is the concentration of EPO in the bone marrow microenvironment. Under normal conditions, the EPO concentrations in the blood and the marrow are relatively low, and the Fas expression on the CFU-E/Pro-EBs is sufficiently high that the resultant level of caspase activity causes most of them undergo apoptosis [93]. The relatively low concentrations of glucocorticoid hormone present under normal conditions results in only a few CFU-E/Pro-EBs undergoing self-renewal. Therefore, of those CFU-E/Pro-EBs that do not undergo apoptosis, most will have sufficient Fas and limited ERK so that they will terminally differentiate, thereby supplying the $2 \cdot 10^{11}$ new erythrocytes required each day to replace those erythrocytes lost to senescent removal.

The normal steady-state erythropoiesis can respond rapidly to changes in EPO concentrations [93]. In kidney disease, anemia develops as less EPO is produced, and more than normal numbers of CFU-E/Pro-EBs undergo apoptosis from the resulting increases in Fas and caspase activities. Exogenous EPO administration or recovery from the kidney disease will lower the Fas and caspase activities, thereby decreasing the apoptosis rate to normal,

and the anemia will resolve. EPO levels increase slightly or moderately with limited bleeding, hemolysis, lung disease, or ascent to high altitude because normal kidneys will produce more EPO in response to slight or moderate hypoxia. The increased EPO will decrease Fas activity and increase the Bcl-xL concentration, thereby reducing the intracellular caspase activities. The decreased apoptosis resulting from the reduced caspase activities is accompanied by an EPO-mediated increase in GATA-1 such that terminal differentiation is increased relative to self-renewal.

Although EPO can increase ERK activity, its effect alone on self-renewal is less than its effect on preventing apoptosis and promoting terminal differentiation. With acute hypoxia due to large amounts of bleeding or hemolysis, the resultant stress erythropoiesis is characterized by large increases in EPO, but the ability of the erythroid progenitor cells that supply the steady-state erythrocyte production to respond to the increased EPO has a maximal limit. Very high EPO concentrations eliminate almost all apoptosis, and EPO-mediated increases in GATA-1 promote terminal differentiation.

Although the total response to very high concentrations of EPO is limited by the number of available CFU-E/Pro-EBs, the erythropoietic response to hypoxic stress is amplified by an increased self-renewal that provides more CFU-E/Pro-EBs. Increased concentrations of glucocorticosteroids and EPO in stress erythropoiesis can raise ERK levels and promote CFU-E/Pro-EB self-renewal, but a major factor in the expansion of CFU-E/proerythroblasts numbers during stress erythropoiesis in mouse spleens is BMP4, a member of the transforming growth factor-family of cytokines, with receptors that signal through the Smad pathway [119]. Splenic macrophages with the same immunophenotype (F4/80 positive) as those that include the central macrophages of erythroblastic islands appear to be the source of BMP4 in murine stress erythropoiesis [110]. Erythroid cells that are directly in contact with central macrophages have a decreased duration of cell cycle that increases their proliferation rate [124], and macrophage function *in vivo* is required for recovery from anemia due to bleeding or hemolysis [130, 48, 121]. The generation of increased CFU-E/Pro-EBs during hypoxic stress requires not only hypoxia but c-Kit and EPO as well as priming by

the cytokine Hedgehog [119]. The source of the BMP4-inducible erythroid progenitors that give rise to an expanded CFU-E/Pro-EB population in the spleen is not certain. They appear to be a separate population of erythroid progenitors that are closely related to, if not the same as, the CFU-E/Pro-EBs of normal steady-state erythropoiesis. However, once they develop to the CFU-E/Pro-EB stage, these BMP-derived progenitors appear to have all of the characteristics of the CFU-E/Pro-EBs present during normal, steady-state erythropoiesis [119].
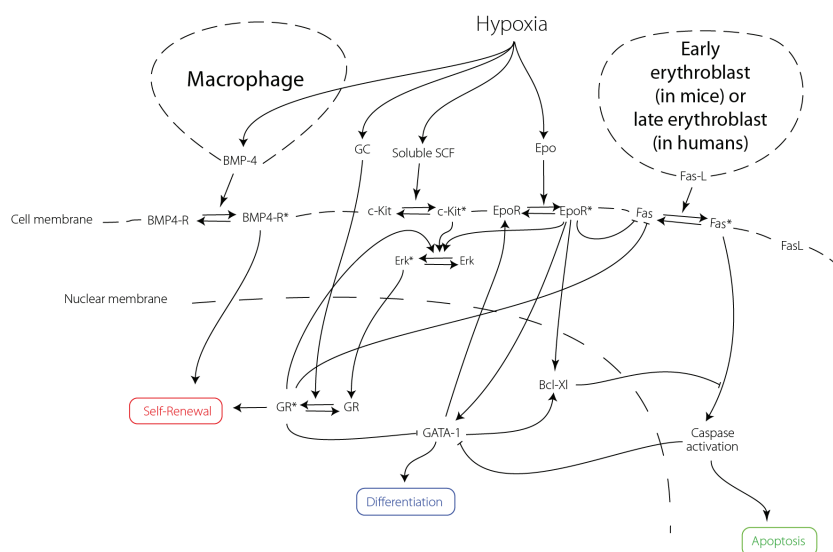
Figure 6.2: Schematic representation of intracellular and extracellular regulation of mammalian erythropoiesis at the stage of the CFU-E/Pro-EB in an erythroblastic island. The scheme uses data from studies of both human and mouse. Macrophages through BMP4, and the microenvironment through KL/SCF and glucocorticosteroids stimulate CFU-E/Pro-EB self-renewal. EPO stimulates CFU-E/Pro-EB survival and differentiation through its down-regulation of Fas and up-regulation of GATA-1. Very early stage erythroblasts in mouse and late stage erythroblasts in human promote apoptosis through their production of Fas-ligand. See text for a detailed description of the scheme.

6.4   Appendix 2. Cell culture experiments

In previously reported studies [124], erythroblastic islands isolated from the spleens of mice in the acute erythroblastosis phase of anemia-inducing Friend virus (FVA)-infection provided the macrophages for experiments that reconstituted erythroblastic islands *in vitro*.

175

Because EPO levels are low in FVA-infected mice [92], most erythroid progenitors do not survive beyond the CFU- E/Pro-EB stages *in vivo*, and a majority of erythroblastic islands in the spleen are populated mainly with CFU-E/Pro-EB. However, when these isolated splenic erythroblastic islands are cultured for 72 hours *in vitro* with EPO under conditions that promote differentiation, the erythroid cells terminally differentiate. Although some erythroblasts lose adherence to macrophages in culture, others remain in the cultured erythroblastic islands. In Figure 2.20, islands at various times of culture were selected to show the stages of erythroid differentiation within the islands *in vitro*.

In order to compare the proliferation and differentiation of the same population of developmentally homogeneous CFU-E/Pro-EBs cultured in erythroblastic islands and cultured without central macrophages, a series of experiments used reconstituted erythroblastic islands [124]. In these experiments, isolated splenic erythroblastic islands were cultured for 6 hours so that their central macrophages bound to the tissue culture plates. Then, after removal of adherent erythroid cells, the macrophages were cultured for another day before CFU-E/Pro-EBs purified from the spleen of another FVA-infected mouse were added in co-cultures for 6 h. Excess unbound erythroid progenitors were then removed, and the co-cultures were continued. Proliferation and differentiation of co-cultured CFU-E/Pro-EBs over the ensuing 3 days were compared to aliquots of the same CFU-E/Pro-EBs that were cultured alone and, thereby, served as controls. In the co-cultures some erythroblasts lost their macrophage adherence. Comparisons of erythroid cells that remained adherent to the macrophages with non-adherent erythroid cells of co-cultures or the control cells cultured without macrophages demonstrated that central macrophage adherence promoted more rapid cell proliferation due to shortened G1 phase of cell cycle [124].

6.5   Appendix 3

In the models considered in this work, some parameters are known : cell size, cell number, duration of cell cycle [75], diffusion coefficient [45]. Some other parameters, especially

reaction constants in intracellular regulation are not known. Such parameters were varied in a large range in order to see how the results depends on them. In the description of the experiments, unknown parameters were fitted.

Initial quantities for the systeme (2.2.13)-(2.2.16) are as follows: $z = 1$, $u = 0.5$, $v = 0.5$, $w = 0.25$ (mice); $z = 1$, $u = 0.5$, $v = 0.5$, $w = 0.5$ (human). At the moment of cell division, the two daughter cells inherit half of quantities z, u, v, w of the mother cell.

Parameter	Value	Unit
Cells cycle length T	18	h
Cells cycle variation	3	h
space variable x		NU
time variable		h
a_0^0	0.001	h^{-1}
a_0^1	0	h^{-1}
a_1^1	0.0001	h^{-1}
a_1^0	0.0000005	h^{-1}
a_2^1	0	h^{-1}
a_2^0	0.00077	h^{-1}
a_3^1	0.0001	h^{-1}
a_3^0	0.000001	h^{-1}
b_1	0.0004	h^{-1}
b_2	0.0045	h^{-1}
b_3	0.43	h_{-1}
w_{cr}	0.09	NU

Table 6.9: Values of intracellular parameters used in Figure 2.14 (right). NU denotes nondimensional unit

Parameter	Value	Unit
Cells cycle length T	18	h
Cells cycle variation	3	h
space variable x		NU
time variable		h
a_0^0	0.001	h^{-1}
a_0^1	0	h^{-1}
a_1^1	0.00025	h^{-1}
a_1^0	0.0000005	h^{-1}
a_2^1	0	h^{-1}
a_2^0	0.000825	h^{-1}
a_3^1	0.0001	h^{-1}
a_3^0	0.000001	h^{-1}
b_1	0.0004	h^{-1}
b_2	0.0045	h^{-1}
b_3	0.51	h^{-1}
w_{cr}	0.509	NU

Table 6.10: Values of intracellular parameters used in Figure 2.14 (left)

Parameter	Value	Unit
AC Cells cycle length	6.5	h
Cells cycle variation	0.5	h
space variable x		NU
time variable		h
a_0^0	0.001	h^{-1}
a_0^1	0	h^{-1}
a_1^1	0.000035	h^{-1}
a_1^0	0.000035	h^{-1}
a_2^1	0	h^{-1}
a_2^0	0.00035	h^{-1}
a_3^1	0.0001	h^{-1}
a_3^0	0.000001	h^{-1}
b_1	0.0004	h^{-1}
b_2	0.0045	h^{-1}
b_3	0.4	h^{-1}
w_{cr}	0.5	NU

Table 6.11: Values of intracellular parameters for AC. Figure 2.18

Parameter	Value	Unit
NAC Cells cycle length	16	h
Cells cycle variation	0.5	h
space variable x		NU
time variable		h
a_0^0	0.001	h^{-1}
a_0^1	0	h^{-1}
a_1^1	0.00003	h^{-1}
a_1^0	0.0000005	h^{-1}
a_2^1	0	h^{-1}
a_2^0	0.00044	h^{-1}
a_3^1	0.0001	h^{-1}
a_3^0	0.000001	h^{-1}
b_1	0.0004	h^{-1}
b_2	0.0045	h^{-1}
b_3	0.4	h^{-1}
w_{cr}	0.485	NU

Table 6.12: Values of intracellular parameters for NAC. Figure 2.18

Parameter	Value	Unit
σ_1	0.01	h^{-1}
$D1$	0.25e-5	$L^2.h^{-1}$
w_1	0.00005	$molecules.L^{-2}.h^{-1}$
σ_2	0.005	h^{-1}
D_2	0.05e-4	$L^2.h^{-1}$
w_2	0.0005	$molecules.L^{-2}.h^{-1}$

Table 6.13: Values of extracellular parameters. L is an arbitrary length unit

6.6 Value of parameters of myeloma simulation

Parameter	Value	Unit
Cell cycle length	720	min
Cell cycle variation	180	min
α	0.026	h^{-1}
β	1	$h^{-1}.NU^{-1}$
a	0.265	h^{-1}
b	0.03	$h^{-1}.NU^{-1}$
c	0.05	h^{-1}
d	0.025	h^{-1}
E_{cr}	0.3	NU
F_{cr}	0.6	NU
E_0 Value of initial quantity E	0.3	NU
F_0 Value of initial quantity F	0.3	NU

Table 6.14: Value of parameters without macrophage

Parameter	Value	Unit
Cell cycle length	1440	min
Cell cycle variation	360	min
α	0.01	h^{-1}
β	2	$h^{-1}.NU^{-1}$
kalpha	0.1	$h^{-1}/GF molecules$
a	0.53	h^{-1}
b	0.06	$h^{-1}.NU^{-1}$
c	0.1	h^{-1}
d	0.05	h^{-1}
kg	0.03	$h^{-1}.NU^{-2}$
E_{cr}	0.55	NU
F_{cr}	0.48	NU
E_0 Value of initial quantity E	0.3	NU
F_0 Value of initial quantity F	0.3	NU

Table 6.15: Value of parameters with macrophages, Figure 3.9.

Parameter	Value	Unit
Cell cycle length	720	min
Cell cycle variation	180	min

Table 6.16: Value of parameters without macrophage

Parameter	Value	Unit
Cell cycle length	1440	min
Cell cycle variation	360	min

Table 6.17: Value of parameters with macrophages, Figure 3.9.